IN VIVO IMAGING OF EXPERIENCE-DEPENDENT PLASTICITY IN THE RETROSPLENIAL CORTEX FOLLOWING UNILATERAL HIPPOCAMPAL LESIONS

MEGAN ELIZABETH TORRY
Bachelor of Science, University of Lethbridge, 2006

A Thesis
Submitted to the School of Graduate Studies
of the University of Lethbridge
in Partial Fulfillment of the
Requirements for the Degree

MASTER OF SCIENCE

Department of Neuroscience
University of Lethbridge
LETHBRIDGE, ALBERTA, CANADA

IN VIVO IMAGING OF EXPERIENCE-DEPENDENT PLASTICITY IN THE RETROSPLENIAL CORTEX FOLLOWING UNILATERAL HIPPOCAMPAL LESIONS

MEGAN ELIZABETH TORRY

Date of Defence: March 25, 2019

Dr. Bruce L. McNaughton Supervisor	Professor	Ph.D.
Dr. Robert Sutherland Committee Member	Professor	Ph.D.
Dr. Bryan Kolb Committee Member	Professor	Ph.D.
Dr. Majid Mohajerani Committee Member	Associate Professor	Ph.D.
Dr. Masami Tatsuno Chair, Thesis Examination	Associate Professor	Ph.D.

Abstract

Mechanisms of learning and memory influence brain connectivity. Hippocampal outflow targets the ipsilateral retrosplenial cortex (RSC) and thus influences plasticity in the neocortex. Evidence from fixed tissue suggests that hippocampal lesions prevent the increase in dendritic spines due to an enrichment environment; however, may prevent observation of a larger effect on synaptic turnover across time. Longitudinal two-photon microscopy was used to compare specific ipsilateral and contralateral RSC locations *in vivo*, before and after enrichment. Consolidation theory predicts that in the absence of one hippocampus the ipsilateral RSC will undergo asymmetry in plasticity following enrichment exposure. In both hemispheres, synaptic turnover persists during home-cage housing with a slight transient increase following transfer to enrichment. There was greater axon growth and a lasting $\sim$7% increase in spine density in the RSC ipsilateral to the lesion. Irregularities in transgenic mouse genetics, and particulars regarding the functionality between pre and post-synaptic elements remain enigmatic.

Acknowledgments

First I would like to thank my supervisor, Dr. Bruce McNaughton for his wisdom, expertise, scientific vigor, creativity and continuing to be an inspiration to me. You are a great leader. To all of the people at the University of Lethbridge, from past to present, from professors to fellow students, for laughs, encouragement, and friendship, Thank-you. To the many people who took the time to answer my questions, and work with me over this experience, you helped me keep going and develop my skillset. Thank-you to my examination committee members, Drs. Robert Sutherland, Bryan Kolb and Majid Mohajerani, especially for any cleverness, additional guidance, or access to resources. To professors John Vokey for continuing to remain a comfortable and logical go-to for me, and Denton Fredrickson for your interest in turning my data into 3D printed hand-held objects. With utmost respect I thank Dr. JianJun (a.k.a. JJ), Ricardo Morgado, and all of the animal/technical/administrative support teams at the CCBN, the entirety of this project would not have been possible without you all. Finally, I would like to thank and dedicate this work to those who have and continue to surround me with love and support. Family and friends near and far, you have helped me more than you will ever know.

Contents

List of Tables

List of Figures

Introduction

The hippocampus is a key component of the limbic system found deep within the brain's medial temporal lobe. Rodents rely upon similar neuroanatomical structures, including the hippocampus and the RSC, as are required for functional declarative memory in humans. Multiple human patient and animal studies dating back to the 1950s have provided increasing support that declarative memory, spatial navigation, and information encoding deficits follow bilateral damage to the hippocampus (Squire and Wixted, 2011; Penfield and Milner, 1958; Scoville and Milner, 1957; Mao et al., 2018). Together, such findings support that in the absence of hippocampal activity, the cortex loses the ability to acquire new episodic memory and semantic knowledge.

The seminal hypotheses and contributions from inspiring researchers such as Santiago Ramón y Cajal, Donald Hebb, and David Marr laid much groundwork for studying the nature of memory. Cajal for the discovery and lifelong support of dendritic spines and their functional involvement in connecting cells to one another. Hebbian theory for acknowledging intrinsic associative learning in that cell assemblies are adaptive, reinforced, and modify in response to stimuli. Finally, Marr for his additional support of associative learning and models of long-term memory in relation to how the hippocampus memorizes unique patterns of activity from sensory experiences that are then reactivated back to the neocortex for later experiential recall (Marr, 1971).

The reactivation of indexed patterns is believed to be a coordination of memory traces that transfers information between the hippocampus and neocortex. Reactivation of neuronal patterns may function to provide important potentiation and depression influencing the strength of synapses. During retrieval of a memory, pattern completion of the index occurs while creating lability for the possibility of new information to be inserted. Thus,

synaptic ensembles remain modifiable upon later experience and reconsolidation of a previous memory may lead to reconstruction upon retrieval (Tronson and Taylor, 2007). One possible mechanism for network modifications is the maturation of new dentate gyrus stem and progenitor cells, as they provide new available connections within pre-exisiting circuitry (Bergami, 2015).

The transmission of activity between neurons is a time-dependent process. Spike time-dependent plasticity relies on the Hebbian learning concept that synapses between cells strengthen (long-term potentiation) when the presynaptic cells leads to co-activation of a postsynaptic cell. One way for long-term depression to occur is when the post-synaptic cell activity precedes the pre-synaptic cell's, likely due to other pre-synaptic inputs. In addition, memory trace reactivations occur bidirectionally, in both the forward and backward direction, implying balance between sequence based, time-dependent processes (Atherton et al., 2015).

Synaptic potentiation/depression likely occurs between the hippocampus and neocortex in order to refine or forget experiences that are not considered necessary. According to Marr's initial theory, the neocortex is continually classifying the most important aspects of hippocampal memory-related input/output (Marr, 1970). Dendritic spines change shape as a function of long-term potentiation or depression; however, an effect on turnover is unclear. Sharp-wave ripple oscillations in the hippocampus during slow wave sleep trigger overall greater synaptic depression in the hippocampus that results in a decrease in dendritic spine tip size but not density (Norimoto et al., 2018). Other research conducted by Roo et al. (2008) found that, bursting activity promotes the replacement of pre-existing spines with new spines, and enlarged spines are more stable with new spine formations occurring close-by in a clustered manner.

A neuroanatomical avenue for the transfer of information from the hippocampus to the neocortex is through abundant ipsilateral connections that originate in the subiculum and project through the granular RSC. Experiment 127795906 from the Allen Brain Atlas sup-

ports that over 85% of connections from the hippocampus are ipsilateral (Oh, 2014). The RSC receives both excitatory and inhibitory connections originating in the hippocampus (rodent: Van Groen and Wyss, 2003; Vogt and Miller, 1983; Miyashita and Rockland, 2007; and monkey: Aggleton et al., 2012). In addition to hippocampal outflow, the RSC and hippocampus contain intrinsic and reciprocal connections. For example, Wyss and Groen (1992) observed axons originating in the RSC that project back to the hippocampus through the entorhinal cortex. For further review on connectivity see: (Sugar et al., 2011).

In addition to circuit level connectivity the hippocampus and RSC share similar functions. A study by Sutherland and Hoesing (1993) found that when one hemisphere's hippocampus is lesioned, as well as the contralateral RSC, spatial navigation deficits are indistinguishable from rats with bilateral hippocampal lesions. The RSC further integrates information to and from additional areas of the neocortex (Zingg et al., 2014). Yamawaki et al. (2016) found that the RSC has monosynaptic connections to the motor cortex, additional connectivity required for successful navigation. In addition, in 2001, Raichle et al. (2001) described an active 'default mode network' that includes simultaneous activity in the hippocampus and RSC (and other structures) during times of quiet wakefulness. This important quiet-time network supports that the hippocampus and the RSC are further involved in successful formation of conjunctive memory-based thought representations, such as internal scenes, self-awareness, remembering the past, and planning for the future.

An additional study by Sutherland et al. (2010a) found evidence from fixed tissue that in rats with unilateral hippocampal lesions there is a decrease in density of basilar dendritic spines in the ipsilateral posterior parietal cortex but an increase in the sham hemisphere, when rats are housed in a complex environment. Conversely, they found a significant complex housing effect indicating an increase in density of apical dendritic spines in both the ipsilateral and contalateral hemispheres. An *in vivo* experiment involving sensory whisker trimming drives both the gain and loss of dendritic spines without influencing the overall density (Trachtenberg et al., 2002). Together such research led to interest in quantifying

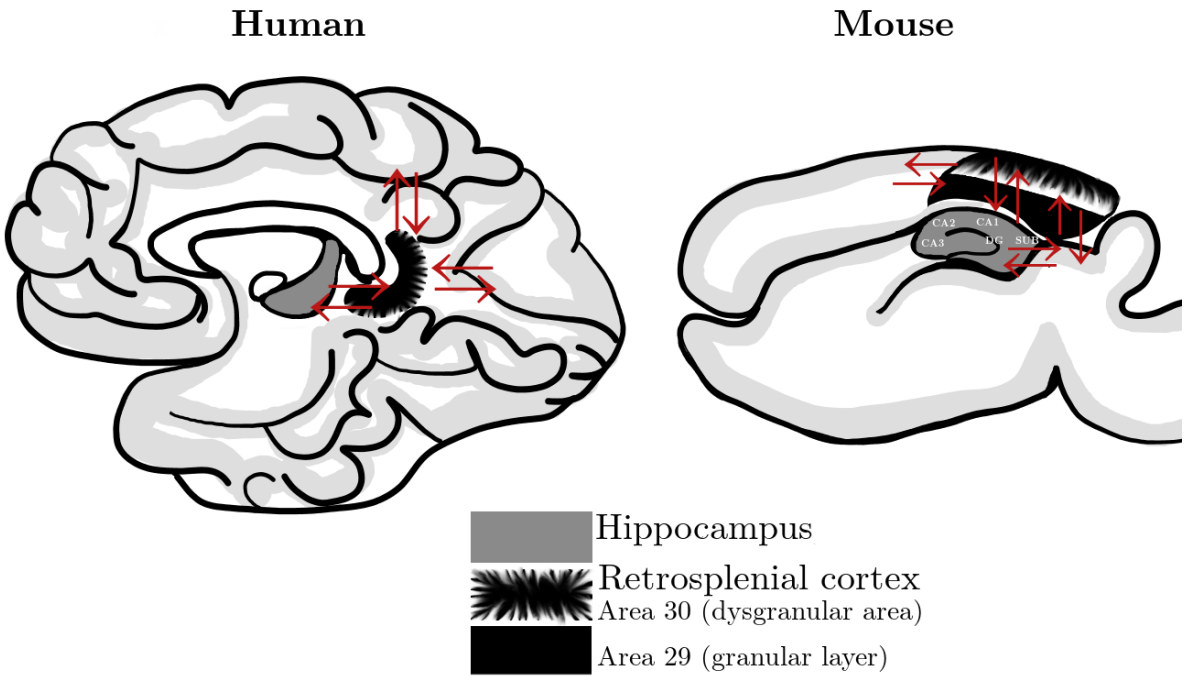

Figure 1.1: In humans the RSC is found deep within the neocortex (a.k.a the cingulate cortex), posterior to the hippocampal formation. In the rodent, the RSC is larger than in humans, making up one of the largest neocortical regions. The surface of the RSC in rodents is easily accessible for direct two photon imaging through a cranial window. The structures are reciprocally connected and involved in spatial navigation, learning and memory.

both the density and turnover of dendritic spines and axonal boutons, before and after enrichment, in mice with unilateral hippocampal lesions.

The cytoarchitecture of the neocortex has six layers containing millions of excitatory pyramidal cells in columnar modules. Numerous dendrites extend above (apical) and below (basilar) from the cell body and are scattered with post-synaptic dendritic spines. In addition, each pyramidal cell contains one axon collateral that potentially extends long distances and is less densely scattered with pre-synaptic boutons. The long lengths of axons makes them challenging and currently less studied due to difficulty tracking their origin and target locations in structural studies. Axons have been captured growing *in vivo* in a unidirectional manner, changing directions and extending hundreds of microns over days (Paola et al., 2006). The following thesis captures the same type of axonal growth data, but it remains an issue regarding their undetermined origin and target locations.

Synapses contain pre-synaptic and post-synaptic elements. The pre-synaptic side serves to transfer information via specialized activity that results in varying synaptic potentials in the post-synaptic side. Synaptic potentials can be excitatory or inhibitory and influence post-synaptic membrane potentials in a complex manner. For example, activation of inhibitory neurons can reduce hyper-excitability via post-synaptic contacts on pyramidal neurons without leading to spine loss. Zuo et al. (2018) performed a stress study where mice exposed to environmental enrichment maintained activation of paravalbumin interneurons that prevented the loss of dendritic spines due to stress. Enriched mice further reestablished competence on a texture discrimination task back to unstressed control levels. In another study, these same inhibitory interneurons responded with a transient increase in axonal bouton density following a lever-pressing motor learning behaviour (Chen et al., 2015).

Dendritic spine and bouton turnover comes in the form of gaining new spines or losing previously existing spines. There are mainly 4 characterized dendritic spine shapes (filopodia, thin, mushroom, and stubby) and two characterized bouton shapes (terminaux and en passant). These actin dense cytoskeleton shapes are thought to coincide with varying functional properties or synaptic weights across time. For example, stubby spines are currently recognized as being the most stable and hold greater weight for activation within a network. Conversely, thin spines are currently recognized as more immature and thus, more susceptible to long term potentiation/depression (Tavosanis, 2011).

A specialized area called the Post Synaptic Density (PSD) is found at the tip of dendritic spines and plays an important role in stability and potential to bear a synapse. The PSD contains varying amounts of ionotropic glutatmate receptors (AMPARs and NDMARs), and scaffolding proteins (PSD-95) that influence the overall size and activity of spines. In order for synaptic potentials to induce the NMDA calcium influx required for an action potential, AMPA receptor activity is often rquired to remove a magnesium cation initially blocking the NMDA receptors. Thus, if a dendritic spine does not contain AMPA receptors it may be potentially silent. In addition, the scaffolding protein PSD-95 must be present in

order for spines to undergo long term potentiation, and is further involved in pathologies such as dendritic beading/blebbing and epilepsy (Campbell et al., 2009). Around 20% of spines do not contain PSD-95 and are consequently short lived with little impact on long-term circuitry, and are often removed without returning (Berry and Nedivi, 2017).

The shrinkage in dendritic spine shape has the potential to disrupt the performance of a learned task (Hayashi-Takagi et al., 2015). Changes in the size of spines was not taken into account in the following thesis due to questionable two-photon microscopy resolution, however; all previously characterized spine types were observed. A finding in Villa et al. (2016) is an additional caveat of the following thesis relating to differentiating functionality of synaptic structures. They observed that the largest and most structurally stable dendritic spines have the potential for two synapses, a structurally stable excitatory synapse paired with a modulatory inhibitory synapse. The inhibitory synapse was observed to move in location between the spine tip and dendritic shaft playing a modulatory role in overall excitability. Such plasticity in these inhibitory synapses subsequently influences the synaptic weight of these structurally stable dendritic spines without leading to structural turnover.

In relation to enrichment, it was anecdotal evidence observed by Hebb (1947) where rats allowed to roam in his home outperformed on tests in comparison to those reared in laboratory housing. Their enhanced cognition was thought to be due to an enriched environment that required a greater diversity of natural rat behaviours. Thus, the behaviour utilized in the following thesis was exposure to an enriched environment in order to induce learning in response increased complexity. Early research supports that, when rodents are housed in environmental enrichment, there is an overall increase in synaptogenesis, spine density, dendritic fields, complexity of arbours, and overall cortical thickness (Weiler et al., 1995).

Grutzendler et al. (2002) observed that dendritic spines in the adult visual cortex are mainly stable. In addition, filopodia (highly plastic immature spines not containing a synaptic connection) are non-existent, however; there is general consensus that functional circuits

in the adult neocortex continue to adjust to novelty and sensory experiences offered by an enrichment environment (Rosenzeig et al., 1972; Holtmaat et al., 2006). There is additional evidence from adult female mice that increased connectivity and enhanced flexibility of dendritic spines manifests from enrichment learning, while conversely, greater stability results without enrichment experiences (Jung and Herms, 2014).

Other studies on experience-dependent plasticity support that overall stabilization of new spines is more likely (Holtmaat and Svoboda, 2009). One study found that during a forelimb reaching task stabilization only was evident after multiple subsequent learning trials (Xu et al., 2009). Interestingly, an *in vivo* experiment indicated that exposure to new experiences results in gain and increased turnover of dendritic spines on the apical tufts of layer 5 pyramidal neurons, only after a period of sleep (Yang et al., 2014). Structural plasticity is theorized to be maximal during slow wave sleep when the hippocampus is believed to coordinate memory trace reactivation in the cortex. Permanent housing in an enriched environment provides both multiple learning experiences and sleep cycles; the development of learning and memory slowly over time.

With the continuation of additional research it has become apparent that results vary between studies depending on methods, sex of the animals, time-lines and areas of cortex in question; how, when and where you look matters (Comeau et al., 2010). Evidence supports that metabolic activity increases in the RSC only one-two days after exposure to a hippocampal dependent learning task (Mendez-Lopez et al., 2013). An experiment on peptides indicates that an increase occurs in the RSC for two weeks in rats between 8-9 months but not 22-23 months of age, regardless of the length of enrichment exposure (Rapley et al., 2018). There are also documented sex differences in response to an enriched environment (Juraska, 1990; Kolb et al., 2003).

In vivo two photon laser scanning microscopy (2PLSM) was used in the following study for longitudinal imaging of the same locations. 2PLSM has greater depth penetration and less photobleaching by exposing less tissue to light absorption in comparison to regular

confocal scanning microscopy (So, 2002). A fluorophore that is activated by one photon at a specific wavelength (λ) can often be excited by two photons at twice the wavelength (2λ) increasing the viability of samples and allowing the imaging of living tissue. In the following experiment, transgenic mice that contain a sparse-medium endogenous expression of yellow fluorescent protein in subsets of pyramidal cells, allowed the desired sample size of 1000 dendritic spines/mouse to be tracked across time.

The purpose of this thesis is to study both synaptic and systems consolidation in relation to learning and memory. Methods include unilateral hippocampal lesions to study possible downstream systems level disruption of the transfer of information from the hippocampus to the RSC over time. The outflow of information from the hippocampus into the ipsilateral RSC is destroyed in only one hemisphere, allowing a within animals comparison between RSC hemispheres of the effects of hippocampal injury on experience-dependent plasticity. Longitudinal in vivo two photon imaging was used to capture changes in density, turnover of dendritic spines and axon boutons, and changes in axon lengths across home-cage and subsequent enrichment housing conditions. The working hypothesis is that experience-dependent dendritic spine and axon modifications that occur in the RSC may be largely dependent on a functional hippocampus. Consolidation theory predicts that after damaging one hippocampus, experience-dependent plasticity will no longer occur in the ipsilateral RSC, in response to an enriched environment.

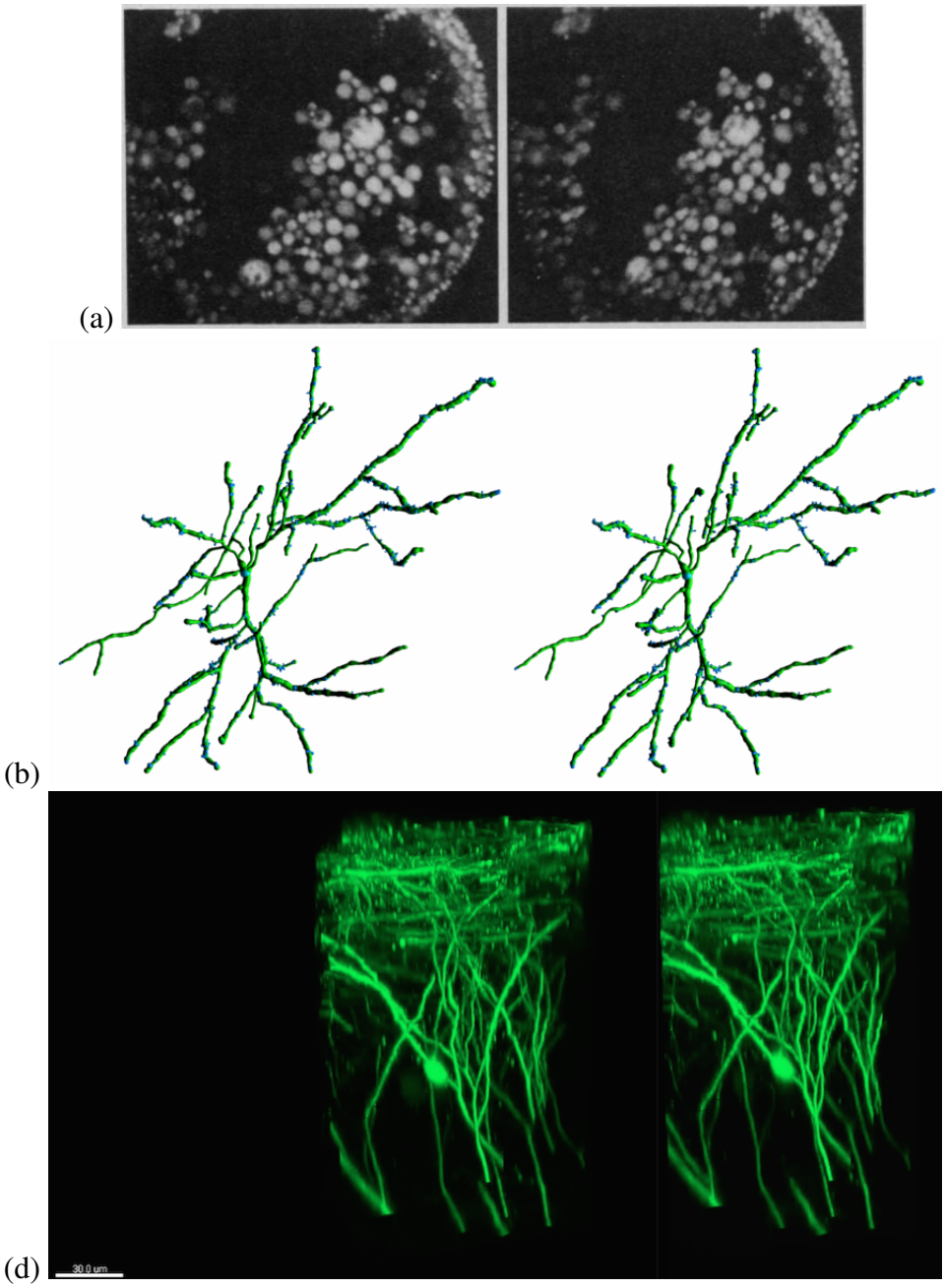

Figure 1.2: Stereo-pairs generated using two photo microscopy were once used to support successful excitation and depth of imaging (a) The first ever stereo-pair generated using two photon images of 9 μm latex test beads (Denk et al., 1991). (b) A stereo pair of a spiny neuron (c) A stereo pair of z-axis orientated raw data, showcasing a layer 2 pyramidal cell body in the RSC, scale bar = 30 μm. Current software technology allows the visible rotation of two photon images for better representation; however, stereo-pairs can still assist in representing depth on paper.

Methods

2.1 Experimental design

Adult female and male mice between three and five months of age underwent unilateral hippocampal lesions and were implanted with a cranial window. A cranial window exposes the surface of the brain by removing a designated area of skull that is then covered with a coverglass. After a minimum of two weeks for recovery, two photon imaging was conducted once every 5 $\pm$1 day for a total of 8 imaging sessions. Animals were housed in a home cage until after the 4th imaging session, whereupon they were transferred to a complex/enriched environment for the remainder of the experiment (last another four imaging sessions). The experiment was a within-subject longitudinal design with two repeated factors (lesion versus control/sham hemisphere and baseline home-cage, followed by enrichment housing). All six mice were measured in all conditions. In unilateral hippocampal lesion mice, hippocampal based consolidation is occurring in only one hemisphere of the cortex rather than equally between the two, creating an important divide for within animal comparisons.

A minimum of six bilateral (three from each hemisphere) image stacks were acquired. The two photon microscope was pre-set to take an image every 0.5 microns, starting from the brain's surface to variable final z-axis depths. All images were subsequently located each imaging session and aligned in order to image the same locations. Across animals, a total of 41 imaging locations were acquired eight times, for a final total of 328 image stacks that were analysed for experience-dependent plasticity measures. In addition, average pixel intensity per image plane was measured for all 41 locations using a randomly selected session.

Our experience-dependent plasticity measures consist of density of structures (how many per unit length of dendrite or axon), and turnover (how many changes via formation/gain or elimination/loss) of both dendritic spines and axon boutons. Changes in the lengths of axons were also measured. Dendrites and axons were analysed separately but each by the same analyst across all images. Analysists were blind to which hemisphere was lesioned, and imaging session order; a double blind design. Statistical analysis consisted of repeated measures analysis of variance (RMANOVA) followed by appropriate post-hoc Bonferonni-adjusted pairwise comparisons.

2.2 Animals

Male transgenic mice B6.Cg-Tg(Thy1-YFP)HJrs/J were ordered from Jackson Laboratories (stock number:003782) then bred in-house by crossing with C57 wild-type animals. Three of the experimental mice came from the same breeder pair in which the sire was Thy1-YFP+ and the mother was the C57 wild-type. Conversely, the other three were siblings from a breeder pair in which the female was Thy1-YFP+ and the sire was the C57 wild-type. There is not present evidence that the sex of the transgenic positive parent in heterozygous breeding makes a difference in the levels of expression in their offspring.

Positive expression of yellow fluorescent protein (YFP) could be detected by shining a Nightsea blue star flashlight with a blue excitation spectrum (440-460nm) on the animal's ear notches while wearing filter glasses. YFP is non-selectively expressed endogenously under regulatory sequences of the Thy1 gene, also referred to as CD90, a cell surface glycoprotein that is present on heterogenous neurons. In these transgenic mice, neurons produce a 'golgi-like' expression pattern in which the entirety of the cell is labelled from the tip of the axon terminal to the tips of thousands of spines. Expression is considered a medium-level; with a greater number of cells containing the fluorophore than the sparse green fluorescent protein (GFP) mouse-line. For additional discussion on the nature of neuronal subsets showing expression, please review the inventor's paper, (Feng et al., 2000).

[a]

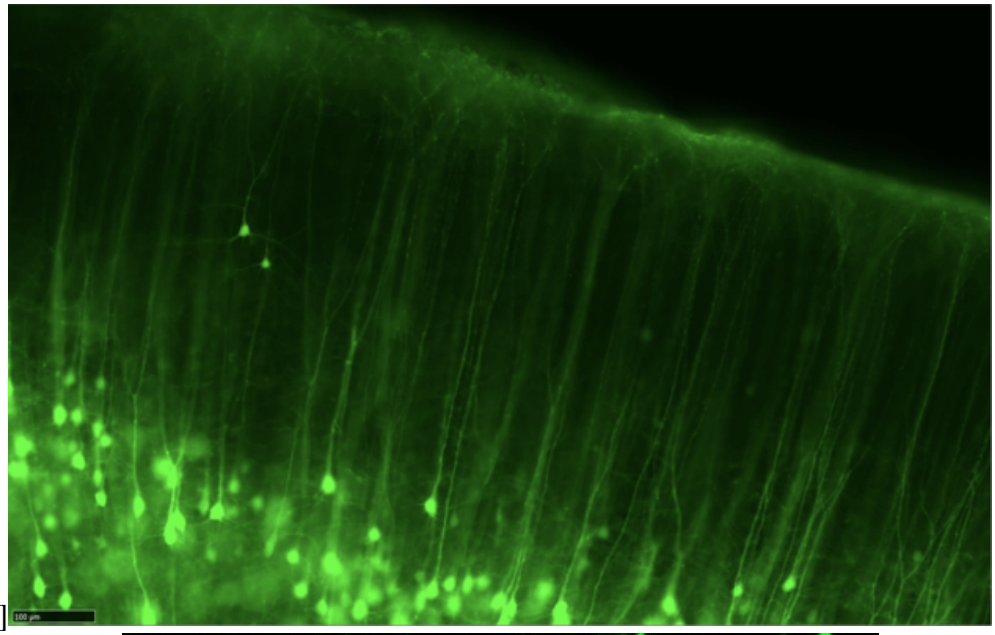

[b]

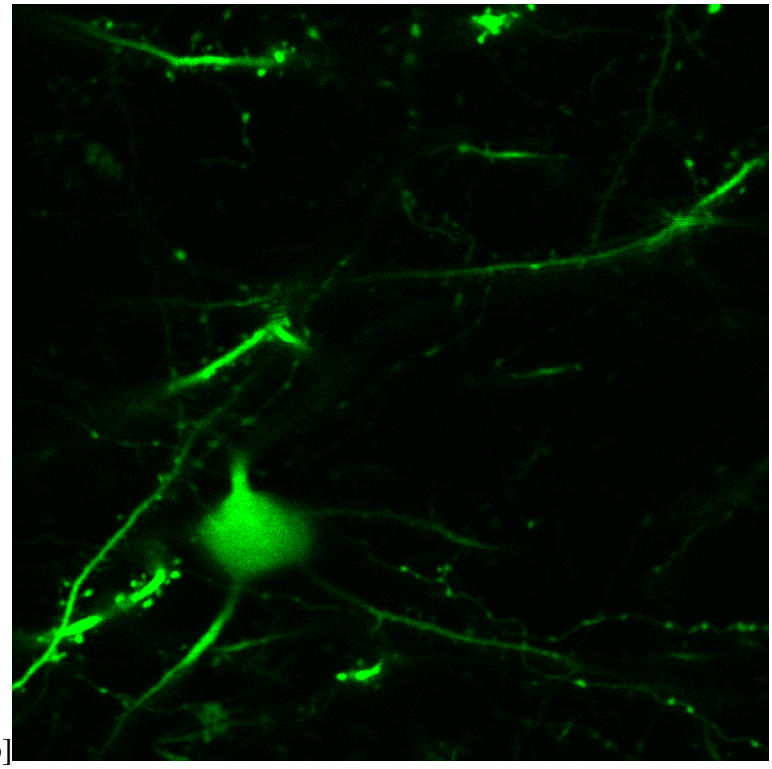

Figure 2.1: [a] Showcasing YFP in subsets of pyramidal cells throughout the neocortex of Thy1-YFP-H line mice. The most dense expression is in excitatory pyramidal cells of layer five (L5) with additional very sparse labeling in layers two and three (L2/3). The majority of the structural data acquired stems from L5, however, the dendrites of L2/3 pyramidal cells are currently undistinguishable and therefore remain possible components of the data. [b] An example of capturing the presence of a L2/3 cell-body within an image. [a] Scale bar =100 μm [b] field of view of each image in the x-y dimension =96x96 μm.

2.3 Surgery

2.3.1 Preparation

The following surgeries were performed using aseptic technique. Animals were double-checked for transgenic expression then received a one hour pre-operative subcutaneous injection of phenobarbital at 30 mg/kg. Mice were initially anesthetized within a mouse induction chamber using 3% isoflurane gas with oxygen set at 3 L/min. Following induction mice were moved to a heating blanket on the surgical table where isoflurane gas was decreased to 1-2% and oxygen flow to 0.5-1.5 L/min. Mice were carefully placed between the blunt ends of ear bars within the surgical plate. All mice were monitored throughout surgery to ensure a surgical plane of anesthesia. Other vitals such as breath rate and temperature were monitored throughout.

Meloxicam was administered subcutaneously at 7 mg/kg followed by an intramuscular injection of dexamethasone at 7mg/kg to reduce inflammation. The local anesthetic Lidocaine was injected under the skin of the scalp at a dose 3mg/kg for further pain management. The scalp hair was removed, and the eyes were protected using a thick layer of eye gel, before the surface skin was disinfected by swabbing alternately with chlorhexidine soap and 70% isopropyl alcohol three times. The surgeons then scrubbed in, and finally the body of the animal was covered with press and seal saran wrap to increase sterility of the surgical field.

2.3.2 Headplate mounting

The scalp skin and periosteum were removed, and cleaned from any hair using 0.9% sterile saline solution. Bregma and the rectangular cranial window were outlined using permanent marker. A plastic custom headplate (3D printed at the University of Irvine) was positioned as straight and centrally as possible on clean dry bone. Once in place, the headplate was securely attached to the skull using a combination of Metabond, Vetbond, bone cement and super glue. Proper headplate attachment was crucial in order for the

[a] 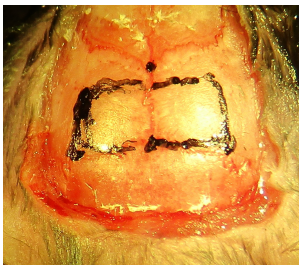 [b] 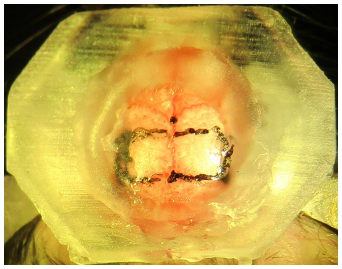 [c] 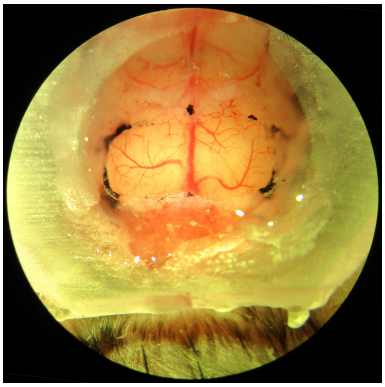

Figure 2.2: Showcasing mouse cranial window surgery a) bregma and the cranial window are outlined b) a mounted headplate c) completed craniotomy with no bleeding or inflammation

mouse to be held securely during chronic imaging.

2.3.3 Craniotomy

A high-speed dental burr was used to drill slowly along the outline of the desired window until there was complete separation of the bone into a rectangular 'skull island'. Fine tip forceps were used to lift the skull island quickly from the surface of the brain while causing as little bleeding or damage as possible. Maintaining the intact superior sagittal sinus and confluence of sinuses was vital as damage can lead to excess bleeding and a poor quality window. Each craniotomy was bilateral, measuring around 6.4 mm wide, allowing access to all necessary imaging and lesion coordinates. Once the skull bone was removed, the surface of the brain was cleaned and a minimum of 10 minutes was allowed in order for the surface to settle under constant moisture.

2.3.4 Unilateral hippocampal lesions

N-Methyl-D-aspartic acid (NMDA) was aliquoted into microcentrifuge tubes containing $0.5\mu L$ at a concentration of 100mM (1.7mL phosphate buffered saline into 25mg NMDA powder) in preparation for surgery. NMDA results in excitotoxic destruction of local tissue. A total of 6 sites and 7-8 injections were used to destroy the hippocampus of one hemisphere in each animal. A stereotaxic frame was used to determine site coordinates be-

fore a nano-injector equipped with a glass pipette was used to inject 50 nL (0.05μL) of 100 mM NMDA into each site. After each injection, the nano-injector was moved to the opposite sham hemisphere, then lowered into the surface of the brain at the same coordinates. NMDA was not injected in the sham and there were no signs of leakage.

The lesion hemispheres were selected at random for each animal with an attempt for a final counterbalance of lesion hemispheres. In total, experimental animals consisted of 4 mice with right hemisphere lesions and left hemisphere shams, and 2 with left hemisphere lesions and right hemisphere shams. See the table below for site coordinates, sites highlighted in grey were interchangeable depending on the blood vessel pattern of each animal. If a blood vessel was obstructing the site, another site was used. Any bleeding was controlled and cleaned before the craniotomy was covered with a single round 7mm coverglass to complete the cranial window. All liquid was removed from the skull's surface, and the coverglass was glued down to the skull using Vetbond, superglue, and bone cement. The bregma markings were visible under the coverslip.

Table 2.1: Sites highlighted in grey were interchangeable depending on blood vessel patterns to avoid damage

Site #	Anterior Posterior	Medial Lateral	Dorsal ventral
1	-1.1	±0.7	-2.0
2	-1.7	±1.5	-2.0
3	-1.7	±2.5	-2.5
4	-2.3	±2.0	-2.5 -3
5	-2.7	±2.7	-3.0
6	-2.9	±2.7	-3.0 -3.5
7	-2.9	±2.0	-2.5
8	-3.3	±3.0	-2.8 -3.3

2.3.5 Postoperative care

The mouse was removed from isoflurane slowly and provided an initial intraperitoneal 5mg/kg injection of diazepam to control seizure activity, and a subcutaneous injection of enrofloxacin at 10 mg/kg in case of infection. The animal was then removed from the surgical suite to an appropriate housing cage on top of a heating pad. The mouse received a subcutaneous injection of saline solution to replace lost fluids, and kept warm. A second dose of diazepam was administered upon awakening. Once the animal was ambulating, each was provided with protein rich food mash and water. Post-operative care continued for three days. The mouse's weight, activity levels, food and water consumption were assessed twice daily during this time. In addition, meloxicam and enrofloxacin were administered once daily for three days in order to control pain, inflammation, and prevent infection. After three days the mice were housed individually in laboratory housing and recovered for a minimum of two weeks before testing.

2.4 Histology

2.4.1 Tissue preparation

Post-euthanasia, animal brains were drop-fixed in 4% paraformaldehyde (PFA) for a minimum of two days and then transferred to 30% sucrose containing azide in order to preserve tissue until slicing. Brains were sliced at $40\mu m$ with either a coronal or sagittal alignment. Block-face imaging was performed after each slice was taken, which provided an image stack from which preliminary lesion extent could be rapidly estimated. Tissue was mounted in serial order and all sections were imaged using a Nanozoomer at 20x magnification and 1x green exposure without any required staining.

2.4.2 Lesion quantification

The lesions were quantified by outlining healthy tissue using Fiji tracing software. The proportion of hippocampal tissue remaining in the lesion hemisphere was calculated by dividing the amount traced by the amount traced in the sham hemisphere (see figure 3.3 and 3.4).

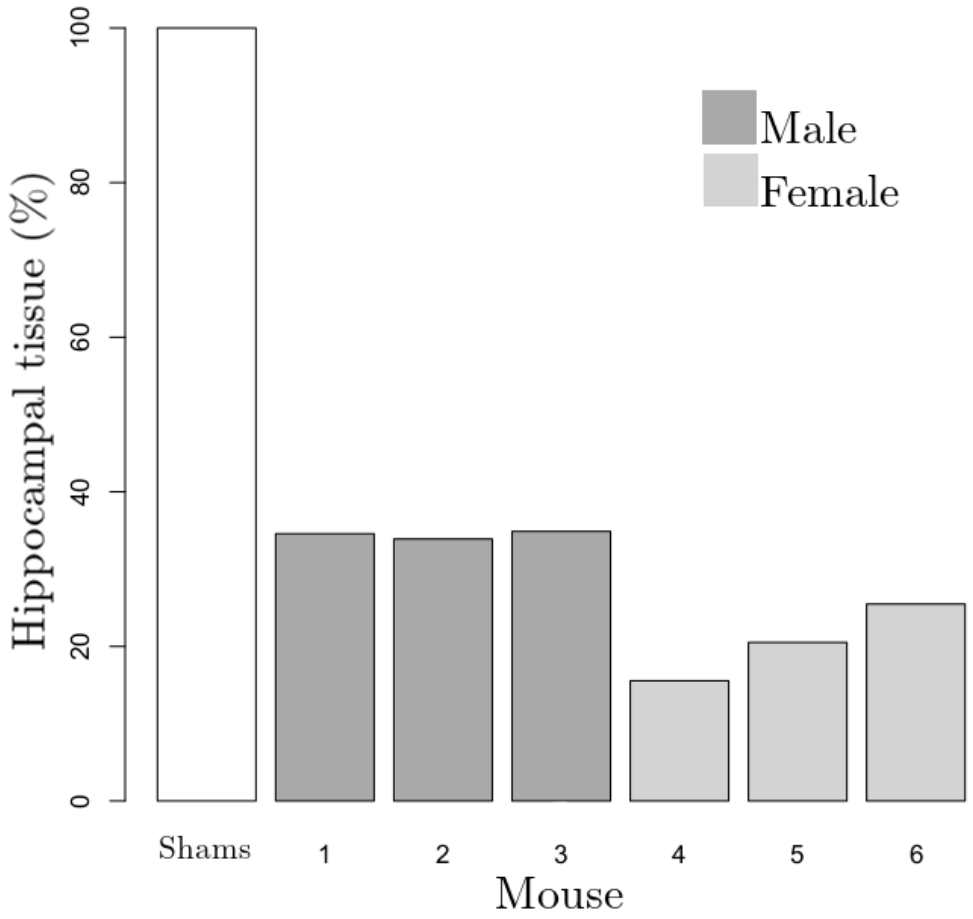

Figure 2.3: Comparing sham hemispheres with full intact hippocampus with their corresponding unilateral lesion percentage of healthy tissue. Males suffered slightly less complete lesions but the overall outcome was successful for a final mean percent damage of 75.37% across animals.

2.5 Housing treatments

2.5.1 Home cage housing

Mice were socially housed in laboratory home-cages for breeding, weaning and pre-surgery. Post-surgery mice were housed individually due to increased aggressive behaviour observed in male mice with unilateral hippocampal lesions, and the sensitive nature of the cranial windows. The home-cage environment consists of direct exhaust ventilation racks that support a non-variable which minimize sound, odour and other outside disturbances. While in home-cage housing all mice were provided with food, water, and one type of nesting material ad libitum. The first four imaging sessions were performed while the animal was housed in this home-cage environment.

2.5.2 Complex housing

The last four imaging sessions were performed while the animal was housed in the following complex housing. The laboratory complex housing environment allows mice to perform more natural behaviours, such as jumping, balancing, exploring, and foraging. Mice were able to remember foraging locations, learned to climb narrow edges, scale lego, jump higher than normal, and knock over objects to look inside. In addition, mice learned that some objects would roll or fall while others were stable. Mice were motivated by chocolate treats, and while in complex housing learned to reach more efficiently challenging locations where a reward could be found.

Complex housing consisted of the mouse's original home-cage being moved to a separate room and being placed without a lid inside a larger aquarium. Objects and the aquarium itself were randomly adjusted for sequential exposure to novelty. Mice were provided with additional types of nesting material including regular bedding, shredded paper towel, crimped paper, and nesting squares. Food consisted of standard mouse feed, the addition of dried pasta, cereal, peanut butter, and a variety of chocolate and yogurt treats. Toys, tunnels and other objects were made of various materials such as paper, plastic, wood, and metal.

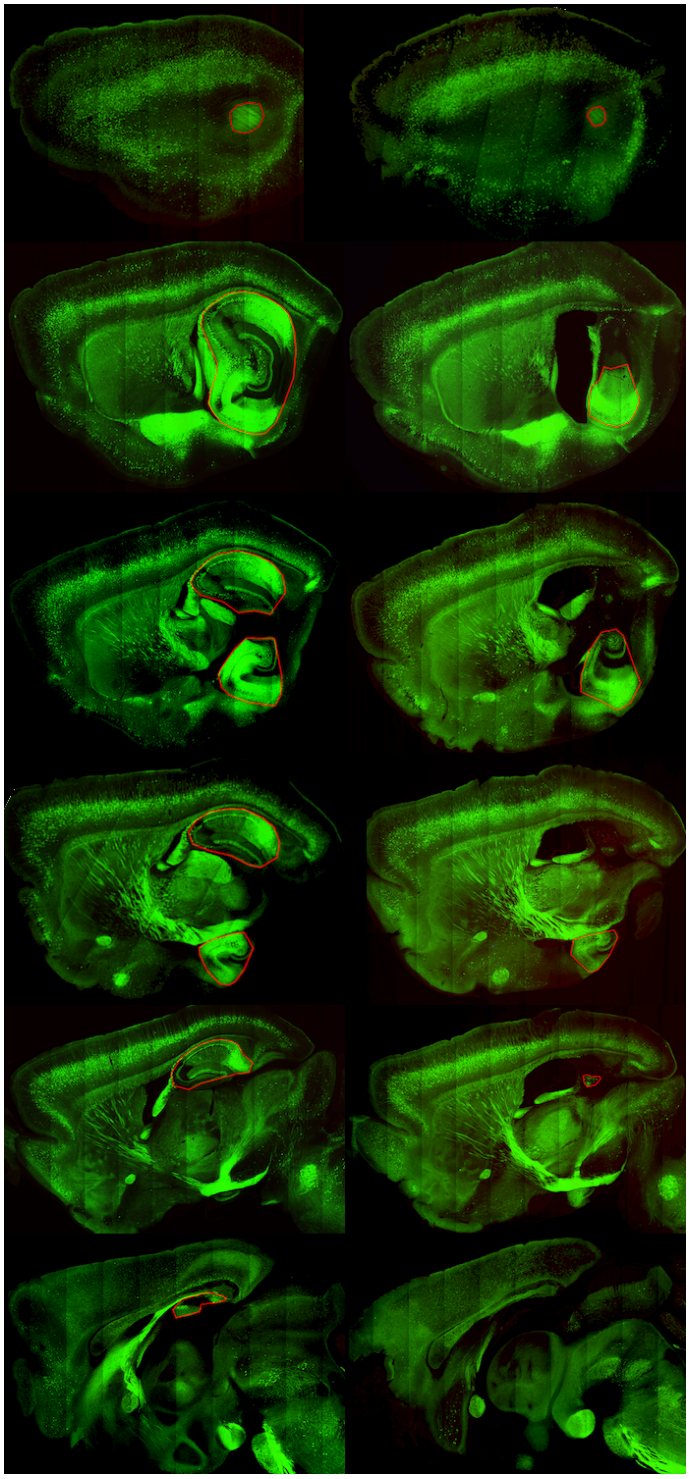

Figure 2.4: An example of sagittal sections with the hippocampus trace-outlined to determine the success of the lesion. Every 10th section was used. The majority of hippocampal sparing was located in the lateral-posterior-ventral regions. In addition, cortical thickness was measured and compared between hemispheres. No apparent differences were identified between hemispheres, though enlargement into the cranial window space was occasionally observed.

Mice were further exposed to music, running water, as well as researchers running other mice on behavioural experiments in the room.

One of the caveats of using only complex housing within a behavioural assay is the variability in behaviour between animals. For example, different levels of exploration and nest building differs amongst mice. Male mice would build larger nests utilizing the majority of provided materials while female mice would build very small nests for themselves in comparison. In addition, animals housed individually may differ in stress responses. For example, females may respond differently to the negative stress of social isolation due to their more social and less territorial nature.

2.5.3 Environmental enrichment

In the following study, environmental enrichment (EE) is defined as the combined experiences of the mice while in complex housing, and other behavioural activities including 'mouse bowling' and foraging through a large open field measuring 61 3/4 inches in diameter. The behavioural activities were introduced in order to expose mice to greater novelty and more consistent exercise levels between each animal. Environmental enrichment functions to stimulate the acquisition of new memories via the exposure to novelty and performance of new behaviours.

Figure 2.5: Laboratory complex housing environment consisting of an original home-cage placed in the centre of a round larger aquarium measuring 28 3/4 inches in diameter. Materials were scattered and the aquarium was cleaned weekly.

[a] 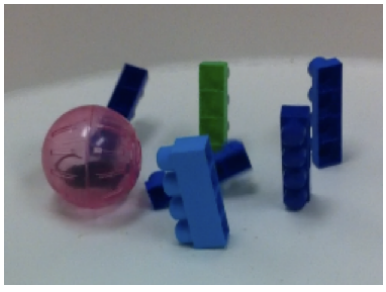 [b] 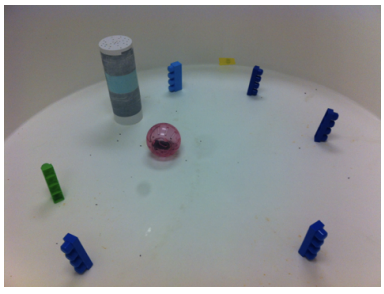

Figure 2.6: Mouse 'bowling': lego set up while mice run in a ball. Natural curiosity led mice to run towards the lego pieces, inevitably knocking them over. Mice were easily able to perform this task with little training, especially male mice. One mouse appeared stressed in the ball and would not run, therefore, was made to run freely in the open field alongside the lego pieces. The behaviour further exposed animals to greater interaction levels with the researcher.

2.6 Image acquisition

2.6.1 Preparation

Mice were initially anesthetized in a mouse chamber using 3% isoflurane gas with oxygen set a 3L/min then moved to a heating pad on the imaging table where isoflurane gas was decreased to 1-1.5% and oxygen flow to 0.5-1.5L/min to maintain a light plane of anesthesia throughout imaging. The mice were attached, levelled, and secured using custom fork-arms that fit into the surgically mounted headplate. Alignment of the mice was carefully performed by eye to increase consistency during future imaging sessions, and aided in efficiency and accuracy, as well as consistency of imaging locations. Eye gel was applied liberally for protection from becoming dry from exposure to light intensity.

2.6.2 Widefield imaging

Wide-field imaging was the first step to locate, focus and image bregma and the surface of the brain. A camera image was taken of bregma at each imaging session and used in future imaging sessions to align the mouse with the same location. The cranial window was cleaned using cotton swabs with sterile saline and ethanol. The microscope stage was then moved to the minimum required x position of 1.7mm posterior from bregma, for RSC imaging. The brain's surface anatomy was brought into focus to locate the correct depth for the two photon objective. The two photon objective was then put in place and water added to the coverglass to connect the two. The mouse is then considered prepared to switch into two photon imaging.

2.6.3 2PLSM

An Olympus two photon laser scanning microscope equipped with a spectra-physics maitai deepsea pulsed IR laser was used at an excitation wavelength of 910nm for image acquisition. A 60x water immersion objective with a numerical aperture of 1.1 was used for a final resolution of 8.3 pixels/μm in the x-y dimensions, and 2 pixels μm in the z-dimension.

The working distance of the objective was 1.5 mm which allowed for successful imaging of superficial cortical layers 1 and 2. The surface of the brain was accurately located by scrolling the objective to determine where expression initially became visible.

All images were acquired at four pixels per second on a 800x800 pixel frame-by-frame basis. Images acquired without any zoom were taken only on day 1 of imaging to aide in finding the same location session after session. Images used for data were acquired using a zoom of 2.2, a final field of view of 96μm in the x-y dimensions and a step size of 0.5μm. The final depth of each image was determined by the visibility of horizontal dendrites that would suffice for analysis (most horizontal dendrites were in superficial cortex and thus images were around 100μm in depth).

In order to prevent inconsistencies in fluorescence throughout the z-axis plane depths, imaging parameters were continually monitored and occasionally adjusted slightly to achieve consistent fluerescence. The overall power of the two-photon was kept as low as possible (ideally ≤ 3 % but ranged from 2.0% - 20.0% across sessions and animals). Animals with more dim expression (mainly males) required a consistent higher power throughout the duration of imaging sessions. The high voltage (HV) settings ranged from 580-620.

2.6.4 Imaging sessions

During the initial imaging session a minimum of six different images were taken, three from each hemisphere. All chosen imaging locations were based on chosen x-y dimension coordinates ($n \geq$1.7mm posterior and $n \leq$1.2mm lateral but as close to midline as possible, in order to remain within the RSC). The most lateral image stack was collected at 1.159 mm lateral to bregma. When the quality of the image was negatively affected by movement of blood within the sagittal sinus, imaging locations were moved more laterally. Regardless of arbitrary boarders, imaging locations may also reside within the posterior parietal or visual cortices. All imaging coordinates were documented during each session in order to assist in finding the same locations repeatedly. Each imaging session took roughly 2 hours

to complete.

2.7 Dendritic spine and axon bouton counting using IMARIS

All eight image stacks across time for each mouse were acquired before counting began. The images were then shuffled in order for the manual counter to be blind to both hemisphere and imaging session order. The first manual counter was responsible for counting all of the dendritic spines, and the second manual counter was responsible for counting all of the axon boutons and quantifying the changes in their lengths.

All imaging sessions for the same location were opened and displayed side-by-side in IMARIS software (see figure 1.8). Dendrites or axons were chosen from one of the images and a template was drawn digitally using the plugin 'Filament tracer' (see figure 1.9). Using Filament Tracer (under the 'autodepth' setting) allowed the program to automate locating the area of interest and filled in a graphic cylinder as the computer mouse cursor traced the area. The cylinder was then 'centred' in the program to fill in the length of the axon or dendritic shaft more accurately. The manual counter then manually zoomed in along the length of the template and added each spine or bouton manually.

When paired with the Ortho-Slicer IMARIS plugin, the volume of the 3D image can then be turned on to view the image in 3D and 2D simultaneously, or turned off in order to remove any distracting parts of the image outside the chosen planes of interest. Ortho-Slicer and Filament Tracer were the two main IMARIS plugins used. The plane of focus can be easily changed by scrolling through the 3D image volume. While counting, few image planes were displayed to better isolate areas of interest.

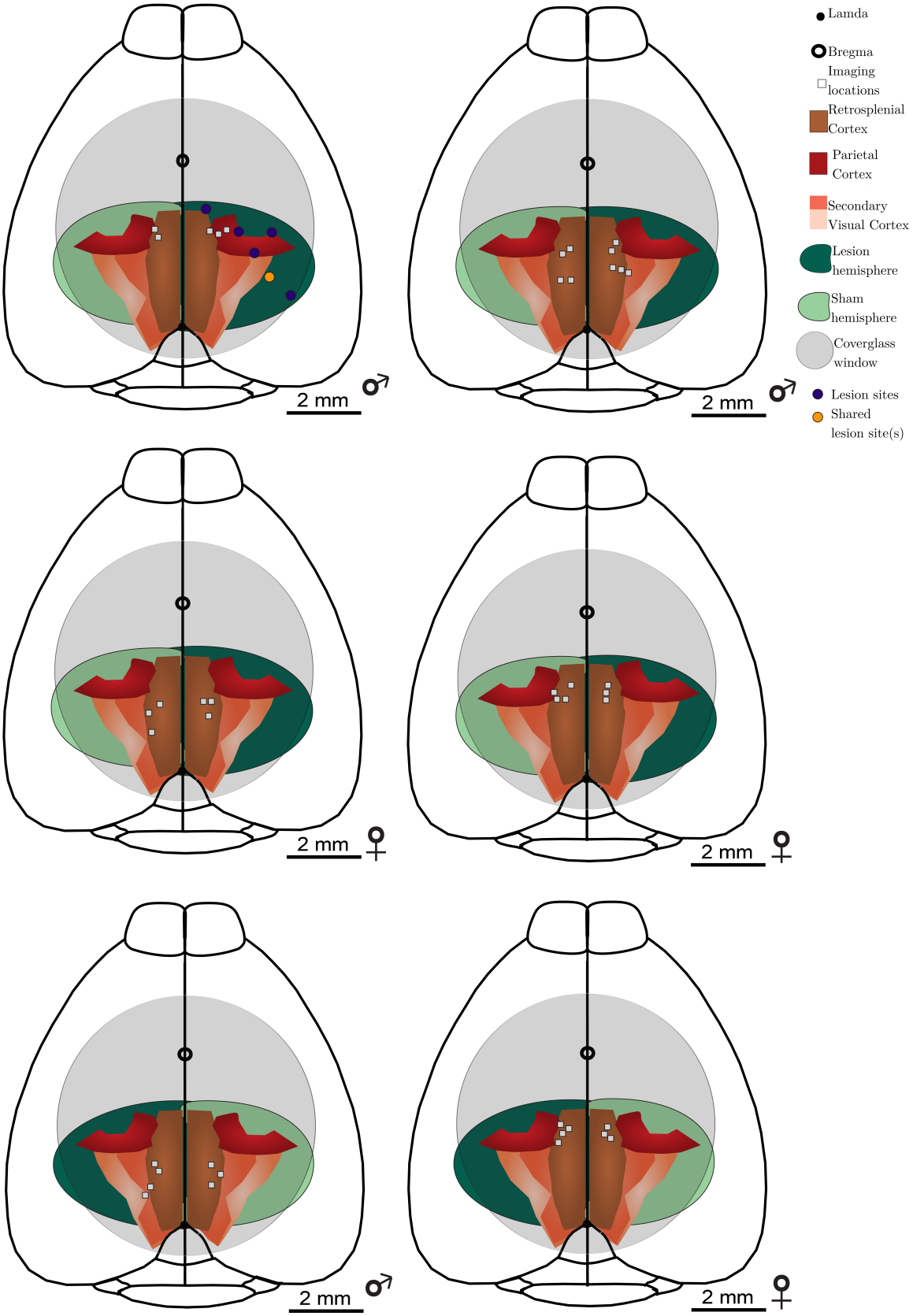

Figure 2.7: Final schematics showing the imaging site locations, treatment hemispheres, and sex for each animal. The top left example shows the lesion/sham site locations that remained the same for each animal.

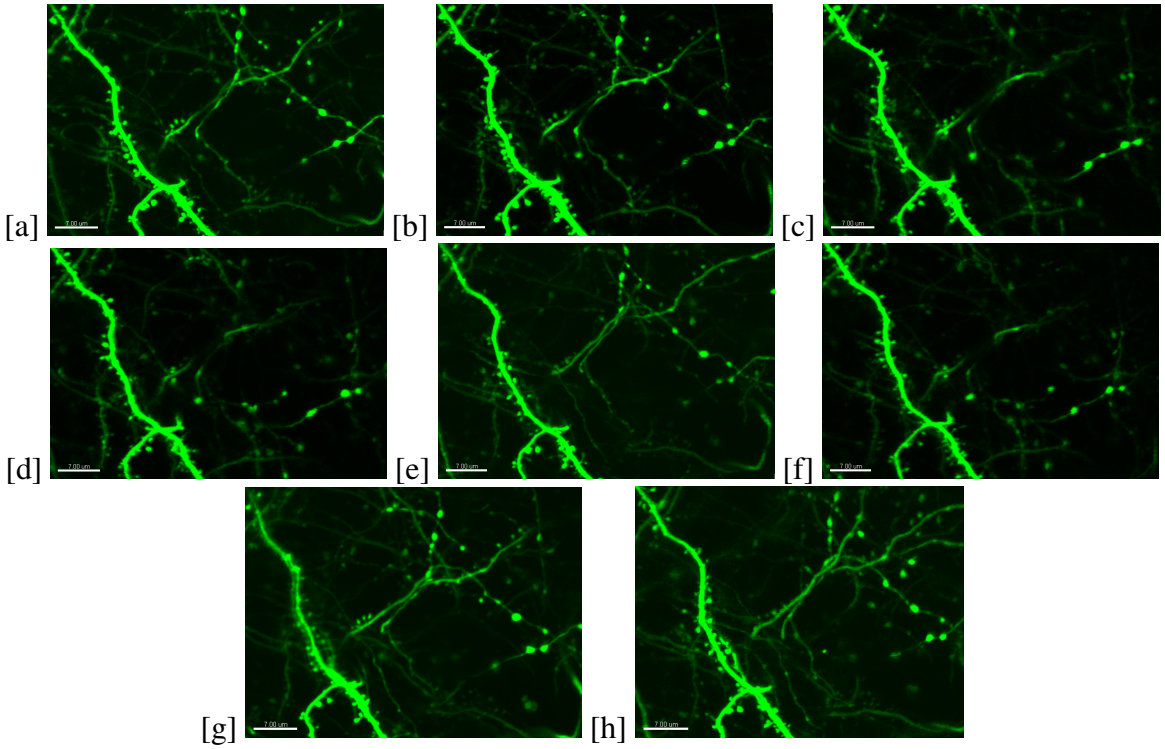

Figure 2.8: An analyzable dendrite isolated from all image stacks with unknown treatments. Images for 8 sessions were collected, and then shuffled and randomly assigned a letter. Image order (housing treatment), and whether or not the image was taken from the lesion or sham hemisphere (lesion treatment) remained unknown; a double blind experimental design.

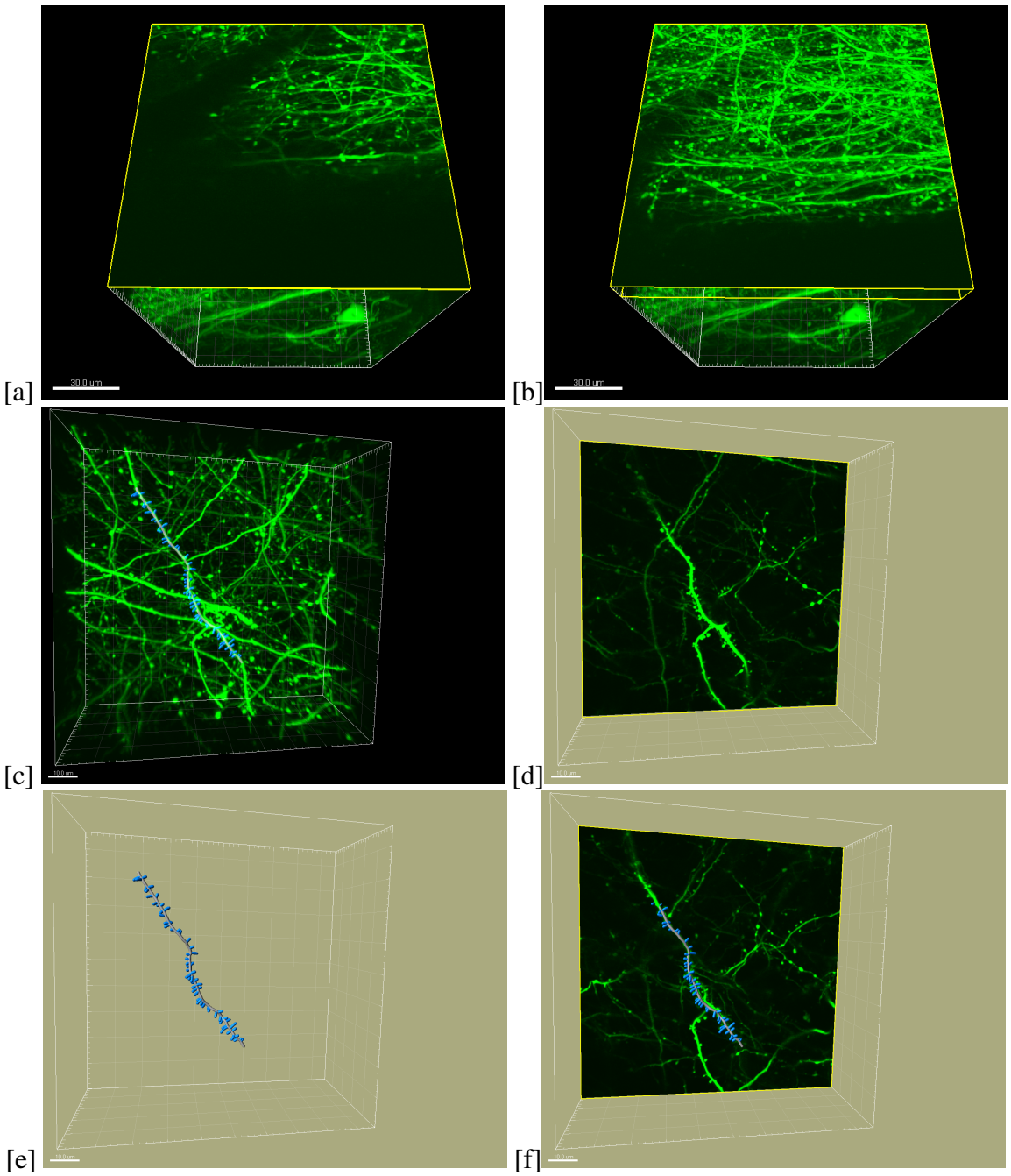

Figure 2.9: [a]The Ortho-Slicer plugin set at one image plane and therefore highlighting 0.5 μm of tissue]b] Ortho-Slicer set at a depth of 3.0 μm and therefore highlighting 6 planes from the entire image stack. [c] The entire image volume and dendrite template [d] No volume and a single plane. [e-f] the traced template dendrite. Both the template and ortho-slicer are easily switched on and off in order for multiple vantage point comparisons. Each image measures 96 μm by 96 μm by variable z-depths. Scale bars [a-b] = 30μm and [c-f] = 10μm

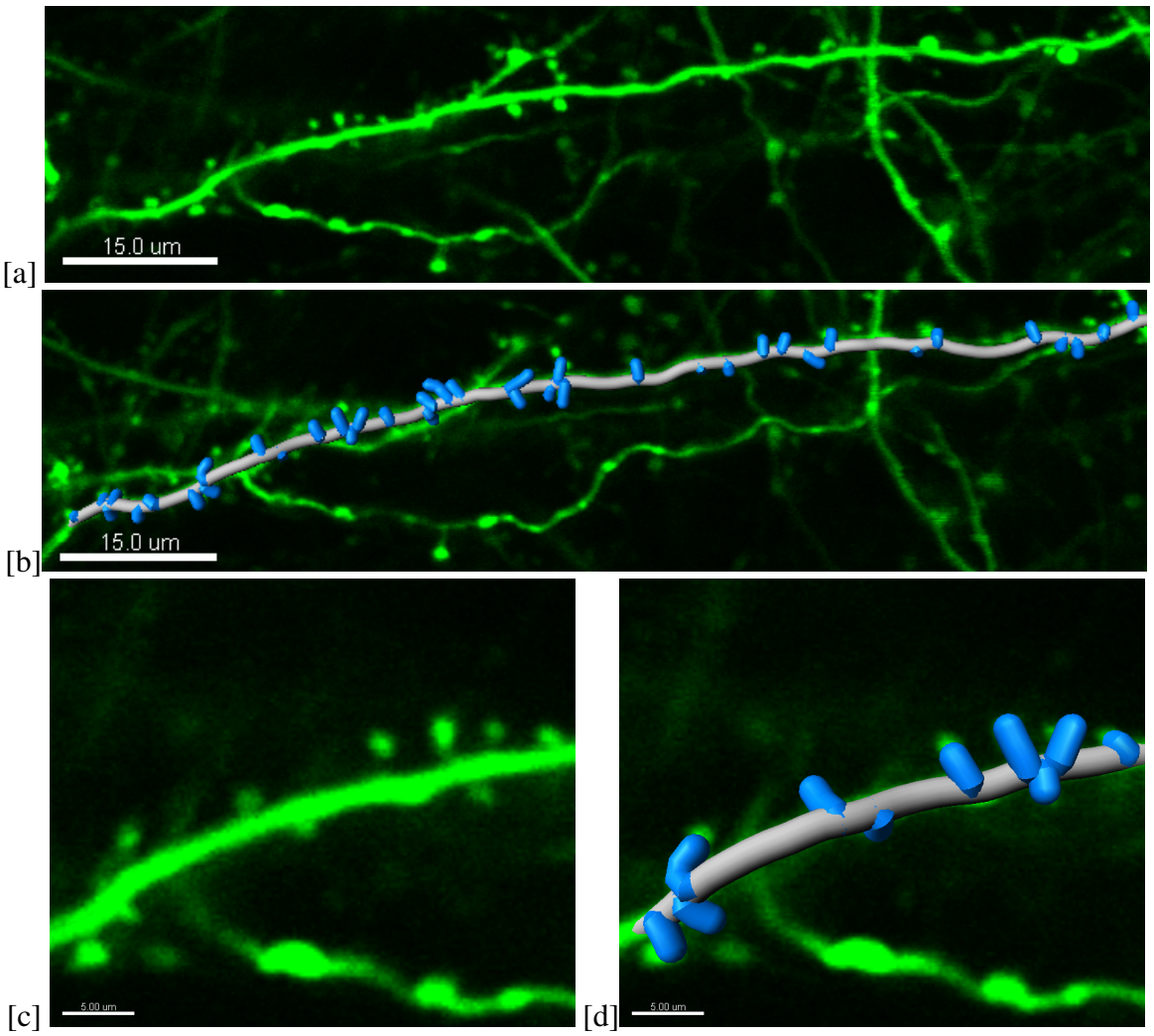

Figure 2.10: Horizontal dendrites have better x-y resolution and were therefore selected for analysis. [a-d] A dendrite template turned off [a] or on [b]. [c-d] IMARIS has the ability to digitally zoom in on selected areas further assisting in accuracy of analysis, scale bar= 5.0 microns.

2.8 Ambiguous data imputation

Data imputation was used to replace our ambiguous or undetermined data with a substituted score based on the previous imaging sessions result. Ambiguous spines and boutons were those not easily labeled as *there* (1) or *not there* (0) by eye. Slight differences in imaging depth, angle, or movement of the structures themselves, are reasons that may have resulted in ambiguity. During analysis, if the counter was unsure of the presence of a spine or bouton, that structure was scored as A for that specific imaging session. Imputation allowed for spines and boutons that were labeled as ambiguous to not be deleted from the data but result in a complete final data set with no missing values. Ambiguity was overall quite random and less than 10% of all data.

2.9 Statistical analysis

The density on each individual day was determined by taking the total number of spines that were observed to be present that day and dividing by the total length of dendrite. There was a total of 16 density scores for each animal, two hemisphere treatments across eight imaging sessions, a $2*8$ repeated measures design. Turnover was calculated by finding the total number of gains, losses and stable spines between subsequent imaging sessions, resulting in a total of 14 turnover scores per animal, a $2*7$ repeated measures design.

$$Density = \frac{There(1)\ Count}{Length(\mu m)\ of\ dendrite\ or\ axon}$$

$$Turnover = \frac{Sum\ of\ Gain/Loss}{Initial\ image:\ There(1)\ Count}$$

2.9.1 Post hoc power analysis

Post hoc power analysis was ran for a within subjects repeated measure analysis of variance with a sample size n=6. Additional parameters included alpha=0.05, power=0.8,

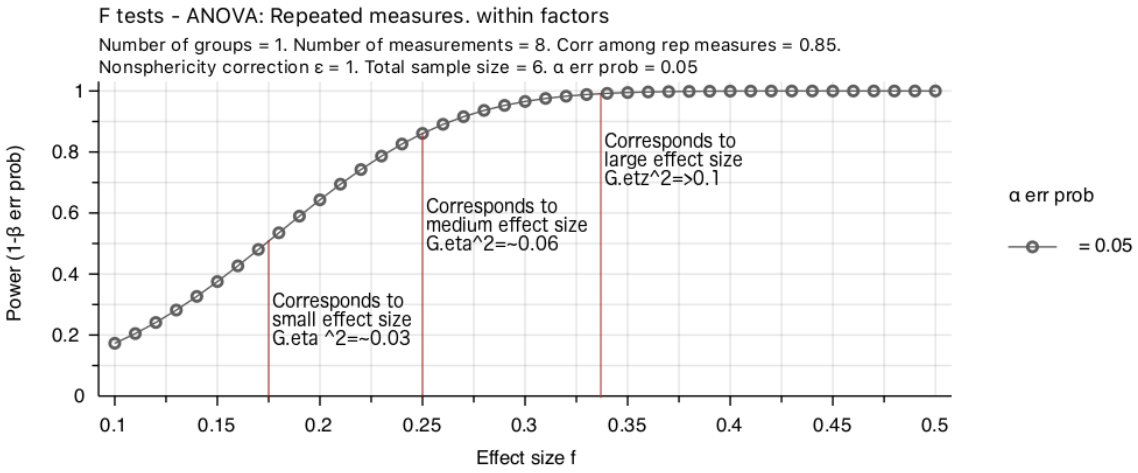

Figure 2.11: A small effect size corresponds with a low power in the following study, $\eta^2_G = 0.03$ corresponds with $\sim$50% power, and a medium $\eta^2_G = 0.06$ corresponds with $\sim$85% power.

and a correlation of 0.85 between the 8 images taken from the same locations. To achieve 80% power, a medium effect size f=0.2387189 was calculated using G*power. Effect size quantifies the size of the difference between factors, offering additional insight into when statistical significance paired with a small effect size would be better justified with a larger sample size. See Bakeman (2005) for a consensus in reporting generalized eta squared when reporting results for a two factor repeated measures ANOVA.

Time-series models rely on a relationship between observations. The main goals of our time series analysis: first, to identify and describe the nature of experience dependent plasticity in the RSC represented sequentially during specific housing conditions; secondly, to identify any differences between the RSC hemispheres ipsilateral versus contralateral to the hippocampal lesions during these housing conditions. Our within-subject ordered observations contain quantitative characteristics in which each animals serves as its own control. Alpha was 0.05 and all calculated p-values below 0.05 were considered significant in rejecting the corresponding null hypothesis.

Repeated measures analysis of variance (RMANOVA) was initially conducted, a 2x8 design for density and 2x7 design for turnover between weeks. The 'ez' package in R was

used to run 'ezanova' to facilitate comparison of within-subjects factors of hemispheres across time. Sphericity corrections were automatically applied and provide the Greenhouse-Geisser and Hugynh-Feldt epsilon values, and corresponding corrected p-values when applicable (Lawrence, 2011). Animals were further categorized and compared using RMANOVA with the between-factor of sex in order to obtain addition p-values supporting sex differences. There are particular limitations with interpreting RMANOVA data alone, therefore, pairwise comparisons with bonferonni corrections were made in order to obtain more specific information about the time that differences occurred.

RMANOVA plots visualize mean averages surrounded by the standard error of the mean, but do not show details related to individual animal variation. More specifically, the trends visualized in the RMANOVA plots are inaccurate on an individual animal basis. RMANOVAs average individual variation in starting points and carry over effects, and do not model possible autocorrelation between imaging sessions or hetereoscedasticity between hemispheres.

2.9.2 Categorizing synaptic structures

The complexity of possible data configurations grows with the number of imaging sessions. With a total of eight imaging sessions and binary scores of 0 or 1 there are a total of $((2)(2)(2)(2)(2)(2)(2)(2)) - 1 = 255$ possibilities for dynamic configurations for each spine/bouton across time. One configuration being removed (0,0,0,0,0,0,0,0), a spine must be detected at least once to be meaningful. In addition, the possibility of a configuration does not mean it necessarily occurred in the data, for example, (0,1,0,1,0,1,0,1) occurred zero times in the spine lesion hemisphere, and would be considered more likely a measurement error as such a high amount of turnover is unlikely in nature. The most common configuration for both spines and boutons was complete stability: (1,1,1,1,1,1,1,1).

Example 2.1. The following matrices represent configurations that represent a spine/bouton that shows one-time-turnover. The line down the middle separates home-cage housing

versus enrichment housing, as the time of occurrence. There are six configurations for both stable-gains and stable-losses, making up a total of 12 of the 255 possible configurations. Stable-gains/losses are non-dynamic; gained/lost at some point and remained that way for the remaining imaging sessions.

$$
\begin{array}{l}
Stable-gain \\
\\
\end{array}
\left(\begin{array}{cccc|cccc}
0 & 0 & 0 & 0 & 0 & 0 & 1 & 1 \\
0 & 0 & 0 & 0 & 0 & 1 & 1 & 1 \\
0 & 0 & 0 & 0 & 1 & 1 & 1 & 1 \\
0 & 0 & 0 & 1 & 1 & 1 & 1 & 1 \\
0 & 0 & 1 & 1 & 1 & 1 & 1 & 1 \\
0 & 1 & 1 & 1 & 1 & 1 & 1 & 1
\end{array}\right)
\quad
\begin{array}{l}
Stable-loss \\
\\
\end{array}
\left(\begin{array}{cccc|cccc}
1 & 1 & 1 & 1 & 1 & 1 & 0 & 0 \\
1 & 1 & 1 & 1 & 1 & 0 & 0 & 0 \\
1 & 1 & 1 & 1 & 0 & 0 & 0 & 0 \\
1 & 1 & 1 & 0 & 0 & 0 & 0 & 0 \\
1 & 1 & 0 & 0 & 0 & 0 & 0 & 0 \\
1 & 0 & 0 & 0 & 0 & 0 & 0 & 0
\end{array}\right)
$$

2.9.3 Pixel intensity quantification

For all image stacks the mean pixel intensity was determined using Fiji software. Intensity values pertaining to each individual z-axis plane were obtained under the heading *Image - Stacks - Plot Z Axis Profile*. All values were averaged across images taken from each hemisphere, for individual mice.

Results: Dendrites and dendritic spines *in vivo*

3.1 Sampled dendrites and dendritic spines in the RSC

Both hemispheres across six mice and eight imaging sessions resulted in a total of 55,704 manual dendritic spine counts. 27,852 make up counts across four imaging sessions while the mice were housed in their laboratory home-cages and the second 27, 852 while housed in enrichment. A total of 6963 spines were sampled along a summed length of one hundred dendrites, measuring 7781μm. 3260 spines were sampled from the sham hemispheres and 3703 from the lesion hemispheres. 3815μm were measured across fifty three dendrites from the sham hemispheres and 3966μm were measured across fifty seven dendrites from the lesion hemispheres.

Dendrites positioned in a horizontal manner were chosen for analysis due to better resolution. Dendrites ranged in thickness and spine density. For example, there were thirty-five examples of thicker dendrites almost completely smooth, without any dendritic spines. Dendrites scattered with spines were chosen for analysis in order to meet counting criteria. It should be noted that taking into account the heterogeneity between spine densities may be a more accurate representation of the overall spine density. In addition, the depths of the dendrites and imaging locations were monitored but not taken into account in the following analysis. Finally, it remains unclear if particular dendrites are apical extensions of pyramidal neurons from layer 5, 2 or 3.

Table 3.1: Sex, lesion hemisphere, total number of sampled spines, total number of sampled dendrites, and the total lengths of all the sampled dendrites combined, measured in (μm) for each mouse.

	Sham			Lesion		
ID/Sex/Lesion	# Dendrites	# Spines	Length	# Dendrites	#Spines	Length
1-♂-Left	9	449	545	12	830	883
2-♀-Right	5	494	449	8	720	695
3-♂-Right	14	715	923	8	495	664
4-♀-Left	6	541	605	9	623	484
5-♀-Right	9	560	558	6	473	504
6-♂-Right	10	501	735	14	562	736
Totals: 6	53	3260	3815	57	3703	3966
3-♀	20	1595	1612	23	1816	1683
3-♂	33	1665	2203	34	1887	2283
2-Left	15	990	1150	21	1453	1367
4-Right	38	2270	2665	36	2250	2599

3.2 Dendritic spine density over time in the RSC

The average density across imaging sessions was 0.6 spines/μm, with a range between 0.36-0.81 spines/μm. The average across all mice for individual imaging sessions was 0.58 spines/μm in the sham hemispheres and 0.62 spines/μm in the lesion hemispheres, calculating to a consistent $\sim$5% greater spine density in the ipsilateral RSC during each session. The total number of spines across all imaging sessions calculates to a 0.85 spines/μm in the sham hemisphere and 0.93 spines/μm in the lesion hemisphere for an overall greater

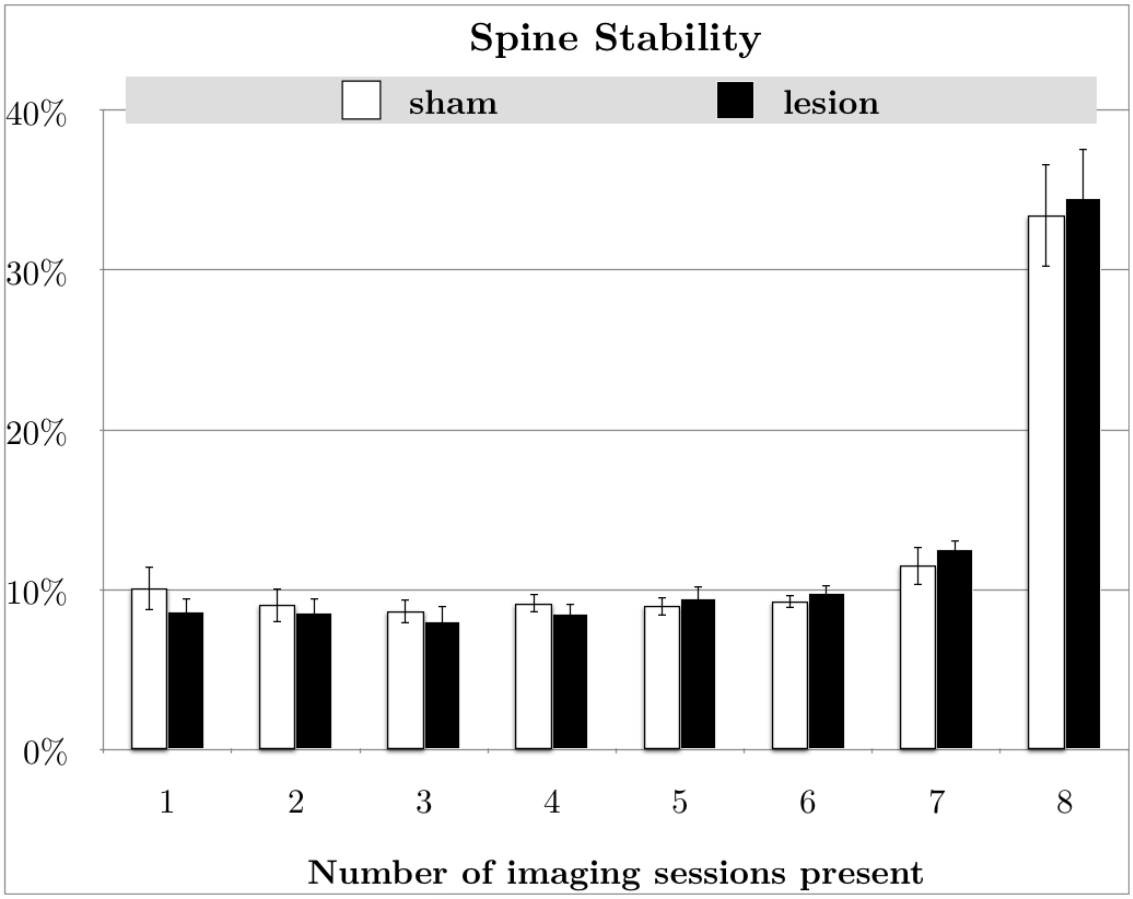

Figure 3.1: The following data represents the number of imaging sessions during which a spine existed, but does not contain information regarding during what specific imaging session(s). The number of days dendritic spines were present for was similar between sham and lesion hemispheres. 32.7% of spines were stable across all eight imaging sessions in the sham hemisphere and 33.9% in the lesion hemisphere. The remaining spines were quite equally distributed in their presence at around 10%. Error bars represent standard error of the mean.

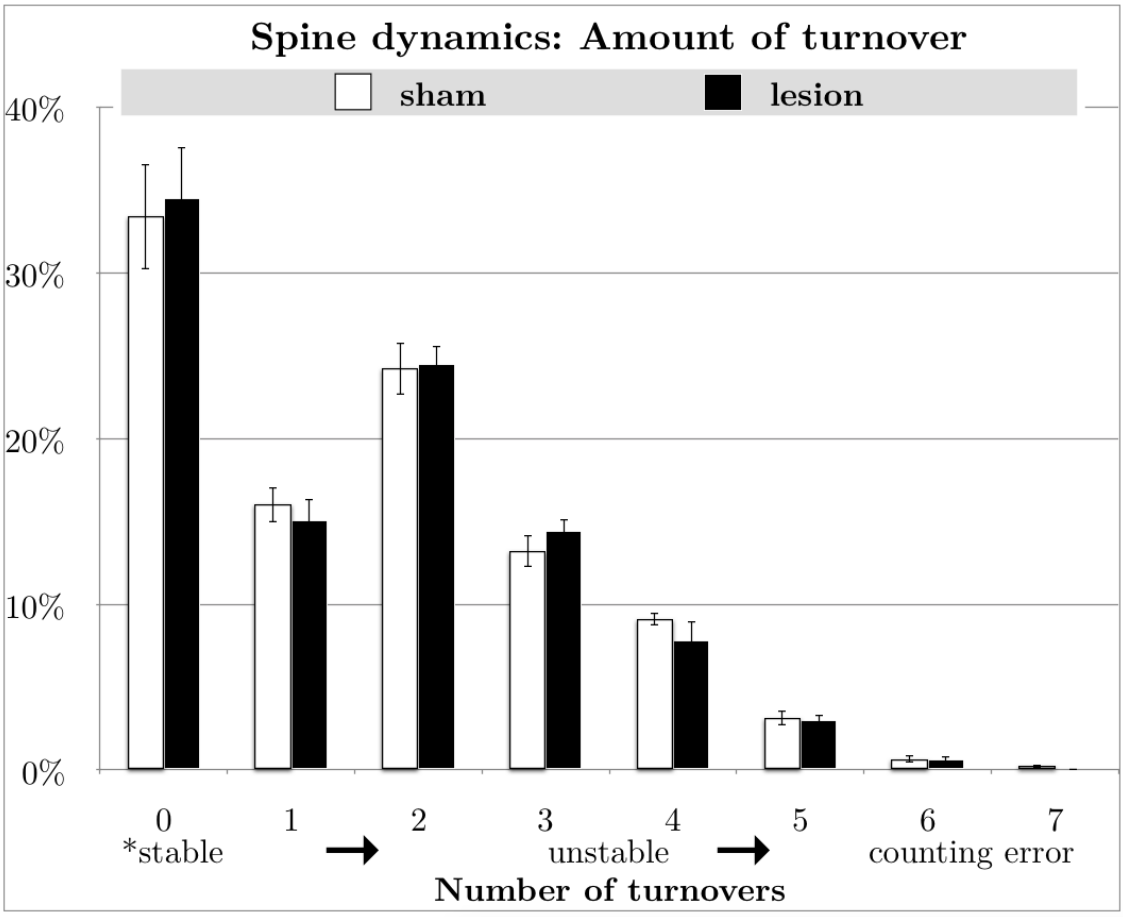

Figure 3.2: Spine turnover represented as the number of counts for how many spines turned over a specific number of times over the eight imaging sessions. The following data are independent of when or what specific imaging sessions the spine showed plasticity. Spines with different levels of turnover were further classified, for example, spines that turned over only one time are commonly classified as stable-gains or stable-losses. Spines that continually turned over each week are considered more likely to be due to experimental error as is biologically highly unlikely. Error bars represent standard error of the mean.

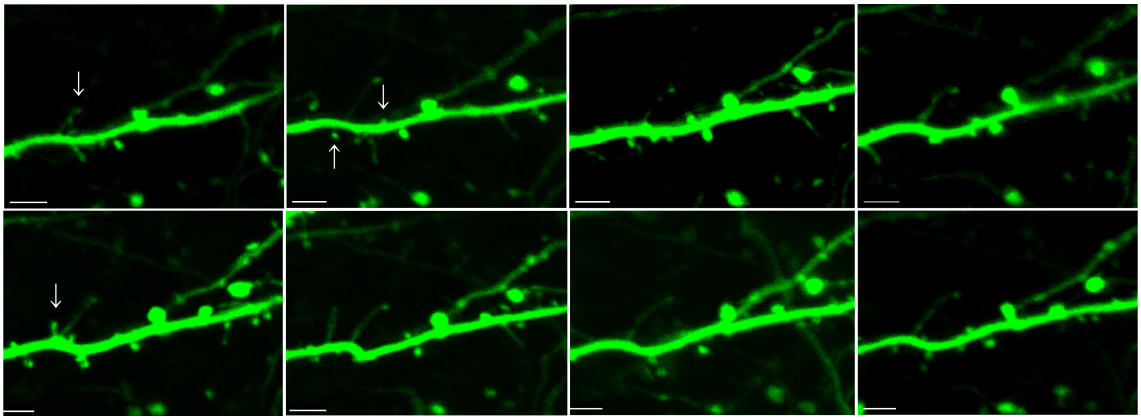

Figure 3.3: The following qualitative example provides evidence for the many shapes of dendritic spines. Stubby and long thin spines both had the capacity to remain stable throughout all imaging sessions. The top four images are while the mouse was housed in laboratory home-cage and the bottom four in enrichment. The white arrow on day 1 represents a filopodia or long spine that remained completely stable throughout all imaging sessions. The white uparrow on day two represents a spine that comes and goes across imaging sessions. The downarrow represents a stable gain during home-cage. There are further structurally plastic changes that are unmarked.

density of $\sim$9% in the lesion hemisphere. A 2*8 repeated measures analysis of variance (RMANOVA) resulted in a significant main effect between the sham and lesion hemispheres, $F(1,5) = 11.3991, p = 0.0198, \eta^2_G = 0.0324$. A main effect of hemisphere rejects the null hypothesis that the RSC has the same spine density between the ipsilateral and contralateral RSC, however; the effect size is small.

In addition, there was a main effect of imaging session. Though often likely in in vivo time-dependent data, sphericity was violated across imaging sessions. Mauchly's test (Mauchly, 1940) for sphericity was significant indicating that there are differences in the variances between imaging sessions. Both Huynh-Feldt (Huynh and Feldt, 1976) and Greenhouse-Geisser (Greenhouse and Geisser, 1959) corrections were calculated and both corrections resulted in a remaining significant main effect of imaging session, $F = 9.7233, p[GG] = 0.0028, p[HF] = 0.0001$. A main effect of imaging session rejects the null hypothesis that the RSC has the same spine densities across imaging sessions. There was no interaction effect, $F(7,35) = 0.7710, p = 0.6153, \eta^2_G = 0.0010$.

Spine stability is defined as how many imaging sessions a spine was present during,

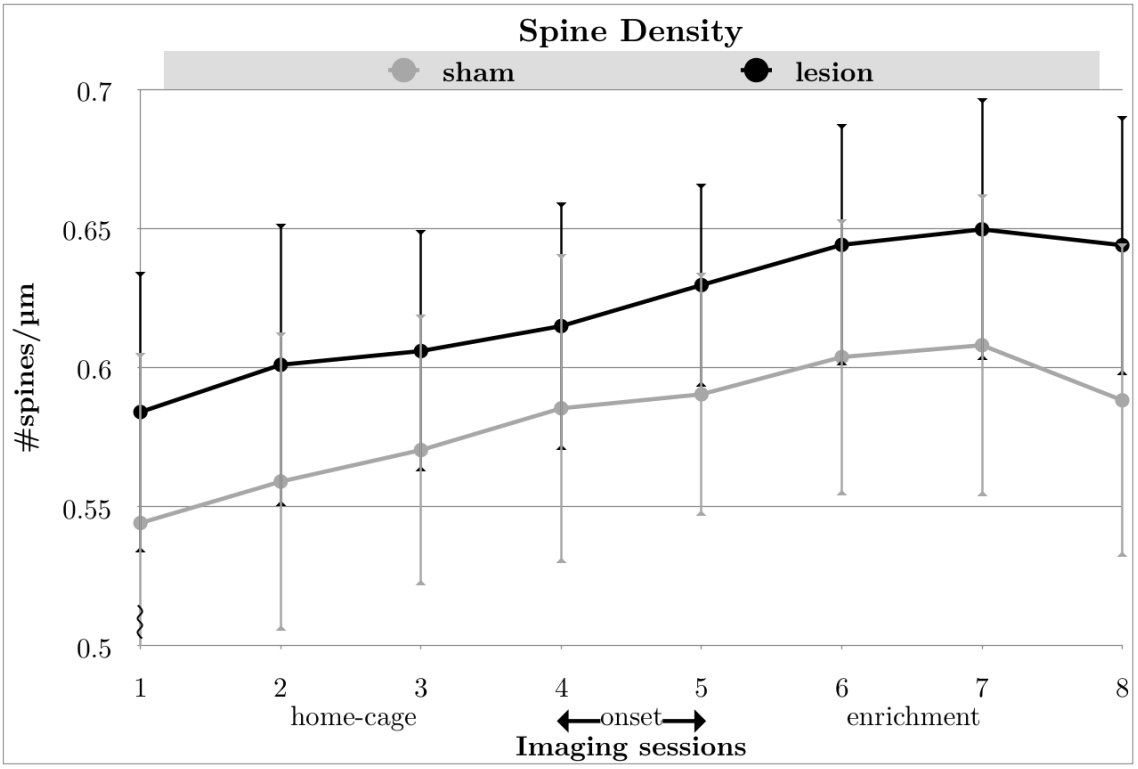

Figure 3.4: Average spine densities across six mice and eight imaging sessions taken every five days. Densities are measured as the number of spines/μm of dendrite. A 2*8 repeated measures analysis of variance (RMANOVA) resulted in two significant main effects of 1) hemisphere and 2) imaging session. 1) Average spine density was greater in the ipsilateral RSC hemisphere, across all eight imaging sessions, $F(1,5) = 11.3991376, p = 0.0197544, \eta^2_G = 0.03242495$. 2) Average spine density shows an increasing linear trend across imaging sessions, and is significant after appropriate assumption corrections, $F = 9.72332, p[GG] = 0.002830,\ p[HF] = 0.00010025$. Error bars represent standard error of the mean. Note: sex differences in the appendix are related to differences in density and an interaction related to housing.

regardless of session order. Completely stable spines existed for a minimum of thirty-five days in total. Spines that only existed for one imaging session have an unknown life-span possibly ranging from 1 day to 5 days. It should be noted that spine stability may correlate with greater density on each individual day.

3.3 Experience-dependent plasticity via turnover of dendritic spines across time

All 6963 spines underwent unique turnover across time (a mixture of gains, losses, and remaining stable). There were a total of 48, 741 turnover counts completed across all eight imaging sessions. 20,889 turnover counts were completed while the mice were housed in their laboratory home-cages and 27,852 were completed while housed in enrichment. Consecutive imaging sessions were compared in order to determine the number of new spines gained or lost each week. A gain is defined as a spine that went from not being present to appearing, a loss is a spine that went from there to disappearing, and a stable count is defined as a spine that remained consistent (either there or not there) between the two consecutive imaging sessions.

Combined gain and loss turnover led to total turnover ranging from $\sim$31%-38% across imaging sessions. Total spine turnover indicated a main effect of imaging sessions. Overall, there are more gains than losses across imaging sessions, further supporting the observed increase in density. There were no significant differences between hemispheres in spine turnover data; however, initial lesion hemisphere turnover was $\sim$4% lower during home-cage housing that increased to sham levels during enrichment. When sex was taken into account there was an interaction effect between gain/loss of spines and imaging sessions, graphs are located in the sex differences appendix.

3.3.1 Dendritic spine turnover in both hemispheres increases transiently following transition to enrichment

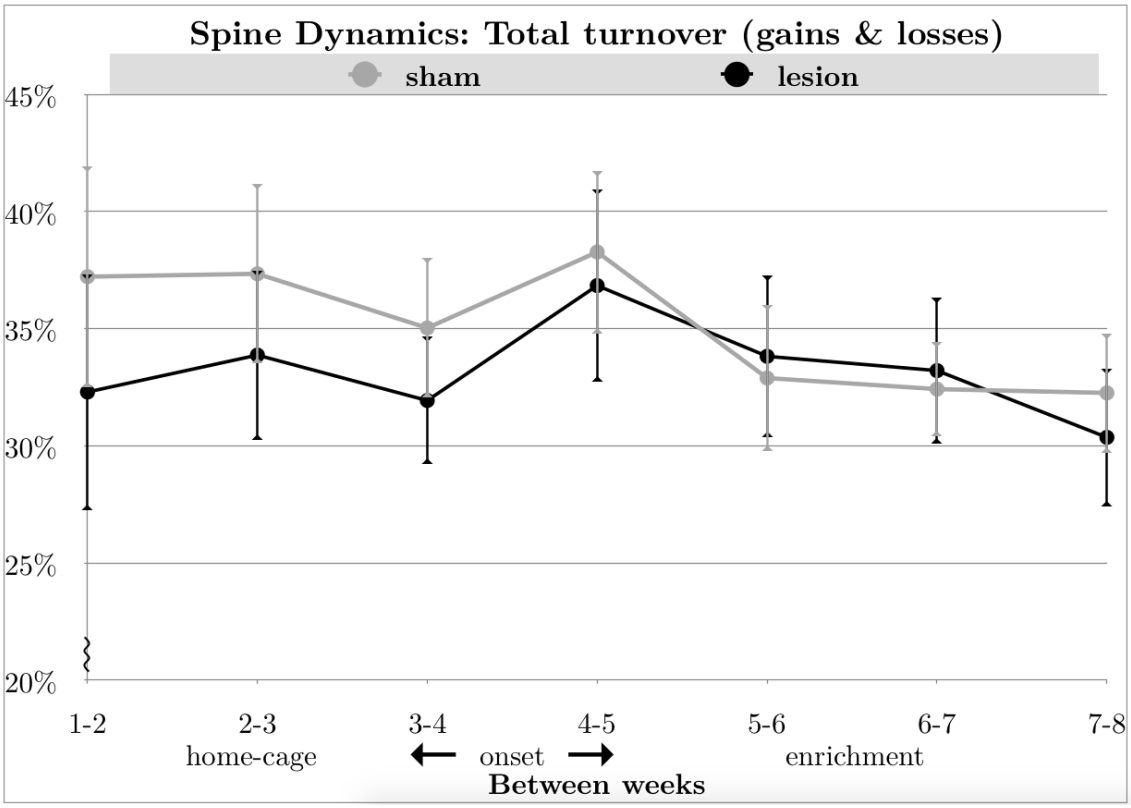

Figure 3.5: Total turnover is defined as all of the gains and losses added together. A 2*7 repeated measures anova results in only a main effect across imaging sessions, $F(6,30) = 3.190376, p = 0.01526907, \eta_G^2 = 0.05538911$. All assumption test were not violated. Pairwise comparisons using paired t-tests with bonferroni corrections resulted in significant differences in turnover during the first and second week and the first and final week during enrichment, p=0.012 and p=0.017. A two-way RMANOVA, found a significant increase between the final week in home-cage and the first week in enrichment (enrichment onset), $F(1,5) = 11.1111, p = 0.020703$. In addition, the first week of enrichment has significantly higher turnover than the second week in enrichment, $F(1,5) = 15.1429, p = 0.011509$ (this agrees with the significant post-hoc pairwise comparison results). The following results support a transient enrichment effect. Error bars represent standard error of the mean. Note additional sex differences in the appendix related to stability and interaction effects.

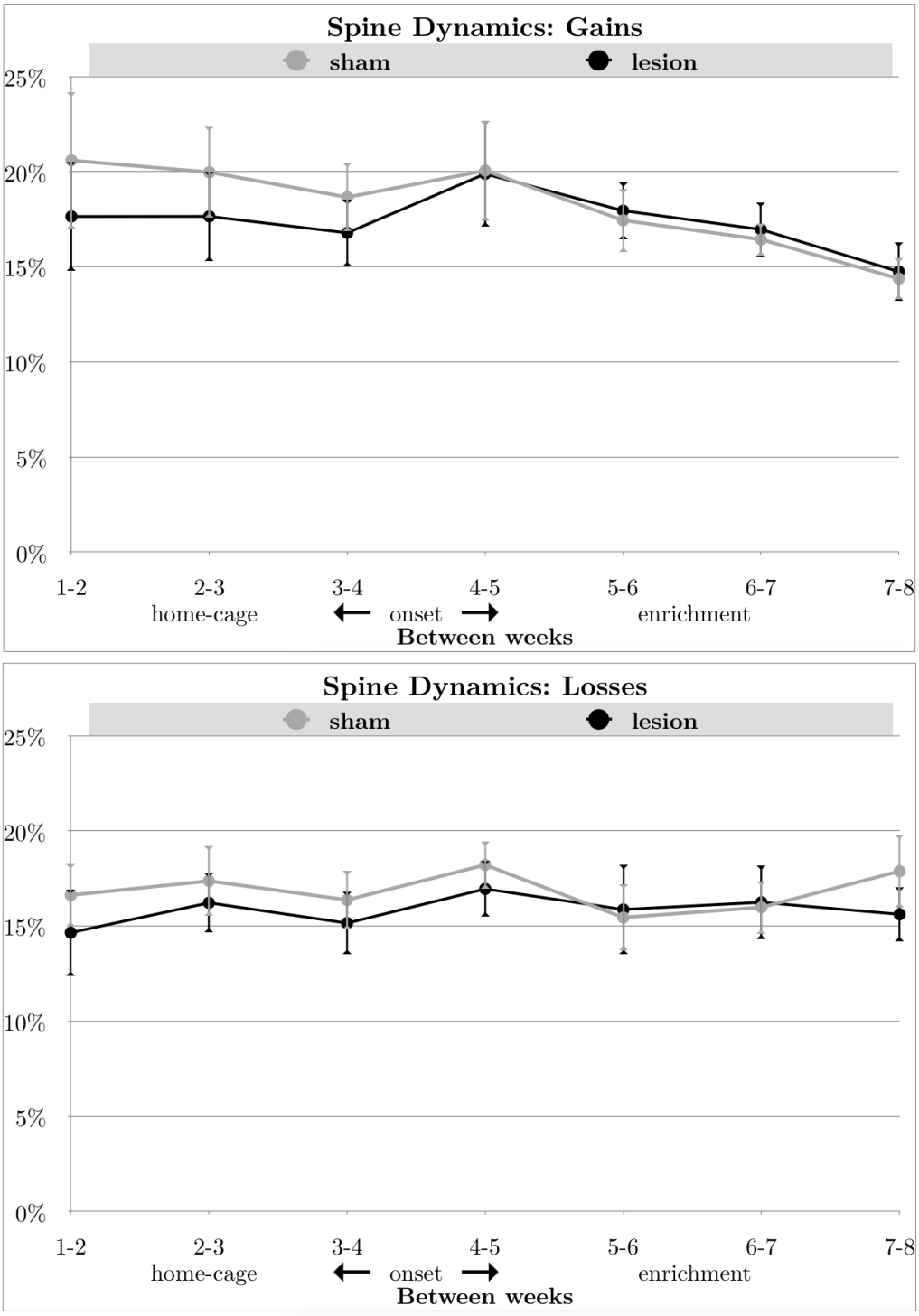

Figure 3.6: There are significantly more gains than losses as is redundant in relation to the increase in density observed across time, $F(1,5) = 19.5871, p = 0.0068553, \eta_G^2 = 0.027567757$. After sphericity corrections for a main effect across imaging sessions, there is only a significant effect if you consider the less conservative Huynh-Feldt correction result, $F = 19.5871, p[GG] = 0.08644915$, $p[HF] = 0.049642$. Post hoc pairwise comparison with bonferroni corrections found significant differences in gains between the first and second week in enrichment and the final week in enrichment, $p = 0.047$ and $p = 0.038$ (consistent with total turnover post-hoc pairwise results). Error bar represent standard error of the mean.

3.4 Enrichment decreases permanency of spine turnover

As previously described in the methods, spine configurations that only had one-time-turnover were categorized as stable-gains/losses. Across all animals there was a total of 567/6963 spines or 8.14% that were categorized as stable-gains, 269/3260 or 8.25% in the sham and 298/3703 or 8.05% in the lesion hemispheres. And a total 292/6963 or 4.2% categorized as stable-losses, 144/3703 or 3.9% in the lesion and 148/3260 or 4.5% in the sham hemispheres. The following categorizations were combined to make an overall comparison of one-time-turnover (consisting of around $\sim$12% of spines) between hemispheres and housing conditions. In addition, spines that were present during only one imaging session are considered very transient were another measure of permanency. Spines that only existed during one imaging session were also totalled and compared between hemispheres and housing conditions.

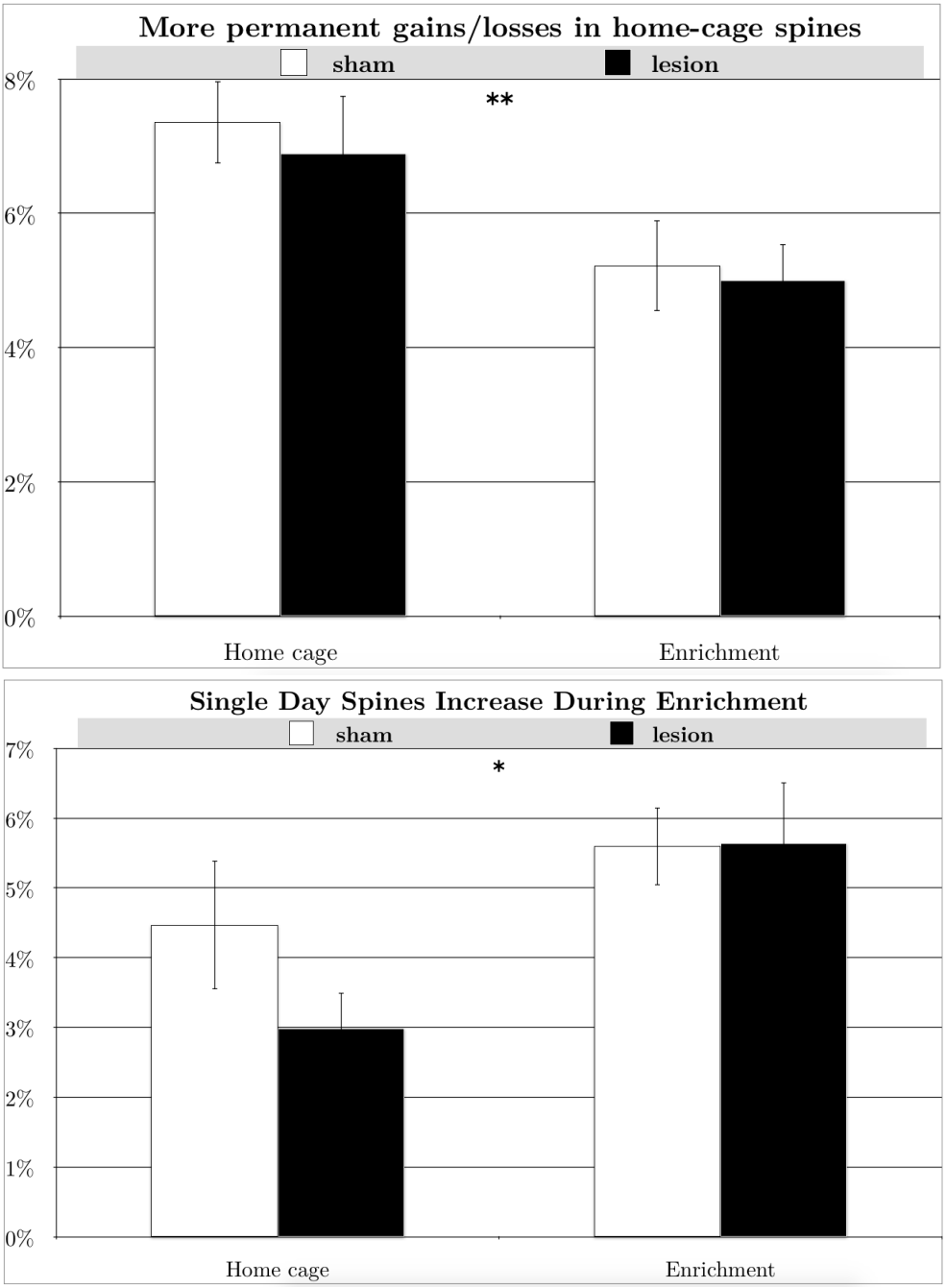

Figure 3.7: Spines that only turned over one time throughout all of the imaging sessions were categorized as stable gains/losses. Stable gains/losses show a significant main effect of housing with more permanency in turnover during home-cage housing, $F(1,5) = 24, p = 0.004478$. Gains alone had a high significant effect, $p =< 0.0001$ while losses are not significant on their own (there were low stable-loss spine numbers so they were combined with stable-gains). Highly transient dendritic spines, that exist during one imaging session only, showed an opposite effect and were significantly greater during enrichment, $F(1,5) = 7, p = 0.045659$. Together, the following results suggest that new spines are more unstable during enrichment and likely to have subsequent turnover.

Results: Axons and axonal boutons *in vivo*

4.1 Sampled axons and axon boutons in the RSC

Both hemispheres across six mice and eight imaging sessions resulted in a total of 17,144 manual axonal bouton counts. 8,572 counts while the mice were housed in their standard laboratory home-cages and 8,572, while they were housed in an enriched environment. A total of 2143 total boutons were sampled along a summed length of axons that measured a total of 24,408μm. 964 boutons were sampled from the sham hemispheres and 1179 from the lesion hemispheres. 11,133μm were measured from the sham hemispheres and 13,275μm were measured from the lesion hemispheres. Only axons that stayed consistent in length across all imaging sessions were used for density and turnover analysis. A total of fourty-nine axons $\sim$14% were observed to change in length across imaging sessions, twenty-three from the sham hemsipheres and twenty-five from the lesion hemispheres. Axons that changed in length across imaging sessions mainly occurred in male mice and were analyzed for changes in lengths separately from axonal bouton turnover.

Table 4.1: Sex, lesion hemisphere, total number of sampled boutons, total number of sampled axons, and the total lengths of all the sampled axons combined, measured in (μm) for each mouse.

	Sham			Lesion		
ID/Sex/Lesion	# Axons	# Boutons	Length	# Axons	#Boutons	Length
1-♂-Left	22	178	2184	26	215	2495
2-♀-Right	31	178	2411	23	167	1621
3-♂-Right	26	190	2295	31	234	2840
4-♀-Left	19	161	1568	28	217	1996
5-♀-Right	24	130	1263	21	165	1764
6-♂-Right	18	127	1412	28	181	2559
Totals: 6	140	964	11,133	157	1179	13,275
3-♀	74	469	5242	72	549	5381
3-♂	66	495	5891	85	630	7894
2-Left	41	339	3752	54	432	4491
4-Right	99	625	7381	103	747	8784

4.2 Axonal bouton density over time in the RSC

The average density across all animals and imaging sessions was 0.07 boutons/μm, with a range between 0.050-0.096 boutons/μm throughout all imaging sessions. The average across all mice and all imaging sessions was 0.071 boutons/μm in the sham hemispheres and 0.070 boutons/μm in the lesion hemispheres. There was no average difference between the sham and lesion hemispheres and running a two-way repeated measures (ANOVA) with both factors repeated, resulted in no main effects of either hemisphere or imaging

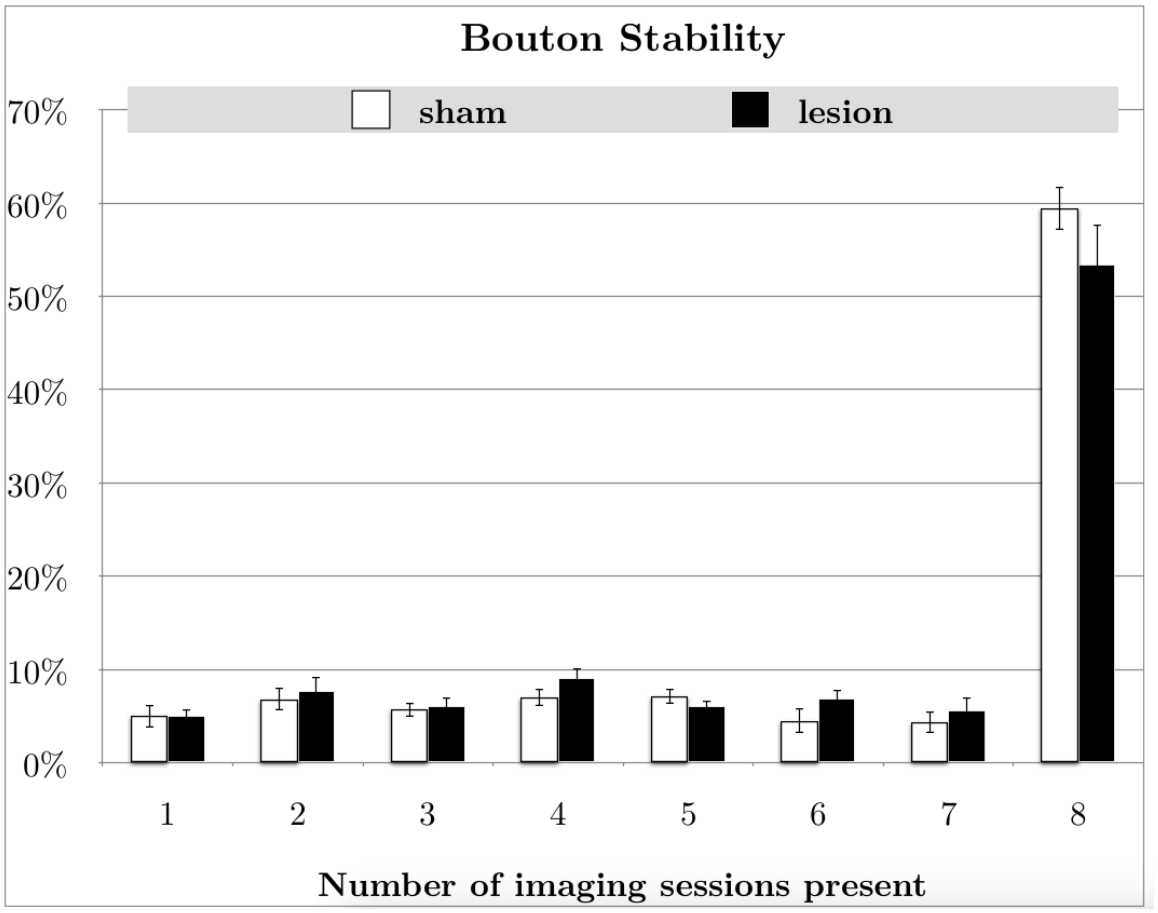

Figure 4.1: The following represents how many imaging sessions a bouton was present for, regardless of order. Between 50-60% of boutons were stable across both hemispheres and all imaging sessions. The remaining boutons that displayed a level of plasticity were evenly distributed in regards to the number of imaging sessions they appeared in.

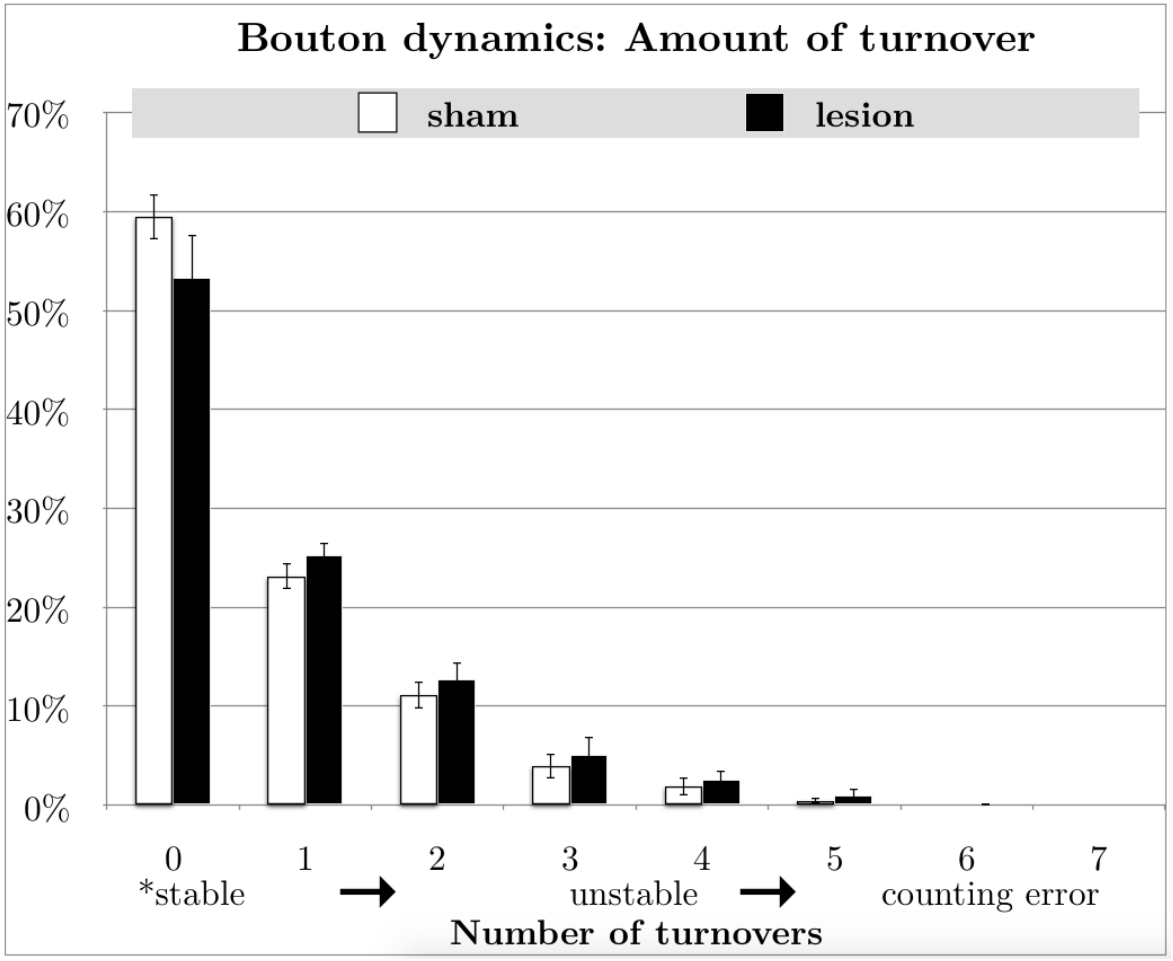

Figure 4.2: The following represents how many times a bouton turned over independent of when; the same as dendritic spine sampling of turnover.

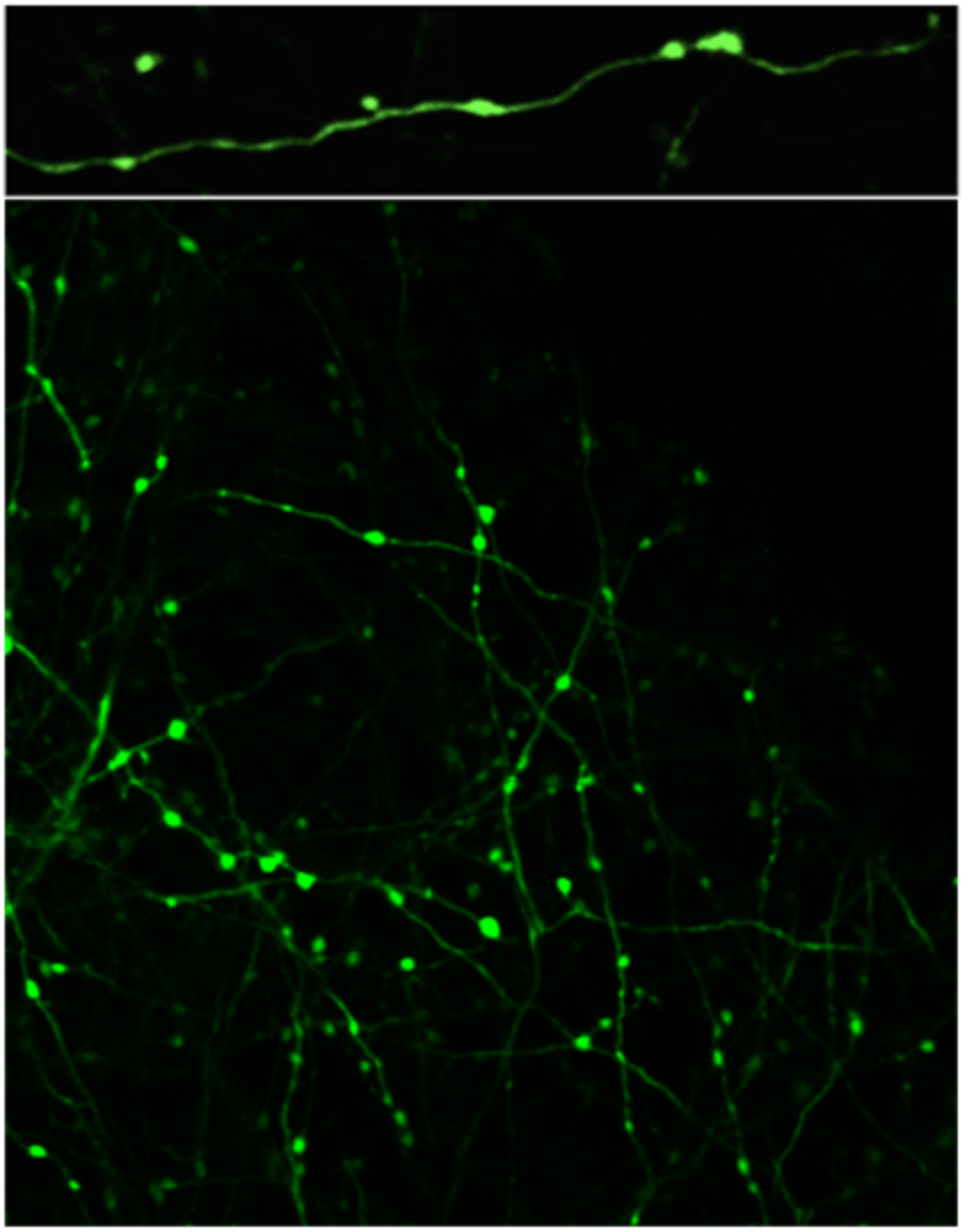

Figure 4.3: The following qualitative example provides a visual representation for a high number of axon branches within one image plane. The image above contains a terminaux bouton with a neck creating an appearance similar to that of a dendritic spine. The image below contains numerous axon branches containing the much more common en passant boutons. Both influence functional circuitry.

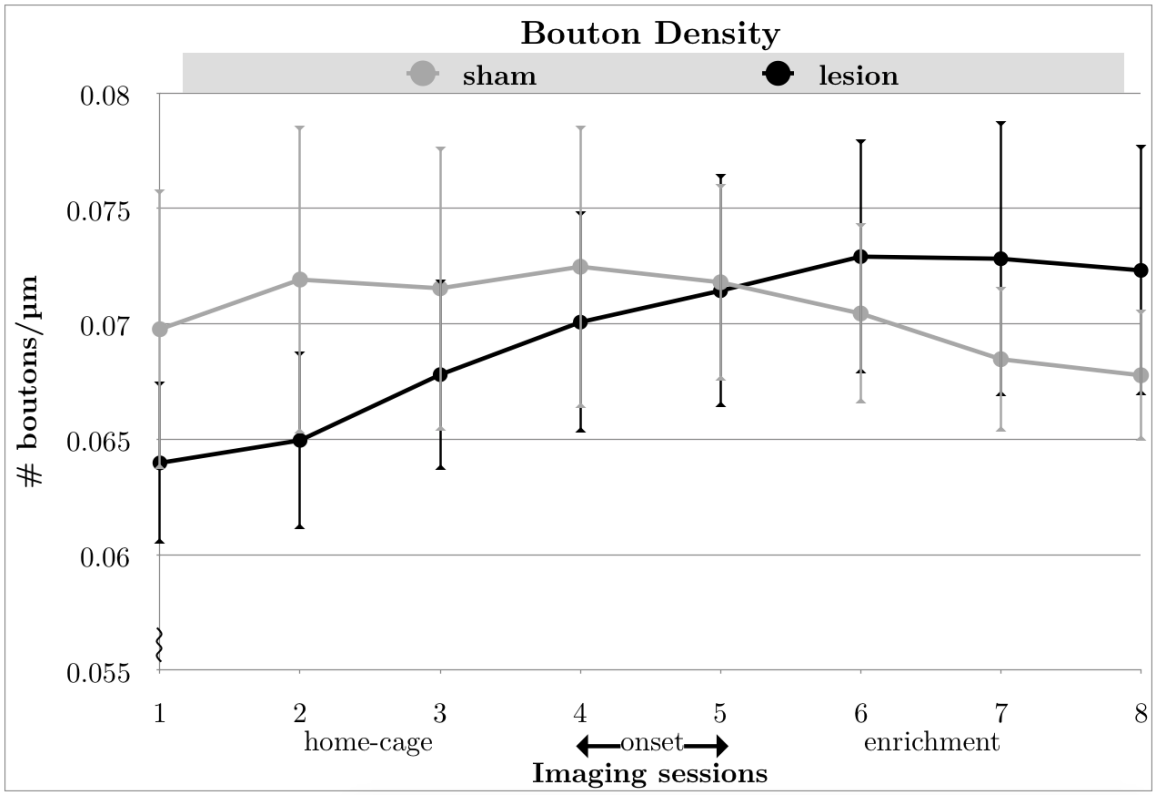

Figure 4.4: Average percent bouton densities across six mice and eight imaging sessions that were taken once every five days. Densities were measured as the number of boutons that are present along 1 μm of axon in the RSC. There was a significant interaction effect before running sphericity corrections: $F(7,35) = 3.2809, p = 0.000870, \eta_G^2 = 0.034558$, however, these data did not remain significant after corrections: $F = 3.2809, p[GG] = 0.28416, p[HF] = 0.27481$. No main effects were significant. Thus, no significant conclusions can be made from the following axonal bouton data after correcting for violations of assumptions, regardless of the observable trend.

sessions. There is an observable trend implying a possible interaction effect, but due to the violation of sphericity the interaction was no longer significant after corrections, before sphericity corrections: $F(7,35) = 3.2809, p = 0.000870, \eta_G^2 = 0.034558$ versus after: $F = 3.2809, p[GG] = 0.28416, p[HF] = 0.27481$. Thus, there were no significant effects found in density of axon boutons in vivo.

4.3 Experience-dependent plasticity via turnover of axonal boutons across time

All 2169 boutons underwent unique turnover across imaging sessions (a mixture of gains, losses, and remaining stable). There were a total of 15,183 turnover counts that account for all changes that occurred across eight imaging sessions taken once every five days. 6507 turnover counts were made while the animals was housed in their laboratory home-cages and 8676 while the animal was housed in an enriched environment. Consecutive imaging sessions were compared in order to determine the number of new boutons gained or lost each week. Total bouton turnover data including gains and losses showed only a main effect of imaging sessions. When sex was taken into account there was an interaction effect between hemispheres and they type of turnover (see sex appendix for further details).

4.3.1 Axonal bouton turnover in both hemispheres increases transiently following transition to enrichment

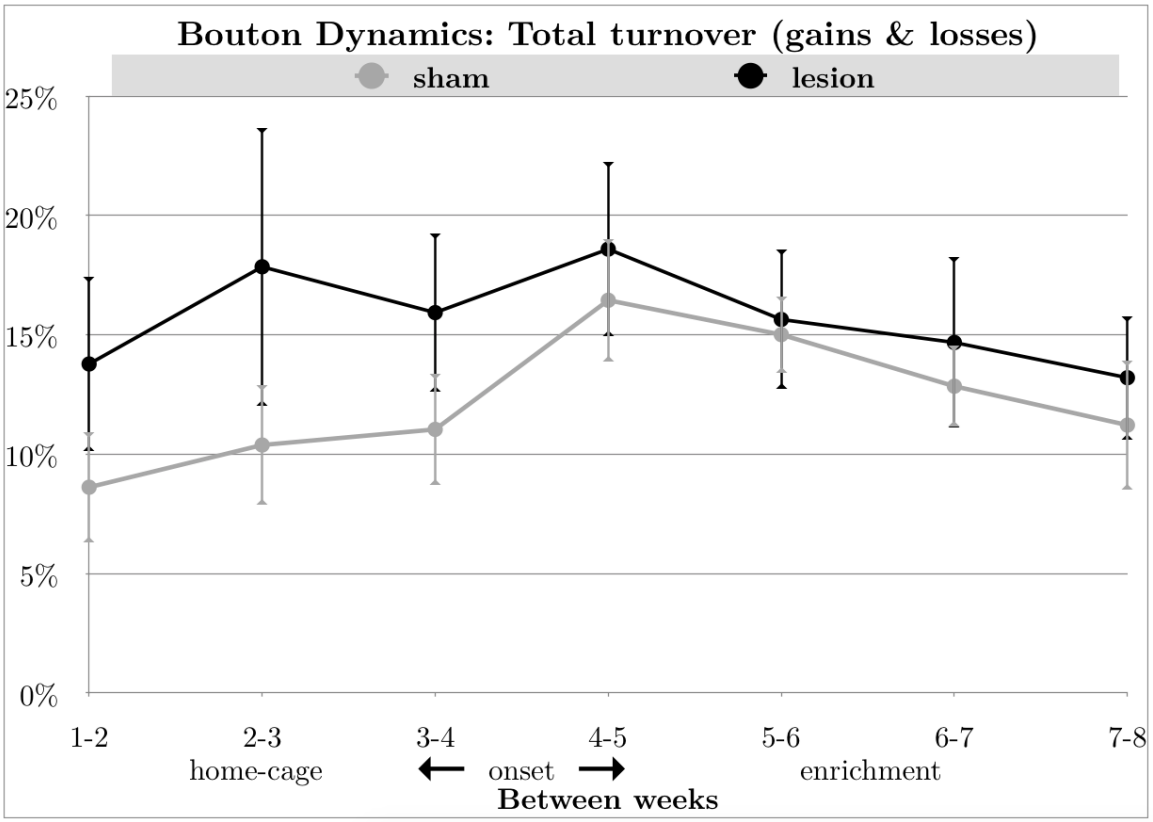

Figure 4.5: Axonal bouton turnover showed a significant main effect of imaging sessions after the less conservative Huynh-Feldt correction but not the more conservative Greenhouse-Geisser, $F = 2.979007, p[GG] = 0.07609473, p[HF] = 0.02388375$. A two-way repeated measures ANOVA on just home-cage data showed no effects, however, when the first week of enrichment was added there was a significant effect of imaging sessions, p=0.012244. Pairwise comparisons identified significance between the first week in home-cage and the first week in enrichment, $p = 0.0078$. A two-way repeated measures ANOVA between the last week in home-cage and first week in enrichment, showed a significant difference with more turnover occurring during the first week of enrichment, $F(1,5) = 7, p = 0.045659$. A repeated measures ANOVA between the first and second week in enrichment was not significant, p=0.079246 but was significantly by the end of enrichment, p=0.048249

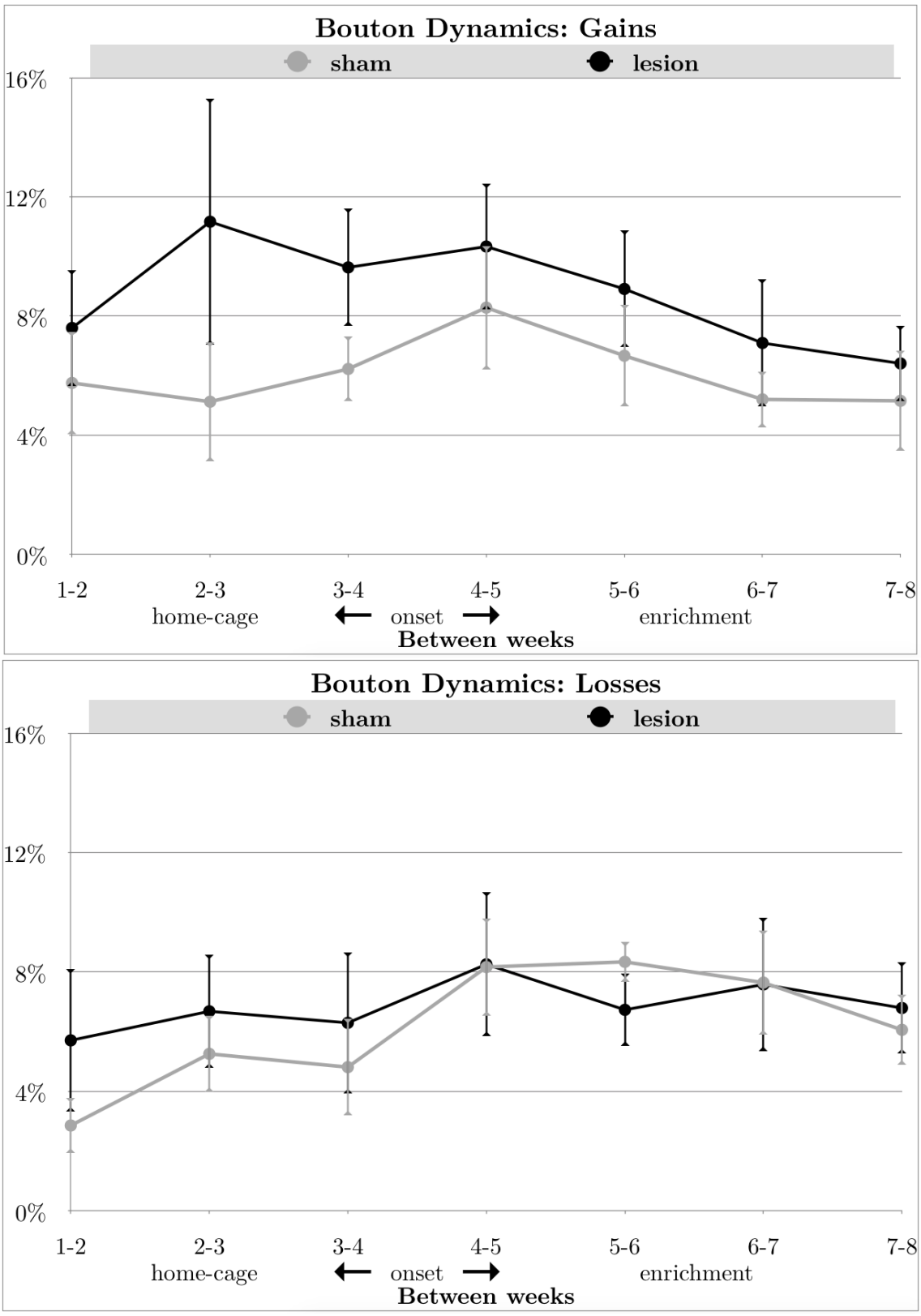

Figure 4.6: A two-way repeated measures ANOVA showed no significant effects of gains or losses. The effect of imaging session on turnover remains, $F(6,30) = 2.979007, p = 0.02104693, \eta^2_G = 0.04932010$.

4.4 Axons modify in length in the retrosplenial cortex across time

Structural changes including axonal growth, retraction, and the combination of both have yet to be documented across longer time periods in vivo, in the RSC. While analysing dendritic spines it was observed that axons change quite drastically in length between imaging sessions. The data for changes in axon length arequalitative in nature, as we only observed a total of 48 axons out of an unknown total amount of axons that could potentially be in the thousands. In addition, 25 boutons were noted to switch between having an elongated neck and being situatied along the midline of the axon.

There were large discrepancies in these axons between the sexes that will be further discussed in the sex-difference appendix. For example, the male mice contained 42 of these axons while the female mice only 6 (and in one female we found zero changes in length). The following figures below are particular instances that showcase growth, retraction, and the combination of both across imaging sessions. No specific relationship to our experimental paradigm of unilateral hippocampal lesions or home-cage versus enrichment could be determined. Such qualitative data though interesting, warrants much further investigation to fully understand the phenomenon. For example, information that would compliment the following data includes identifying where axons originate from that are projecting to the RSC.

Table 4.2: Sex, lesion hemisphere, total number of axons that changed in length, total growth, and retraction lengths of all the sampled axons combined, measured in (μm) for each mouse.

	Sham			Lesion		
ID/Sex/Lesion	# Axons	# Growth	Retraction	# Axons	Growth	Retraction
1-♂-Left	5	83	-280	12	427	-362
2-♀-Right	0	NA	NA	2	28	-56
3-♂-Right	16	330	-351	3	100	-52
4-♀-Left	1	0	-38	3	79	-58
5-♀-Right	0	NA	NA	0	NA	NA
6-♂-Right	2	62	-6	5	86	-172
Totals: 6	24	475	-675	25	720	-700
3-♀	1	0	-38	5	107	-114
3-♂	23	475	637	20	613	-586
2-Left	6	83	318	15	506	-420
4-Right	18	392	357	10	214	-280

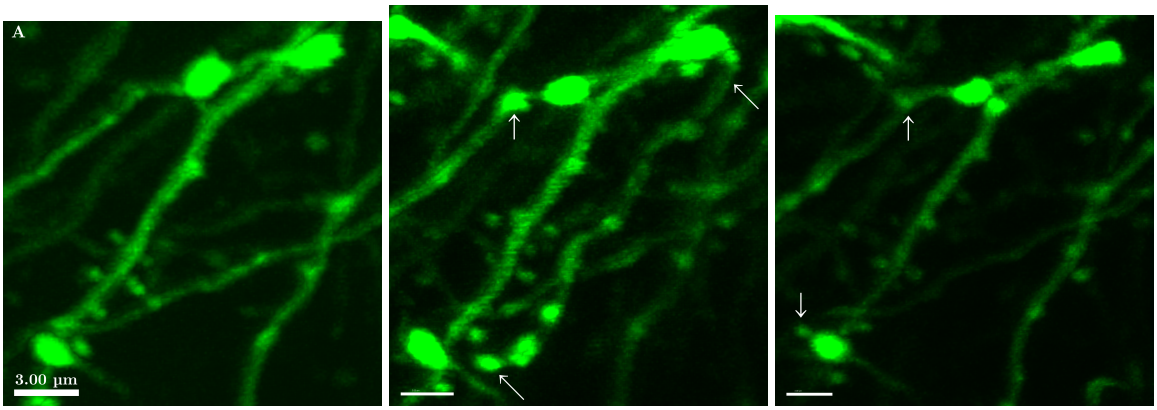

Figure 4.7: Axons display growth, retraction, transient growth/retraction, as well as turnover of boutons. The following three images are consecutive images taken while the animal was housed in an enriched environment (sessions, 5, 6, and 7). The imaging is an example drawn from the sham hemisphere. The unstable axon branch is labelled with the diagonal arrows, and was only present during one imaging session of all eight. Vertical arrows represent changes in axon boutons.

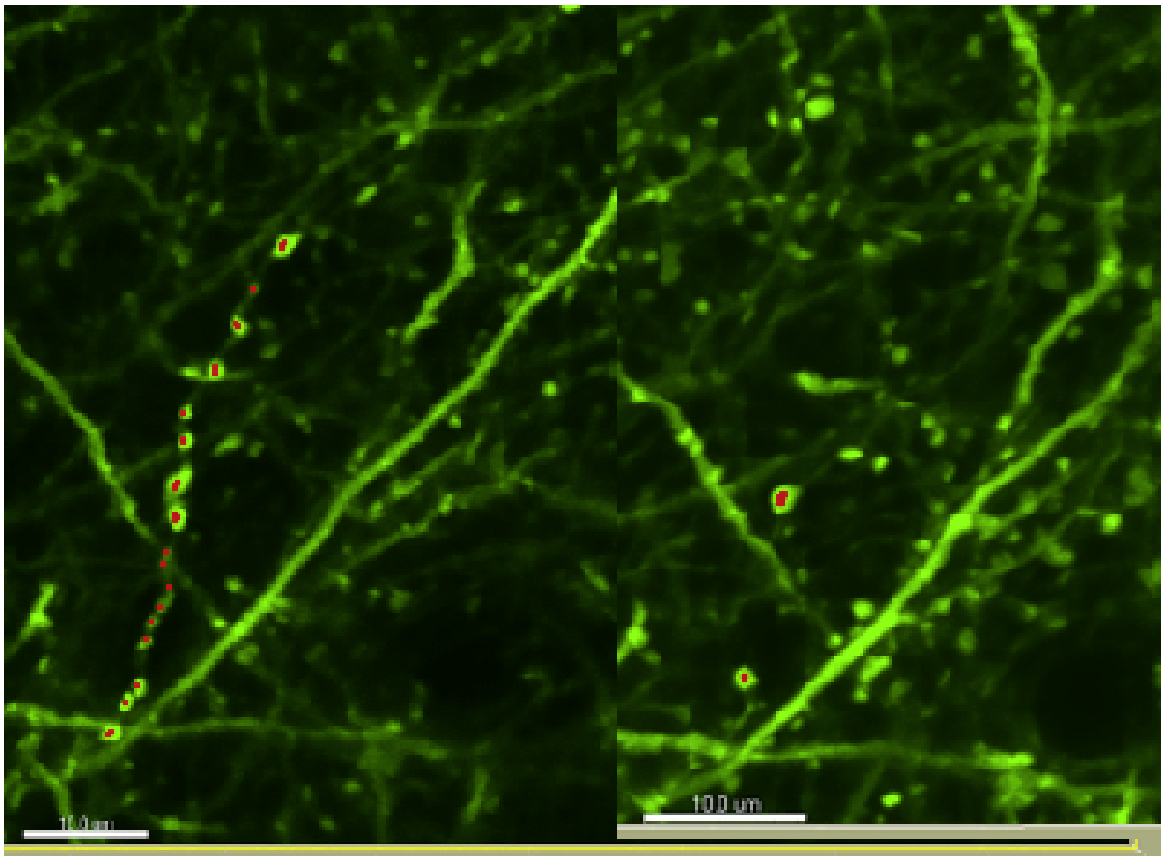

Figure 4.8: Axons that disappeared over time appeared to have some blebbing along their lengths. A possible mechanism of degeneration includes Wallerian degeneration due to damage at the location of the cell body and degeneration of the axon that is slowly taken away by the cytoplasm and microglia. Scale bars for both 10μm

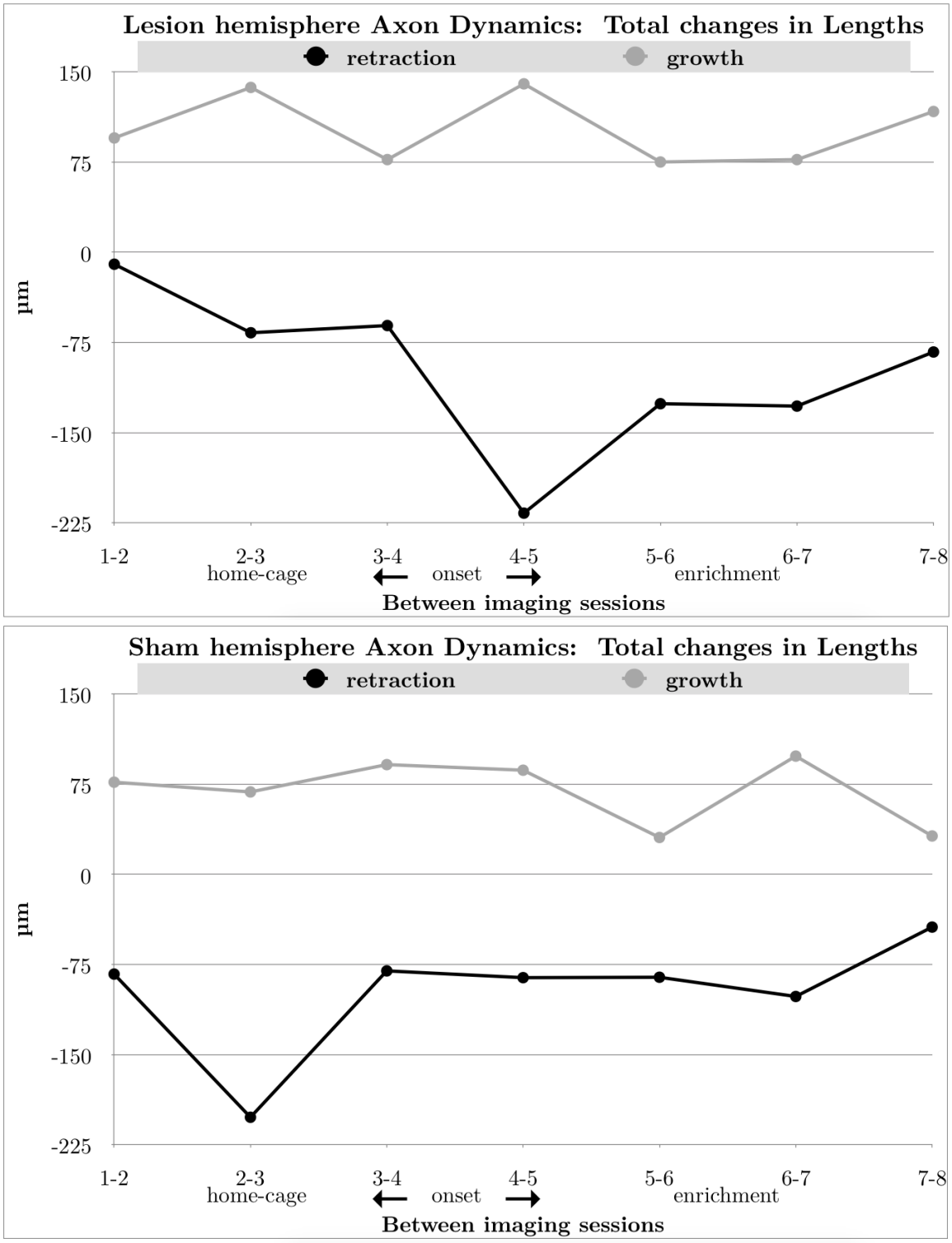

Figure 4.9: Growth and retraction in axon lengths across imaging sessions was dynamic. Qualitative observations include: 1) overall greater axon growth in the RSC ipsilateral to a hippocampal lesion independent of housing and 2) greater retraction of axons during home-cage housing in the sham hemisphere and conversely, greater retraction following enrichment onset in the lesion hemisphere.

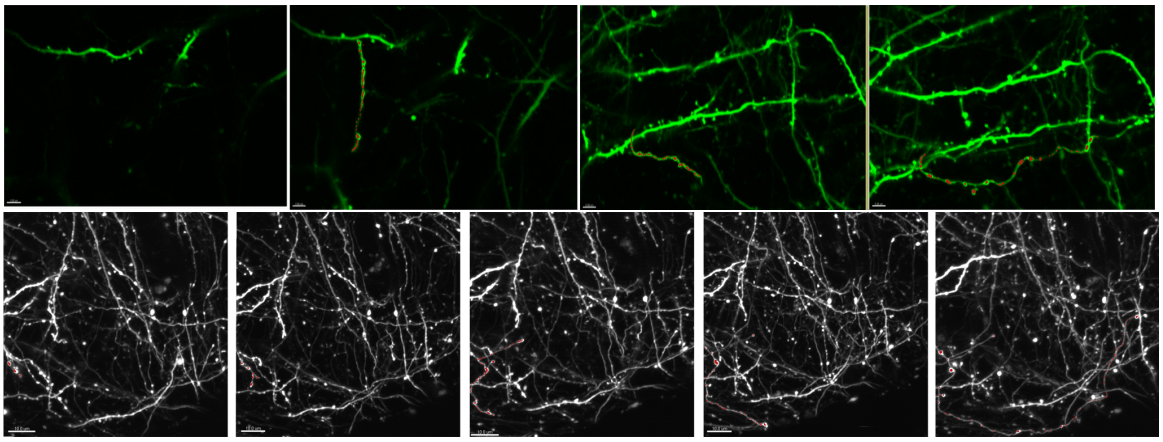

Figure 4.10: Two examples showcasing axon growth across imaging sessions. The top image is an example of growth beginning at enrichment onset, taken from the lesion hemisphere. The image below is from the sham hemisphere and growth began one imaging session prior to enrichment onset.

4.5 Hippocampal axons project to the retrosplenial cortex

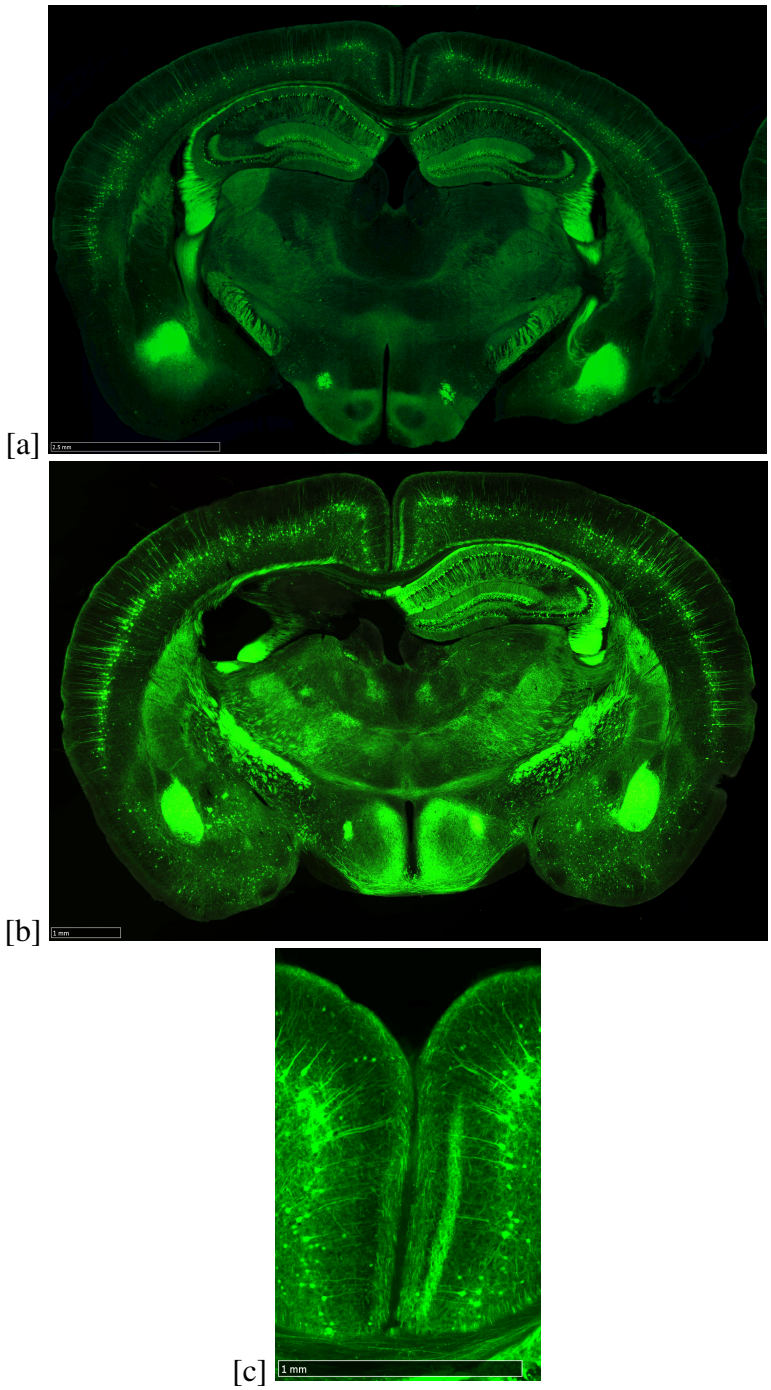

Figure 4.11: a) Healthy bilateral hippocampi, scale bar = 2.5mm b) Unilateral hippocampal lesion pathology scale bar = 1mm and c) absence of hippocampal projections to layer 1 of the granular ipsilateral retrosplenial cortex, without influencing the presence of layer 5 pyramidal neurons. Result is congruent with subiculum lesions after an ibotenic acid lesion observe in:, (Ichinohe et al., 2008)

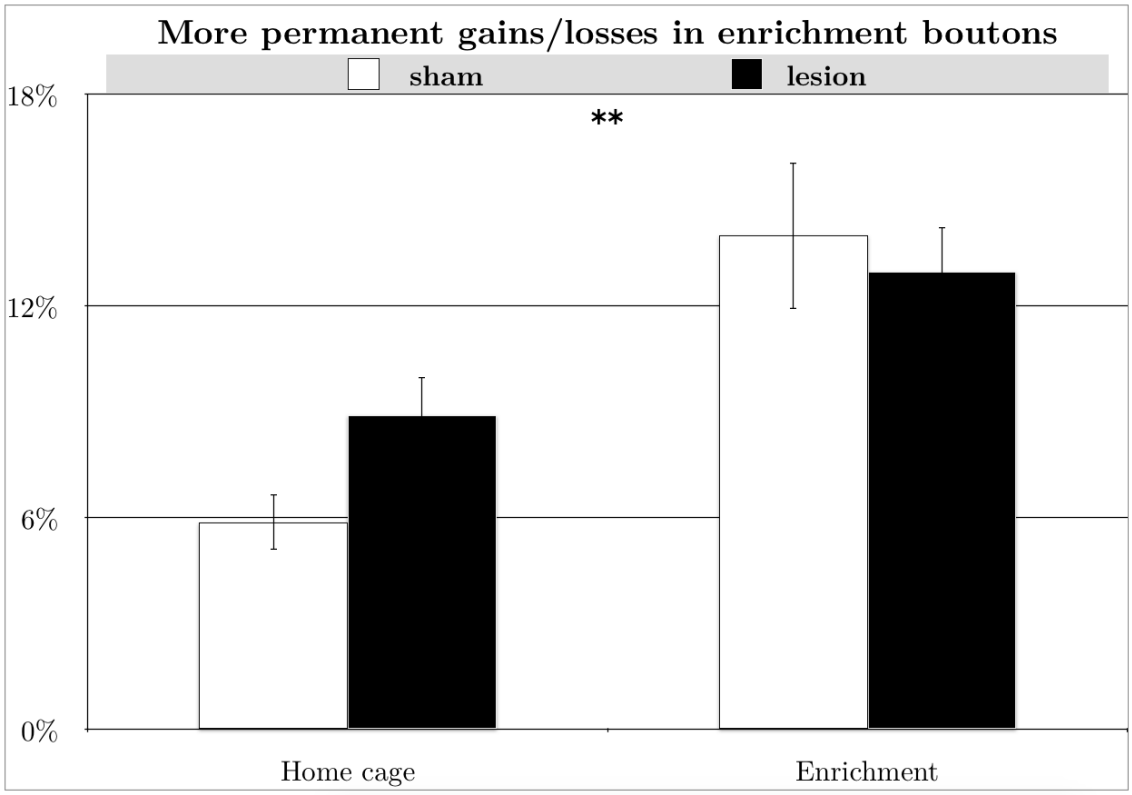

Figure 4.12: Axonaql boutons that turned over one time only throughout the duration of the imaging sessions were categorized as stable gains/losses. Stable gains/losses showed a significant main effect of greater permanency of turnover in enrichment housing, $F(1,5) = 18.667, p = 0.007567$.

4.6 Enrichment increases permanency of axonal bouton turnover

Across all animals there were a total of boutons 266/2143 or (12.4%) that were categorized as stable gains, 178/1179 (15.1%) in the lesion and 88/964 (9.1%) in the sham hemispheres, and a total of 178/2143 (8.3%) that were categorized as stable-losses. 80/1179 (6.8%) in the lesion and 98/964 (10.2%) in the sham hemispheres. One-time turnover categorizations were combined together to (consisting of around 21%).

Discussion

Neurological disorders such as Alzheimer's disease, autism, epilepsy, and stroke have been associated with synaptic dysgenesis and have a negative impact on memory (Phillips and Pozzo-Miller, 2015;DeKosky and Scheff, 1990; Tong et al., 2012). The hippocampus is a highly efficient system that transfers short-term memories into long-term memories. Systems consolidation involves the reorganization of memories that are initially encoded in the hippocampus and later transferred to the neocortex, through mechanisms such as memory trace reactivation. In addition, hippocampal projections to the ipsilateral RSC are a possible avenue in which such transfer of information is likely to occur and further justify unilateral hippocampal lesion models for within animal comparisons. Our turnover and density data oppose the initial consolidation prediction that experience-dependent plasticity would decrease in the RSC ipsilateral to the lesion. Contrary to the standard model postulating that all memories are initially hippocampal dependent, structural plasticity was observed in the ipsilateral RSC regardless of hippocampal damage.

5.1 The hippocampus influences the density of synapses not the proportion that undergo turnover

5.1.1 Compensatory mechanisms in dendritic spines and axons

There was an effect of imaging session on the proportion of dendritic spine and axon bouton turnover, that on closer examination, increased transiently in both hemispheres following transition to enrichment. Additional trends support that dendritic spine turnover during home-cage housing was on average lower in the ipsilateral hemisphere; however, following transition to enrichment, increased more to match sham hemisphere levels ($\sim$37%

maximum turnover in either). The initial lower dendritic spine turnover suggests a possible initial deficit; however a greater increase following transition to enrichment is congruent with the suggestion that environmental enrichment following brain damage instigates a potential compensatory process (Rose et al., 1993).

Due to increased density in the lesion hemisphere, the actual number of spines to calculate a lower proportion was similar between hemispheres. Opposite of the trend in dendritic spines, the proportion of axonal bouton turnover in the sham hemisphere was initially lower, but showed the greater increase to reach lesion hemisphere levels following transition to enrichment. The following trends suggest a possible interaction effect between synaptic structures and hemispheres; however, such a relationship remains unclear and is outside the scope of the following study.

Throughout all imaging sessions there was greater axon growth in the lesion hemisphere, as well as a transient increase in retraction in the lesion hemisphere following transition to enrichment. The increase in growth is likely compensatory in nature. There is evidence that thalamocortical afferents are are characterized by the elongation and retraction of their branches in the RSC (Holtmaat and Svoboda, 2009). Axonal growth has previously been observed to be regulated by the level of spiking activity (Galimberti et al., 2006). A greater density of dendritic spines may result in a higher number of synaptic potentials and support such a relationship between spiking activity and growth of axons. An incompatible finding pertaining to such a relationship is that females had higher dendritic spine density than males, but did not show greater axon growth. The majority of all changes in axon length occurred in male mice. Thus, there my be additional differences in axonal connectivity pertaining to types and origins of axons between males and females in the RSC.

Sutherland et al. (2010a) results indicate, contrary to compensatory mechanisms, that enrichment led to a reduction in dendritic spines in the ipsilateral neocortex to a hippocampal lesion. It should be noted that the deficit only occurred in the right hemisphere as lesions were not counterbalanced. In addition, the effect was marginal due to the initial ANOVA

having an interaction effect p=0.058, which to some researchers would not warrant the continuation into post-hoc analysis. A anterior thalamic lesion study found a reduction in dendritic spine density in both the RSC and the hippocampus. Only the dendritic spines in the hippocampus were ameliorated after animals were housed in an enriched environment while spines in the RSC remained unrecovered (Harland et al., 2014). Such a finding supports less compensatory response in the RSC in comparison to the hippocampus. The lesion effects remained permanent across time and varying experience.

5.1.2 Intrinsic plasticity and spike-time dependent plasticity between hemispheres

There is emerging importance of the concept that intrinsic plasticity plays an important role in memory at possible synaptic, neuronal, and global levels (Shim et al., 2018). Global intrinsic plasticity accumulates when multiple structures are activated, and such distribution may influence whether or not something is stored more long term. Specific mechanisms that allow for initial hippocampal encoding to determine such distribution is unclear. Moreover, optimal intrinsic plasticity levels to acquire memory may be less dependent on the hippocampus when achieved through repetition or great arousal.

The loss of hippocampal input to the RSC in the ipsilateral hemisphere will remove the occurrence of spike-time dependent plasticity as a result of such outflow. The loss of of spike-time dependent plasticity may lead to a homeostatic compensatory increase in synapses in order for intrinsic plasticity levels to persist in the RSC. A study completed by Brown et al. (2010) reports homeostatic mechanisms in spine density remodeling after stroke. Experience-dependent plasticity remains intact in the RSC outside of obvious destruction of hippocampal outflow.

Research by Baumgartel et al. (2018) indicates that dendritic spines in the RSC increase over time in response to cAMP signalling, independent of any training. Our results support continuous signaling, as there was no increase in dendritic spine density in response to an enriched environment but only a gradual steady increase across time. The cAMP pathway

is used in cell communication and thus, regardless of decreased hippocampal input into the ipsilateral RSC hemisphere, other cell communication remains intact. The gradual increase in spine density over time may be a continuation of such a s signalling process during aging.

An experiment conducted by Yu et al. (2008) identified that in YFP-H line mice, cells containing endogenous expression show connectivity that cells without expression do not have. Thus, results only pertain to the neocortical cell populations containing endogenous expression of YFP. Adult mice were used in the following study as it has also been shown that expression levels in these mice can increase over time during development (Porrero et al., 2010). Fortunately if a new cell expresses YFP, they express brightly throughout its entirety. Thus, if a dendrite or axon was chosen during the first imaging session, the entirety of the neuron already contains expression.

5.1.3 Possible mechanisms of hippocampal overshadowing and learning episodes

The concept of hippocampal overshadowing implies competitive-like processes between brain regions. In relation to initial encoding and involvement in turning short term memories into long term memories, the hippocampus is more efficient/dominant and overshadows the neocortex. Thus, when one hemisphere's hippocampus is damaged the ipsilateral neocortex may no longer be overshadowed in the same manner. Downstream long-term depression may serve as a mechanism of hippocampal overshadowing. Hippocampal outflow may lead to greater levels of both long-term potentiation and long-term depression, but with an overall greater level of depression and down-regulation of the number of dendritic spines. Another mechanism that may lead to successful hippocampal overshadowing is its overall higher rate of synaptic turnover in comparison to the neocortex.

Memory is able to overcome hippocampal overshadowing through repetition; the hippocampus and neocortex may independently acquire different representations that support successful memory (Sutherland et al., 2010b). Enrichment offers a form of time dependent distributed learning in that repeated exposures to similar information are experienced.

Novelty followed by more familiarity of experience may account for the observed transient plasticity in the RSC persisting in both hemispheres.

5.1.4 Excitotoxic NMDA lesions may lead to irreversible downstream effects in the RSC

NMDA is an excitotoxin that initially functions as an intense receptor agonist leading to seizure activity by allowing high levels of calcium ion influx. The final result is antagonistic in that neurons are destroyed via apoptosis. Excitotoxicity of the hippocmapus leads to deviation from normal oscillatory activity and such destruction of tissue can be visualized after one week or more (Kirby et al., 2012). The finding in the following study of an increase in dendritic spine density in the ipsilateral RSC to an excitotoxic hippocampal lesion may be a downstream effect of excessive neuron firing during the excitatoxic process. Greater dendritic spine density suggests an increase in potential electrical activity; however, once seizure activity is completely controlled mice do not exhibit future seizure activity. A further interesting observation was that female mice exhibited an observable larger seizure response post-NMDA infusion, during surgical recovery, and have a corresponding greater spine density than male mice but less axon modifications.

5.2 Overall issues with variability

Axon data had high within-group variability leading to issues of violating assumption tests when running RMANOVAs. One possible reason is that we do not have enough boutons counted to obtain a large enough sample size to account for the variation. With such a low number of mice (n=6) even one mouse showing an opposite trend has a substantial influence on the data outcome, resulting in no significant findings. Sex differences warrant such variation and are further discussed in the appendix. In addition, lateralization between hemispheres may warrant future investigation. Lateralization was briefly considered, resulting in the left lesion hemisphere showing higher levels of turnover in comparison to

right lesion hemispheres, possibly accounting for the increased variation observed in the lesion hemispheres.

5.3 Dendritic spine turnover is more unstable during enrichment while axonal bouton turnover is more stable

Previous research results support that exposure to learning leads to greater stabilization of dendritic spines (Roberts et al., 2010). The number of stable spines is thought to increase throughout life and represent long-term memories. Such research would lead to the prediction that the turnover of dendritic spines would be more stable following transition to enrichment. To the contrary, our data results support that when a spine was gained during home-cage it was more likely to remain permanent, and when lost, less likely to reappear. Moreover, when a spine was gained during enrichment it was less stable and likely to show subsequent turnover.

A study by Ruthazer et al. (2006) better supports our finding that more unstable spines following enrichment coincides with an increase in the retraction of axon branches. Their study supports that the stabilization of axon branch dynamics occurs through synaptic maturation. The lesion hemisphere had overall less stable axon dynamics in relation to extension through all housing, and retraction following exposure to enrichment. Thus, offers support for an increase in dendritic spine maturation in the sham hemisphere following enrichment that did not occur in the lesion hemisphere.

The mice were able to remember specific foraging locations/objects and how to manipulate such objects in order to retrieve hidden treats (even soon upon recovery from exposure to isoflurane). Mice were also quite naturally attracted to the lego objects while in the running ball and the behaviour could be exploited for them to learn to knock them over. The characteristic more unstable turnover of dendritic spines may mirror the more ever-changing world experience during enrichment. The opposing more stable turnover of axonal boutons offers another example that mirrors the opposing pre and post-synaptic

functions of the two structures.

5.4 Future research

'Seasonality' in data contains a period with an increase or decrease in the dependent variable during particular conditions. Our data supports the occurrence of seasonality by displaying complex combinations of gradual and transient experience-dependent plasticity. A future experiment may be interested in additional modelling related to particulars of the density and type of turnover (gain or loss) of synaptic structures across time within individual animals. Conclusions could help partial out variations regarding starting points, and overlap between the hippocampus and RSC functionally.

Due to the connections between these two brain structures an obvious avenue for future research is running the same experimental paradigm on mice without lesions and mice with bilateral hippocampal lesions. The addition of such data would allow for within group comparisons for each, as well as between group comparisons. Bilateral hippocampal lesions may offer greater support for our initial prediction due to the complete destruction of hippocampal outflow to the RSC. In addition, any chance for contralateral hippocampal or sham RSC influence would also destroyed.

Obtaining more structural data of Thy1-YFP mice would help examine the origins of axon collaterals throughout the RSC and further shed light on sex differences. The axons in our data may come from multiple sources, such as the thalamus, visual cortex or other intra-cortical layers in the neocortex. Whole-brain imaging on cleared Thy1-YFP brains using light-sheet microscopy could shed light on axon origins and possible target locations.

Future research that could label synaptic structures and their functionality would be beneficial. Currently, it is unknown whether or not each structure we counted contained a functional synapse. Issues related to doing the following in vivo are evident as immunohistochemistry or electron microscope methods are the current standard to determine functionality of synapses. Determining the ratio of functional synapses in the RSC from the

tissue of YFP mice could be helpful, but not ideal to determine turnover levels related to functionality. Tagging specific proteins or receptors (PSD-95 or AMPARs) associated with synaptic function is an option. In addition, a genetically encoded calcium indicator with red-shifted excitation, such as that used in Dana et al. (2018) could be bred with YFP mice in order to attempt co-labeling synaptic structure and neural activity simultaneously. Data collection would be limited to synaptic structures containing dual excitation and help shed light on the relationship between neuronal activity and synaptic plasticity.

Indeed the human eye remains a fundamental pattern detector, however, a future approach would be to incorporate an automated learning algorithm that could successful detect spines, axons, and their subsequent changes over time. Having a successful method of counting spines across time would save a lot of time. A flaw in doing this too quickly is that when you are not sure what you may find, it's hard to train a program. For example, changes in axon length may have never been detected in the following data without a manual counting method in place.

5.5 Conclusion

The RSC ipsilateral to a hippocampal lesion displayed greater dendritic spine density and more growth in the lengths of axons in comparison to the sham hemisphere. Lower synaptic density in the sham hemisphere likely supports a hippocampal role in the formation of a more efficient network with overall less excitability in the RSC. The increase in density in the lesion hemisphere further suggests that a greater amount of turnover is required to achieve the same proportion observed in the sham hemisphere. There were irregularities between spines and boutons in starting points and stability in response to enrichment. In addition, in both hemispheres the turnover of dendritic spines and axonal boutons persisted during both home-cage and enrichment conditions, regardless of the unilateral hippocampal lesion. Remaining turnover in the ipsilateral RSC to the lesion is likely influenced by polysynaptic sham RSC cross-hemisphere connectivity via the corpus callosum.

Bibliography

Aggleton, J., Nicholas, F., Seralynne, D., and Saunders, R. (2012). Medial temporal lobe projections to the retrosplenial cortex of the macaque monkey. *Hippocampus*, 9:1883–1900.

Atherton, L., Dupret, D., and Mellor, J. (2015). Memory trace replay: the shaping of memory consolidation by neuromodulation. *Trends in neurosciences*, 38(9):560–570.

Bakeman, R. (2005). Recommended effect size statistics for repeated measures designs. *Behavior Research Methods*, 37(3):379–384.

Baumgartel, K., Green, A., Hornberger, D., Lapira, J., Rex, C., Wheeler, D., and Peters, M. (2018). Pde4d regulates spine plasticity and memory in the retrosplenial cortex. *Scientific reports*, 8(3895):1–14.

Bergami, M. (2015). Experience-dependent plasticity of adult-born neuron connectvity. *Communicative and Integrative Biology*, (8)3(e1038444).

Berry, K. and Nedivi, E. (2017). Spine dynamics: Are they all the same? *Neuron*, 27(95):43–55.

Brown, C., Boyd, J., and Murphy, T. (2010). Longitudinal in vivo imaging reveals balanced and branch-specific remodeling of mature cortical pyramidal dendritic arbors after stroke. *Jornal of Cerebral Blood Flow and Metabolism*, 30(4):783–791.

Campbell, J., Kurz, J., and Churn, S. (2009). *Dendritic spines: Pathological remodeling of dendritic spines*. New York: Nova Science.

Chen, S., Kim, A., Peters, A., and Komiyama, T. (2015). Subtype-specific plasticity of inhibitory circuits in motor cortex during motor learning. *Nature Neuroscience*, 18(8):1109–1115.

Comeau, W., McDonald, R., and Kolb, B. (2010). Learning-induced alterations in prefrontal cortical dendritic morphology. *Behavioural Brain Research*, 213:91–101.

Dana, H., Novak, O., Guardado-Montesino, M., Fansen, J., Hu, A., Borghuis, B., Guo, C., Kim, D., and Svoboda, K. (2018). Thy1 transgenic mice expression the red fluorescent calcium indicator jrgeco1a for neuronal population imaging in vivo. *PLoS One*, 13(10):1–23.

DeKosky, S. and Scheff, S. (1990). Synapse loss in frontal cortex biopsies in alzheimer's disease: correlations with cognitive severity. *Annals of Neurology*, 27:457–464.

Denk, W., Strickler, J., and Webb, W. (1991). Two-photon laser scanning fluorescence microscopy. *Science*, 248:73–76.

Feng, G., Mellor, R., Bernstein, M., Keller-Peck, C., Nguyen, Q., Wallace, M., Nerbonne, J., Lichtman, J., and Sanes, J. (2000). Imaging neuronal subsets in transgenic mice expression multiple spectral variants of gfp. *Neuron*, 28:41–51.

Galimberti, I., Gogolla, N., Alberi, S., A.F., S., Muller, D., and Caroni, P. (2006). Long-term rearrangements of hippocampal mossy fiber terminal connectivity in the adult regulated by experience. *Neuron*, 50(5):749–763.

Greenhouse, S. and Geisser, S. (1959). On methods in the analysis of profile data. *Psychometrika*, 24:95–112.

Grutzendler, J., Kasthur, N., and Gan, W. (2002). Long-term dendritic spine stability in the adult cortex. *Nature*, 420(6917):812–6.

Harland, B., Collings, D., McNaughton, N., Abraham, W., and Dalrymple-Alford, J. (2014). Anterior thalamic lesions reduce spine density in both hippocampal ca1 and retrosplenial cortex, but enrichment rescues ca1 spines only. *Hippocampus*, 10:1232–1247.

Hayashi-Takagi, A., Yagishita, S., NAkamura, M., Shirai, F., Wu, Y., Loshbaugh, A., Kuhlman, B., and Hahn, K.M. amd Kasai, H. (2015). Labelling and optical erasure of synaptic memory traces in the motor cortex. *Nature*, 525:333–338.

Hebb, D. (1947). The effects of early experience on problem solving at maturity. *American Psychologist*, 2:737–45.

Holtmaat, A. and Svoboda, K. (2009). Experience-dependent structural synaptic plasticity in the mammalian brain. *Nature Reviews*, 10:647–658.

Holtmaat, A., Trachtenberg, J., and Wilbrecht, L. (2006). Experience-dependent and cell-type-specific spine growth in the neocortex. *Nature*, 441:979–83.

Huynh, H. and Feldt, L. (1976). Estimation of the box correction for degrees of freedom from sample data in ranomised block and split-plot designs. *Journal of Educational Statistics*, 1:69–82.

Ichinohe, N., Knight, A., Ogawa, M., Ohshima, T., Mikoshiba, K., Yoshihara, Y., Terashima, T., and Rockland, K. (2008). Unusual patch-matrix organization in the retrosplenial cortex of the reeler mouse and shaking rat kawasaki. *Cerebral Cortex*, 18:1125–1138.

Jung, C. and Herms, J. (2014). Structural dynamics of dendritic spines are influenced by an environmental enrichment: An in vivo imaging study. *Cerebral Cortex*, 24:377–384.

Juraska, J. (1990). The structure of the cerebral cortex: effects of gender and the environment. In Kolb, B. and Tees, R., editors, *The cerebral cortex of the rat*, pages 483–506. Cambridge, MA: MIT Press.

Kirby, E., Jensen, K., Goosens, K., and Kaufer, D. (2012). Stereotaxic surgery for excitotoxic lesion of specific brain areas in the adult rat. *Journal of Visualized Experiments*, 65(4079):1–6.

Kolb, B., Gibb, R., and Gorny, G. (2003). Experience-dependent changes in dendritic arbor and spine density in neocortex vary with age and sex. *Neurobiology of learning and memory*, 791:1–10.

Lawrence, M. (2011). ez: Easy analysis and visualization of factorial experiments.

Mao, D., Neumann, A., Sun, J., Bonin, V., Mohaherani, M., and McNaughton, B. (2018). Hippocampus-dependent emergence of spatial sequence coding in retrosplenial cortex. *Proceedings of the National Academy of Sciences*, pages 1–4.

Marr, D. (1970). A theory for cerebral neocortex. *Proceedings of the Royal Society of London. Series B, Biological Sciences*, pages 161–234.

Marr, D. (1971). Simple memory: A theory for archicortex. *Biological Sciences*, 262(841):23–81.

Mauchly, J. (1940). Significance test for sphericity of a normal n-variate distribution. *The Annals of Mathematicsl Statistics*, 11:204–209.

Mendez-Lopez, M., Arias, B., and Wolff, M. (2013). Reduced cytochrome oxidase activity in the retrosplenial cortex after lesions to the anterior thalamic nuclei. *Behavioural Brain Research*, 250:264–273.

Miyashita, T. and Rockland, K. (2007). Gabaergic projections from the hippocampus to the retrosplenial cortex in the rat. *Eur. J. Neurosci.*, 26:196–206.

Norimoto, H., Makino, K., Gao, M., Shikano, Y., Okamoto, K., Ishikawa, T., Sasaki, T., Hioki, H., Fujisawa, S., and Ikegaya, Y. (2018). Hippocampal ripples down-regulate synapses. *Science*, 359(6383):1524–1527.

Oh, S.W, e. a. (2014). A mesoscale connectome fo the mouse brain. *Nature*, 508:207–214.

Paola, V., Holtmaat, A., Knott, G., Song, S., Wilbrecht, L., Caroni, P., and Svoboda, K. (2006). Cell type-specific structural plasticity of axonal branches and boutons in the adult neocortex. *Neuron*, 49(6):861–875.

Penfield, W. and Milner, B. (1958). Memory deficit produced by bilateral lesions in the hippocampal zone. *AMA Arch Neurol Psychiatry*, 81(6):785–94.

Phillips, M. and Pozzo-Miller, L. (2015). Dendritic spine dysgenesis in autism related disorders. *Neuroscience Letters*, 601:30–40.

Porrero, C., Rubio-Garrido, P., Avendano, C., and Clasca, F. (2010). Mapping of fluorescent protein-expressing neurons and axon pathways in adult and developing thy1-eyfp-h trangenic mice. *Brain Research*, 1345:59–72.

Raichle, M., MacLeod, A., Snyder, A., Powers, W., Gusnard, D., and Shulman, G. (2001). A default mode of brain function. *Proceedings of the National Academy of Sciences*, 98(2):676–682.

Rapley, S., Prickett, T., Dalrymple-Alford, J., and Espiner, E. (2018). Environmental enrichment elicits a transient rise of bioactive c-type natriuretic peptide in young but not aged rats. *Frontiers in behaviroual neuroscience*, 12(142):1–12.

Roberts, T., Tschida, K., and Marguerita, E.K. amd Mooney, R. (2010). Rapid spine stabilization and synaptic enhancement at the onset of behavioural learning. *Nature*, 463(7283):948–952.

Roo, M., Klauser, P., and Muller, D. (2008). Ltp promotes a selective long-term stabalization and clustering of dendritic spines. *PLOS Biology*, 6(9):1850–1860.

Rose, F., al Khamees, K., Davey, M., and Attree, E. (1993). Environmental enrichment following brain damage: an aid to recovery or compensation? *Behavioural Brain Research*, 56(1):93–100.

Rosenzeig, M., Bennett, E., and Diamond, M. (1972). Chemical and anatomical plasticity of brain: replications and extensions. In Macromolecules, I. J. G. and behaviour, editors, *Macromolecules and behaviour*, pages 205–277. New York: Appleton-Century-Crofts, 2 edition.

Ruthazer, E., Li, J., and Cline, H. T. (2006). Stabilization of axon branch dynamics by synaptic maturation. *The Journal of Neuroscience*, 26(13):3594–3603.

Scoville, W. and Milner, B. (1957). Loss of recent memory after bilateral hippocampal lesions. *Journal of Neurology, Neurosurgery Psychiatry*, 20(1):11–21.

Shim, H., Lee, Y., and Kim, S. (2018). The emerging concept of instrinsic plasticity: Activity-dependent modulation of intrinsic excitability in cerebellar purkinje cells and motor learning. *Experimental Neurobiology*, 27(3):139–154.

So, P. T. (2002). Two-photon fluorescence light microscopy. In *Encyclopedia of Life Sciences*, pages 1–5. Macmillan Publishing Group, Nature Publishing Group / www.els.net.

Squire, L. and Wixted, J. (2011). The conitive neuroscience of human memory since h.m. *Annual review of neuroscience*, 34:259–288.

Sugar, J., Witter, M., van Strien, N., and Cappaert, N. (2011). The retrosplenial cortex: Instrinsic connectivity and connections with the (para)hippocampal region in the rat. *Frontiers in Neuroinformatics*, 5(7):1–13.

Sutherland, R., Gibb, R., and Kolb, B. (2010a). The hippocampus makes a significant contribution to experience-dependent neocortical plasticity. *Behavioural Brain Research*, 214:121–124.

Sutherland, R., Sparks, F., and Lehmann, H. (2010b). Hippocampus and retrograde amnesia in the rat model: A modest proposal for the situation of systems consolidation. *Neuropsychologia*, 48:2357–2369.

Sutherland, R. J. and Hoesing, J. (1993). Posterior cingulate cortex and spatial memory: A microlimnology analysis. In Vogt, B. and Gabriel, M., editors, *Neurobiology of Cingulate Cortex and Limbic Thalamus*. Birkhauser, Boston, MA.

Tavosanis, G. (2011). Dendritic structural plasticity. *Developmental Neurobiology*, 72:73–86.

Tong, L., Prieto, G., Kramar, E., Smith, E., Cribbs, D., Lynch, G., and Cotman, C. (2012). Brain-derived neurotrophic factor-dependent synaptic plasticity is suppressed by interleukin-1 via p38 mitogen-activated protein kinase. *Journal of Neuroscience*, 32:17714–17724.

Trachtenberg, J., B.E., C., Knott, G., Feng, G., Sanes, J., Welker, E., and Svoboda, K. (2002). Long-term in vivo imaging of experience-dependent synaptic plasticity in adult cortex. *Nature*, 420:788–794.

Tronson, N. and Taylor, J. (2007). Molecular mechanisms of memory reconsolidation. *Nature Reviews*, 8:262–275.

Van Groen, T. and Wyss, J. (2003). Connections of the retrosplenial granular b cortex in the rat. *J Comp. Neurol.*, 463:249–263.

Villa, K., Berry, K., Subramanian, J., Cha, J., Oh, W., Kwon, H.-B., Kubota, Y., So, P., and Nedivi, E. (2016). Inhibitory synapses are repeatedly assembled and removed at persistent sites in vivo. *Neuron*, 89(4):756–769.

Vogt, B. and Miller, M. (1983). Cortical connections between rat cingulate cortex and visual, motor, and postsubicular cortices. *J Comp. Neurol.*, 216(2):192–210.

Weiler, I., Hawrylak, N., and Greenough, W. (1995). Morphogenesis in memory formation: synaptic and cellular mechanisms. *Behavioural Brain Research*, 66:1–6.

Wyss, J. and Groen, T. (1992). Connections between the retrosplenial cortex and hippocampal formation in the rat: A review. *Hippocampus*, 2(1):1–12.

Xu, T., Xinzhu, Y., Perlik, A., Tobin, W.F. amd Zweig, J., Tennant, K., and Jones, T. amd Zuo, Y. (2009). Rapid formation and selective stabilization of synapses for enduring motor memories. *Nature*, 462:915–919.

Yamawaki, N., Radulovic, J., and Shepherd, G. (2016). A corticocortical circuit directly links retrosplenial cortex to m2 in the mouse. *Journal of Neuroscience*, 36(36):9365–9374.

Yang, G., Lai, C., Cichon, J., Ma, L., Li, W., and Gan, W. (2014). Sleep promotes branch-specific formation of dendritic spines after learning. *Science*, 344(6188):1173–1178.

Yu, J., Anderson, C., Kiritani, T., Sheets, P., Wokosin, D., and Wood, L. amd Shepherd, G. (2008). Local-circuit phenotypes of layer 5 neurons in motor-frontal cortex of yfp-h mice. *Frontiers in Neural Circuits*, 2(6):1–8.

Zingg, B., Hinitiryan, H., Gou, L., Song, M., Bay, M., Bienkowski, M., Foster, N., Yamashita, S., Bowman, I., Toga, A., and H.W., D. (2014). Neural networks of the mouse neocortex. *Cell*, 156:1096–1111.

Zuo, Y., Ding, J., Lu, J., and Chen, C. (2018). Selective activation of parvalbumin interneurons prevents stress-induced synapse loss and perceptual defects. *Molecular Psychiatry*, 23:1614–1625.

Sex Differences

Could opposing spatial strategies such as allocentric versus egocentric be a reason for the greater female expression in the apical fields of the RSC? Is there increased superficial branching in females due to differences in expression levels between the sexes? Does the sex of the YFP+ versus wild-type parent matter? Why do axon branches modify substantially more often in males, only 6/49 or $\sim$12% of all changes occurred in females. Are there anatomically different origins for axons with specific morphologies that are different between males and females? Conversely, why is synaptic density greater in females? Sex differences in transgenic mouse lines and possible structural differences in the RSC between the sexes require additional examination.

A.1 Top-down visual difference in layer 1

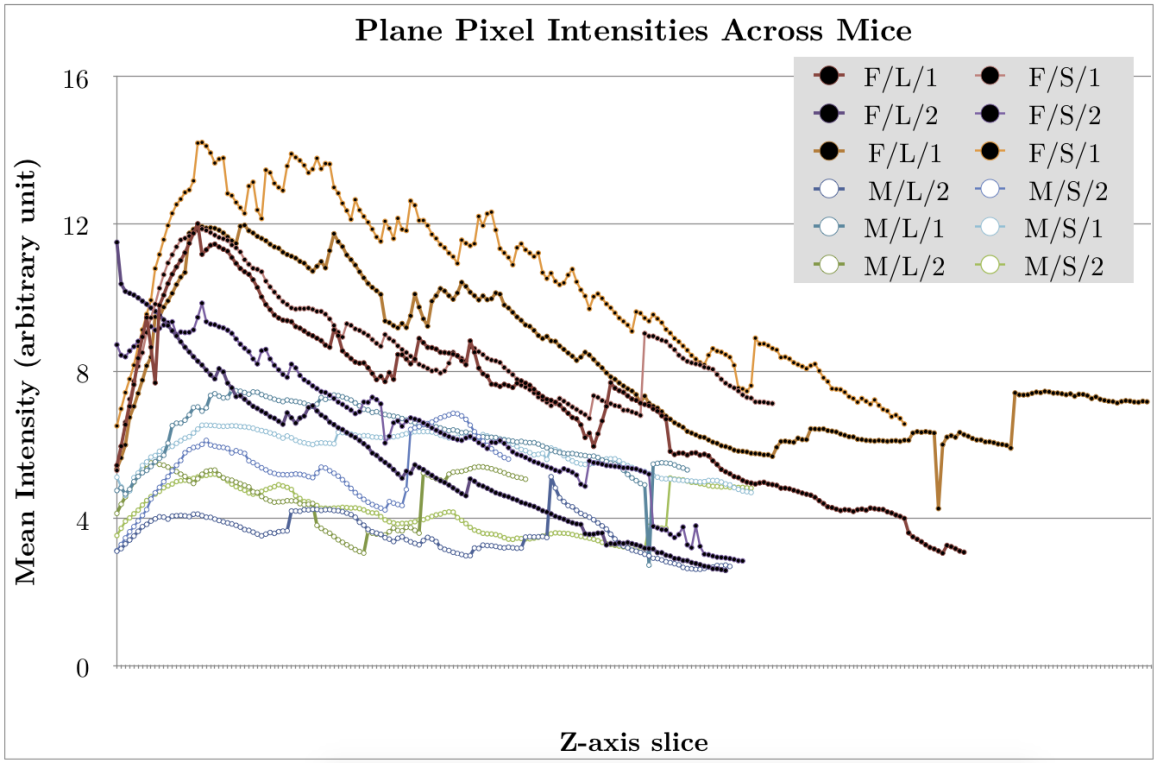

Figure A.1: Qualitative data indicating that females have higher pixel intensity in the superficial layer 1 of the RSC. These data highlight sex/hemisphere/sibling group; 1 siblings had a sire who contained the Thy1-YFP+ phenotype and (2) siblings had a mother who contained the Thy1-YFP+ phenotype.

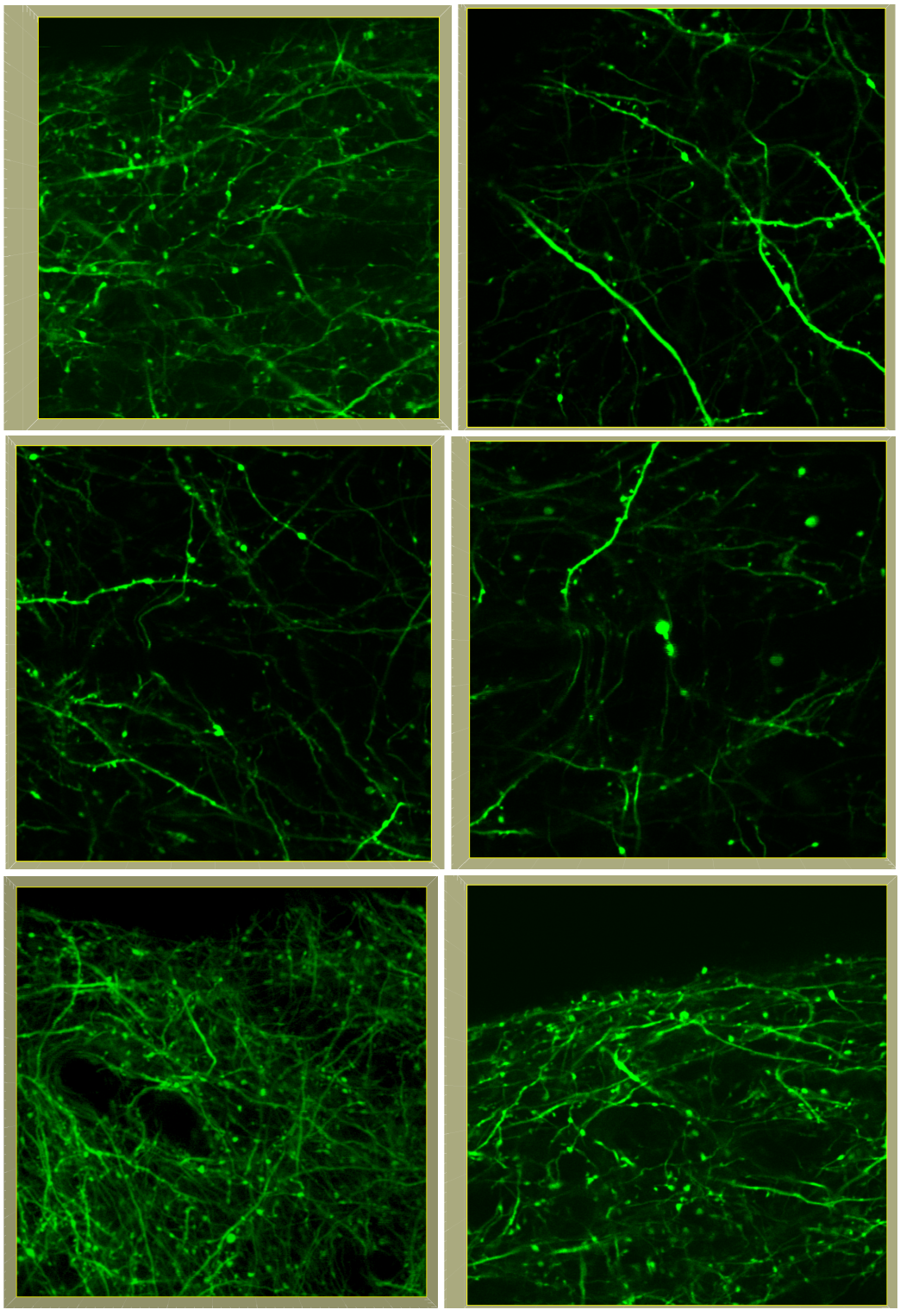

[a]

[b]

[c]

Figure A.2: In addition to pixel intensities, there was also a noticeable visual difference by eye in RSC superficial layers between the sexes. The surface of the brains appeared more convoluted with more dynamic branching in female mice. [a] comparing brain surface (left) female followed by (right) male [b] two male image examples from different mice [c] two female image examples from two different mice.

A.2 Sex difference in histology

Females Males

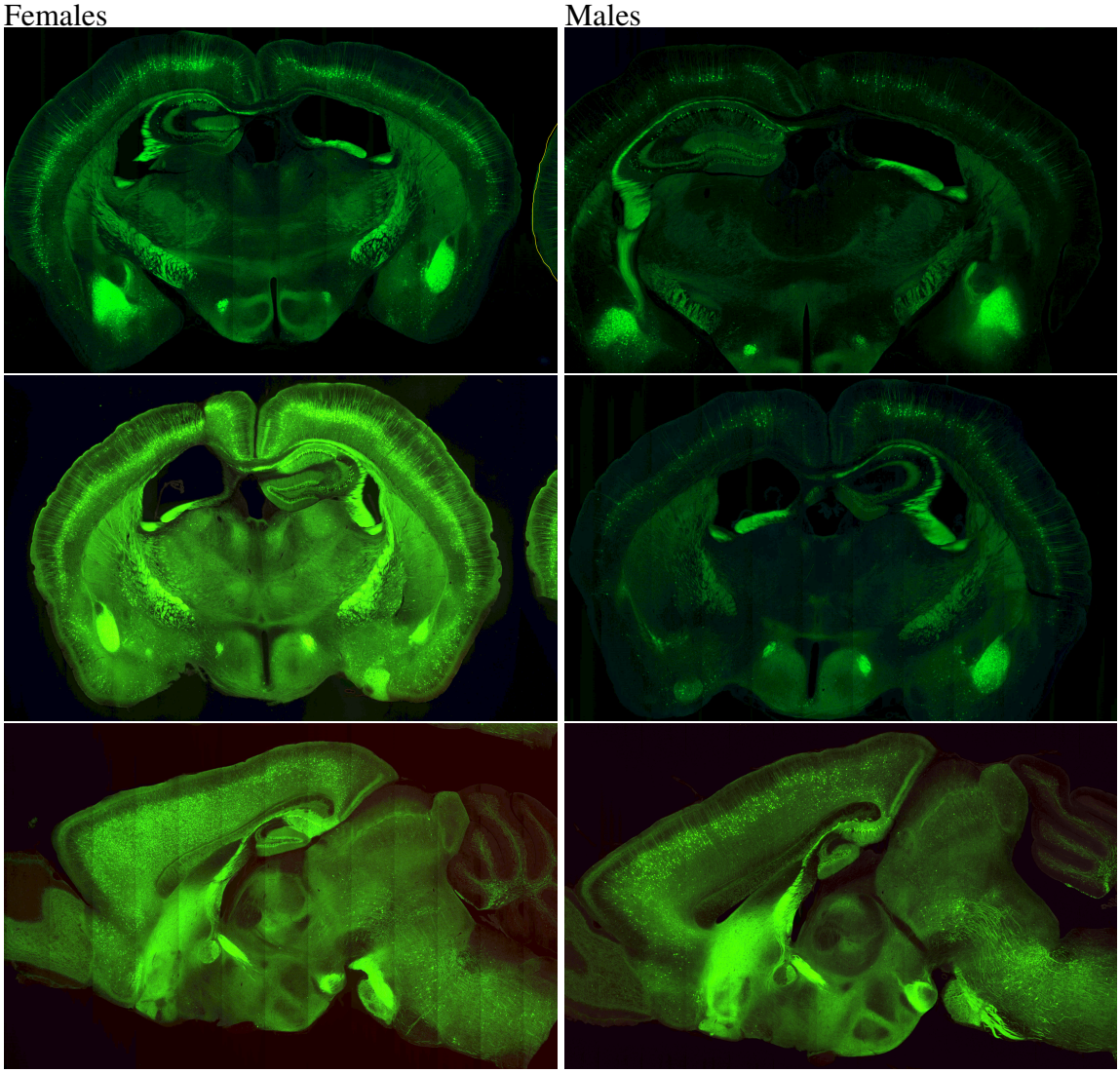

Figure A.3: Female expression appeared brighter and more dense than male expression across the brains of YFP+ transgenic mice. The top left female is siblings with the top 2 males and the bottom male is siblings with the bottom two females which was identified for 2 reasons, 1) a more alike hue between siblings and 2) The male with the highest density was sibling to the females with the highest and the female with the lowest was sibling to the males with the lowest.

A.3 Sex differences in density and stability of dendritic spines and axon boutons

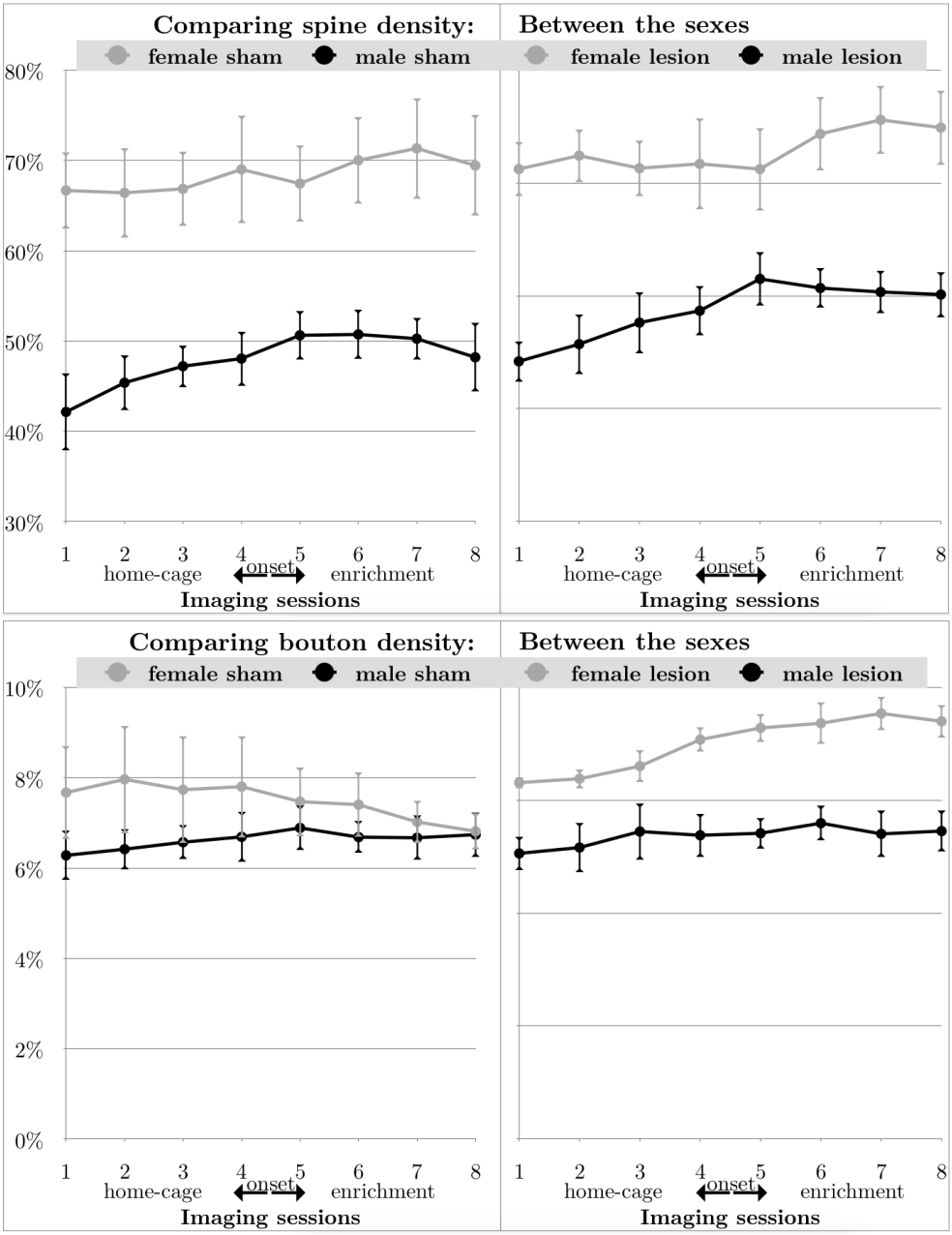

Figure A.4: Adding sex as a factor resulted in a significant difference between the sexes for both dendritc spines and boutons, spines: $F(1,4) = 14.4925923, p = 0.01899043, \eta_G^2 = 0.764528159$ and boutons: $F(1,4) = 7.97208, p = 0.0473589, \eta_G^2 = 0.409789$. In addition, there was an interaction between sex and imaging sessions in dendritic spines only, $F(7,28) = 5.4320340, p = 0.0005123105, \eta_G^2 = 0.044664262$. Females showed a level density during home-cage that increased during enrichment while males showed a greater increase in density during home-cage that levelled off during enrichment.

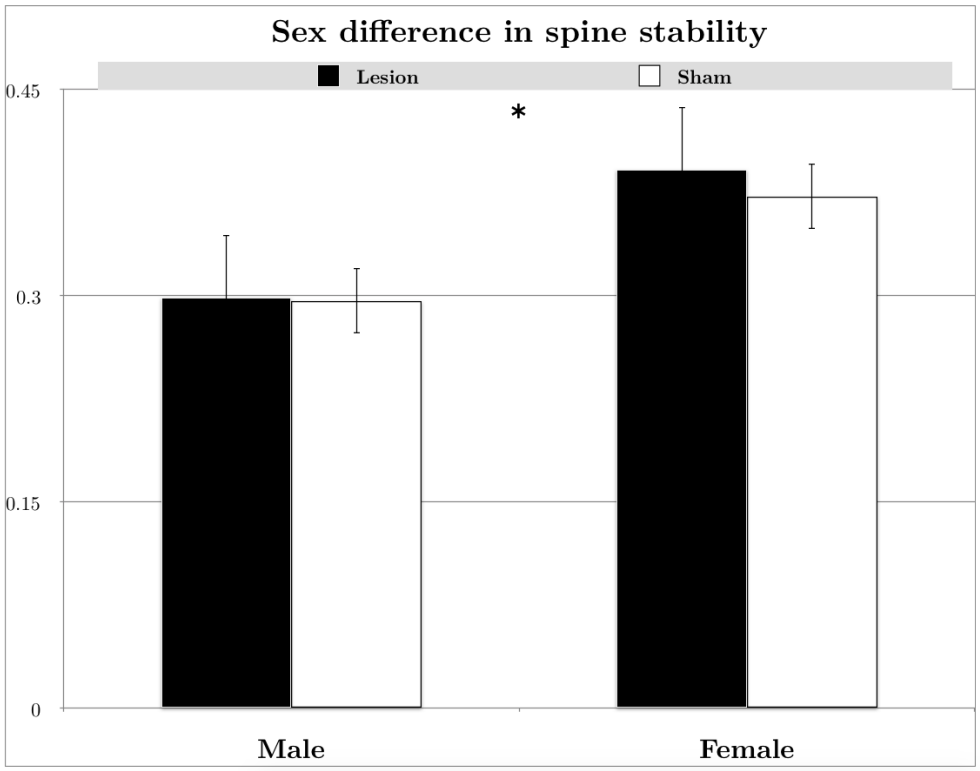

Figure A.5: Females show significantly higher spine stability than males, $p = 0.02067$ and two-tailed, $p = 0.041340$ result. Increased stability may shed light on a possible bias regarding why females have an overall greater spine density than males. Specifically, when more spines stick around across imaging sessions they will be counted a greater number of times. There was no sex difference in axon bouton stability.

A.4 Axonal bouton turnover interaction and variability

A.5 Dendritic spine turnover interactions

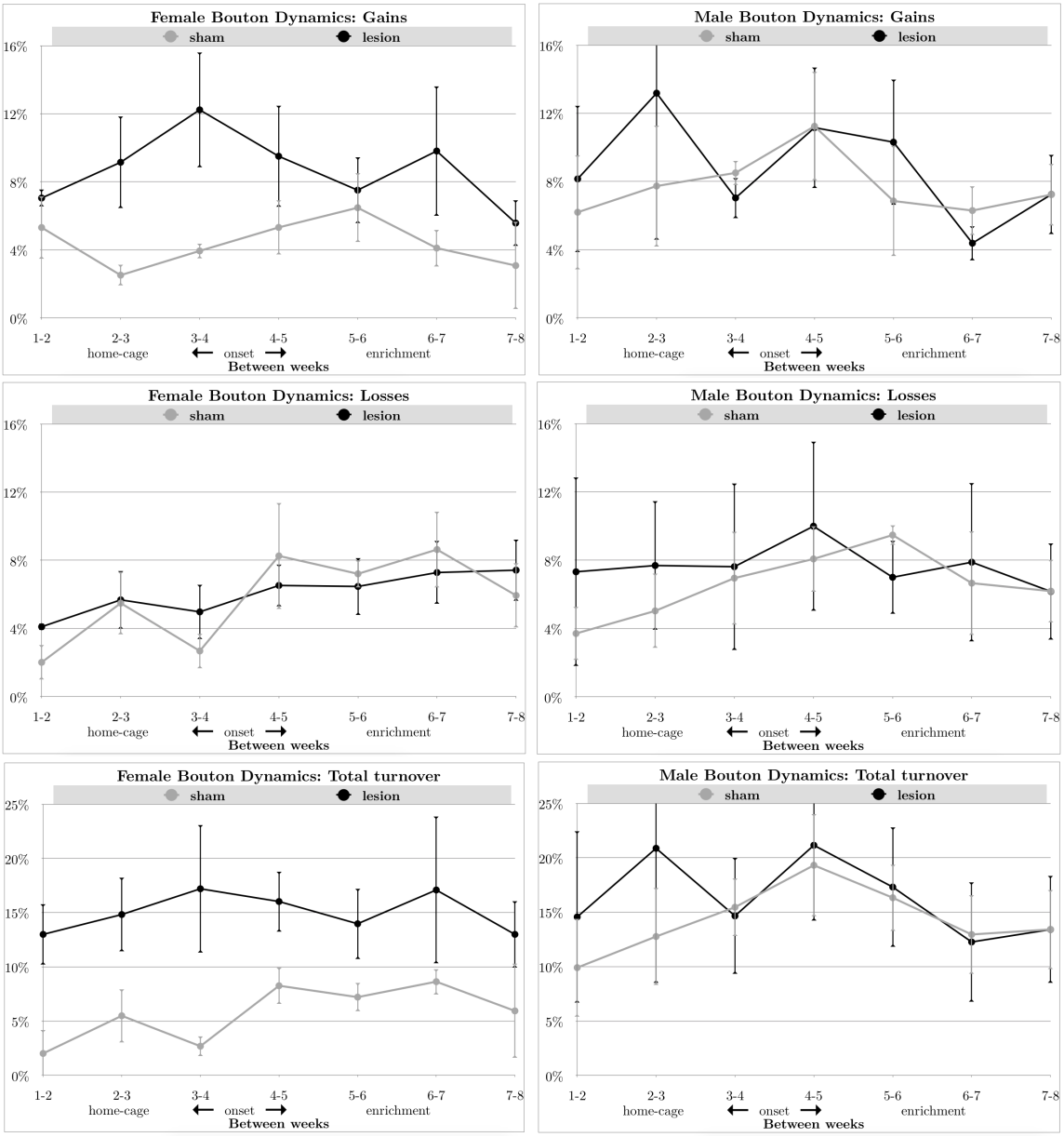

Figure A.6: When the between factor sex was taken into account a repeated measures ANOVA resulted in the addition of a significant Type:Hemisphere interaction, $F(1,4) = 7.7428930, p = 0.04968598, \eta^2_G = 0.014619545$. The variability in data is partially due to sex differences. Both males and females show greater variability in the lesion hemisphere of total turnover, with total variability being higher in males. Females also display a larger difference between hemispheres, with greater turnover being observed in the lesion hemisphere.

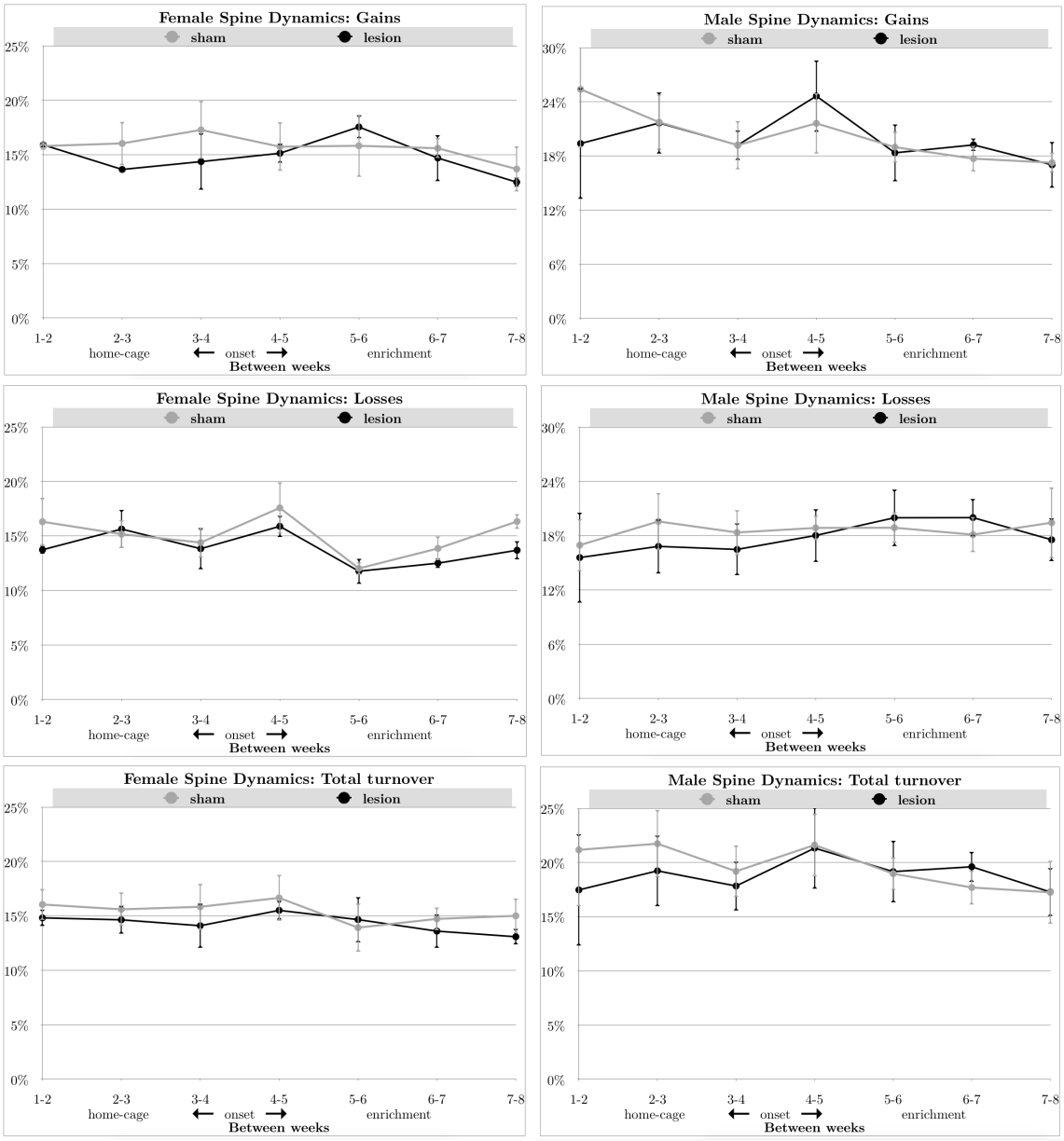

Figure A.7: When the between factor sex was taken into account a repeated measures ANOVA resulted in the addition of a mild significant Type:Sessions interaction, $F(1,4) = 7.7428930, p[HF] = 0.0441, and Sex : Type : Sessions, p[GG] = 0.0265, p[HF] = 0.00399$. The variability in data is partially due to sex differences.

R-Code

B.1 Repeated measures analysis of variance

The following example code is a 2*8 repeated measures analysis of variance for spine turnover data with pairwise comparison post hoc analysis. Similar codes were continually used to perform multiple two-way factorial analysis of variance in which there were 2-8 levels of each of three possible variables, hemisphere, type of turnover, and imaging sessions. Each mouse was measured under all of the possible combinations and therefore these factors are all considered repeated measures. When sex was taken into account and an ANOVA was ran, sex was represented as the only between-subjects factor.

```
%Input data, the following shows partial data
%spine turnover

Input = ("Hemisphere␣Mouse␣Turnover␣Sessions␣Sex
'Lesion'␣␣␣␣␣a␣␣␣␣␣0.523281596452328␣␣␣␣␣␣1␣␣␣M
'Lesion'␣␣␣␣␣b␣␣␣␣␣0.296724470134875␣␣␣␣␣␣1␣␣␣F
'Lesion'␣␣␣␣␣c␣␣␣␣␣0.377162629757785␣␣␣␣␣␣1␣␣␣M
'Lesion'␣␣␣␣␣d␣␣␣␣␣0.304545454545455␣␣␣␣␣␣1␣␣␣F
'Lesion'␣␣␣␣␣e␣␣␣␣␣0.287878787878788␣␣␣␣␣␣1␣␣␣F
'Lesion'␣␣␣␣␣f␣␣␣␣␣0.14804469273743␣␣␣␣␣␣␣1␣␣␣M
'Lesion'␣␣␣␣␣a␣␣␣␣␣0.498973305954825␣␣␣␣␣␣2␣␣␣M
'Lesion'␣␣␣␣␣b␣␣␣␣␣0.314990512333966␣␣␣␣␣␣2␣␣␣F
'Lesion'␣␣␣␣␣c␣␣␣␣␣0.375862068965517␣␣␣␣␣␣2␣␣␣M
'Lesion'␣␣␣␣␣d␣␣␣␣␣0.306666666666667␣␣␣␣␣␣2␣␣␣F
'Lesion'␣␣␣␣␣e␣␣␣␣␣0.256637168141593␣␣␣␣␣␣2␣␣␣F
'Lesion'␣␣␣␣␣f␣␣␣␣␣0.279132791327913␣␣␣␣␣␣2␣␣␣M
...
...
'Sham'␣␣␣␣␣a␣␣␣␣␣␣␣0.316993464052288␣␣␣␣6␣␣␣M
'Sham'␣␣␣␣␣b␣␣␣␣␣␣␣0.32␣␣␣␣␣␣␣␣␣␣␣␣␣␣␣␣6␣␣␣F
'Sham'␣␣␣␣␣c␣␣␣␣␣␣␣0.416107382550336␣␣␣␣6␣␣␣M
'Sham'␣␣␣␣␣d␣␣␣␣␣␣␣0.290076335877863␣␣␣␣6␣␣␣F
'Sham'␣␣␣␣␣e␣␣␣␣␣␣␣0.273364485981308␣␣␣␣6␣␣␣F
'Sham'␣␣␣␣␣f␣␣␣␣␣␣␣0.328571428571429␣␣␣␣6␣␣␣M
'Sham'␣␣␣␣␣a␣␣␣␣␣␣␣0.31438127090301␣␣␣␣␣7␣␣␣M
'Sham'␣␣␣␣␣b␣␣␣␣␣␣␣0.346368715083799␣␣␣␣7␣␣␣F
'Sham'␣␣␣␣␣c␣␣␣␣␣␣␣0.434782608695652␣␣␣␣7␣␣␣M
'Sham'␣␣␣␣␣d␣␣␣␣␣␣␣0.295629820051414␣␣␣␣7␣␣␣F
'Sham'␣␣␣␣␣e␣␣␣␣␣␣␣0.258426966292135␣␣␣␣7␣␣␣F
'Sham'␣␣␣␣␣f␣␣␣␣␣␣␣0.285714285714286␣␣␣␣7␣␣␣M
```

```
")

> Data1SpineTurnover = read.table(textConnection(Input),
+header=TRUE)
> Data1SpineTurnover$Sessions = factor(Data1SpineTurnover$
+Sessions, levels=unique(Data1SpineTurnover$Sessions))

%Check the data to make sure it has been imported  correctly

> str(Data1SpineTurnover)

%Output:
'data.frame':   84 obs. of  5 variables:
 $ Hemisphere: Factor w/ 2 levels "'Lesion'","'Sham'":
 1 1 1 1 1 1 1 1 1 1 ...
 $ Mouse     : Factor w/ 6 levels "a","b","c","d",..:
 1 2 3 4 5 6 1 2 3 4 ...
 $ Density   : num  0.523 0.297 0.377 0.305 0.288 ...
 $ Sessions  : Factor w/ 7 levels "1","2","3","4",..:
 1 1 1 1 1 1 2 2 2 2 ...
 $ Sex       : Factor w/ 2 levels "M","F":
 1 2 1 2 2 1 1 2 1 2 ...

> summary(Data1SpineTurnover)

%Output:
    Hemisphere  Mouse      Density         Sessions Sex
 'Lesion':42   a:14   Min.   :0.1480   1:12     M:42
 'Sham'  :42   b:14   1st Qu.:0.2855   2:12     F:42
               c:14   Median :0.3208   3:12
               d:14   Mean   :0.3412   4:12
               e:14   3rd Qu.:0.3749   5:12
               f:14   Max.   :0.5994   6:12
                                       7:12
%Visual check
install.packages('ez')
library(ez)
> ezDesign(
+       data = Data1SpineDensity
+       , x = Sessions
+       , y = Mouse
+       , row = Hemisphere
+       , col = Sex
+   )
```

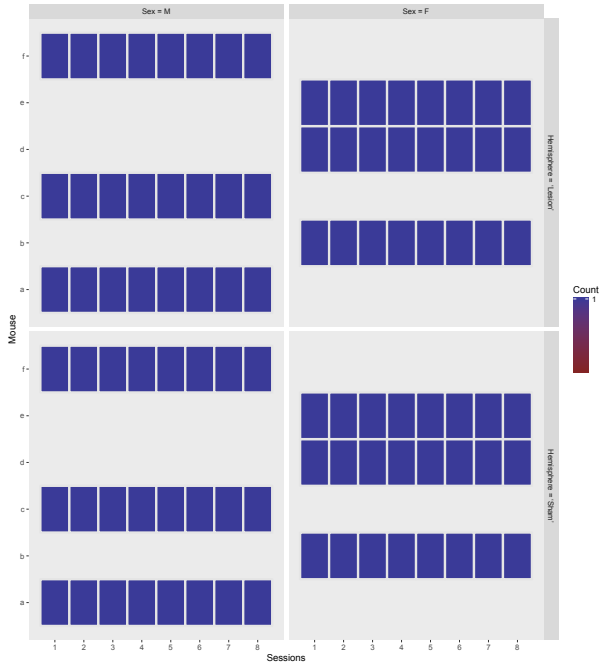

Figure B.1: The following check provides a visual output. All blue indicates that all data is accounted for in the data. A box containing red would indicate a missing value or unequal data frame. Each row pertains to a specific mouse, the four quadrants indicate sex and hemisphere. The eight boxes represent imaging sessions.

```
%Output:
```

```
%Run a repeated measures ANOVA via ezANOVA
% ez packages were written by Mark Lawrence

> SpineTurnoverANOVA = ezANOVA(data=Data1SpineTurnover,
+     wid = Mouse,
+     within = .(Hemisphere, Sessions),
+     dv = Turnover,
+     type = 3)

> SpineTurnoverANOVA

%Output: * represents significance
$ANOVA
      Effect DFn DFd         F          p p<.05         ges
2 Hemisphere   1   5 0.2873332 0.61491282       0.01416410
3   Sessions   6  30 3.1903759 0.01526907*      0.05538911
4 Interaction   6  30 1.2947093 0.28966633       0.01642205
```

```
%Mauchly's Test for Sphericity runs automatically
%only shows when significant
%Sphericity corrections run automatically
% when Mauchly's is significant


%Run pairwise comparison on each hemisphere across time

> lesion=subset(Data1AxonTurnover, Hemisphere == "?Lesion?")
> sham=subset(Data1AxonTurnover, Hemisphere == "?Sham?")
> pairwise.t.test(sham$Density, sham$Sessions,
paired=TRUE, p.adj ="bonferroni")

%Output:

  1     2     3     4     5     6
2 1.000 -     -     -     -     -
3 1.000 1.000 -     -     -     -
4 0.016 0.117 1.000 -     -     -
5 0.240 0.437 1.000 1.000 -     -
6 0.198 1.000 1.000 0.946 1.000 -
7 1.000 1.000 1.000 1.000 1.000 1.000

P value adjustment method: bonferroni
> pairwise.t.test(lesion$Density, lesion$Sessions,
paired=TRUE, p.adj ="bonferroni")

        Pairwise comparisons using paired t tests

data:  lesion$Density and lesion$Sessions

  1 2 3 4 5 6
2 1 - - - - -
3 1 1 - - - -
4 1 1 1 - - -
5 1 1 1 1 - -
6 1 1 1 1 1 -
7 1 1 1 1 1 1

P value adjustment method: bonferroni
```

B.2 Counting all possible data configurations

```
>install.packages('e1071')
>library(e1071)

%Input dataset

>NAME <- read.table(file="~/Desktop/AllAnimalsShamSpines.txt")
%Perform function

>CountShamSpines <-countpattern(NAME)
>CountShamSpines
```